INTERMEDIATE ENERGY ELECTRON COOLING FOR ANTIPROTON SOURCES

by

DELBERT JOHN LARSON

A thesis submitted in partial fulfillment of the

requirements for the degree of

Doctor of Philosophy

(Physics)

at the

UNIVERSITY OF WISCONSIN -- MADISON

© copyright by Delbert John Larson 1986

Intermediate Energy Electron Cooling for Antiproton Sources -- Abstract

Electron-cooling at low energies (γ slightly greater than one) has been shown to be an extremely effective means to increase the phase space density of proton beams. This document starts with a review of the progress made in low energy electron cooling, followed by a brief look at the parameters of intermediate energy electron cooling. (γ of five to ten).

The results of an emittance measurement done on an electrostatic accelerator are presented indicating that such a device would be ideal for intermediate energy electron cooling. A complete electron optics design of the system is done next, solving the beam envelope evolution problem in the presence of emittance, space charge, and acceleration.

Application of intermediate energy electron cooling to the Fermilab antiproton source is theoretically studied. The amount of time it takes for the antiproton beam to cool is calculated including the effects of finite electron beam temperature, betatron oscillations, and intrabeam scattering. A four ampere electron beam will cool the Fermilab antiproton beam in half an hour.

Lastly, the final equilibrium antiproton emittances obtainable are estimated. Equilibrium between the competing processes of intrabeam scattering and electron cooling exists when the transverse antiproton beam emittances are 0.12 π mm-mr and the longitudinal antiproton beam emittance is $\Delta p/p = 1\times10^{-5}$. This represents a phase space density increase of about 15 in each transverse plane, and an improvement of 20 in the energy resolution of the accumulator. Possible instabilities of such a dense beam are investigated.

To my family: Doris Anderson, Delbert A. Larson, Marion Larson, Louis Larson, Mark Larson, Doris & Ted Peterson et. al, Laurie Larson, Michelle Larson, and Gerrie.

Table of Contents

Abstract	i
Dedication	ii
Table of Contents	iii
Where are the Pictures?	v
Table of Tables	vii
1) Introduction	p. 1
A) Overview	p. 1
B) Review of Electron Cooling Experiments	p. 4
C) Parameters of Intermediate Energy Electron Cooling	p. 9
2) Use of an Electrostatic Accelerator as an Electron Beam Source	p. 13
A) Emittance Measurement	p. 13
B) Collector and Gun Designs for the Pelletron	p. 28
C) Pelletron Optics Calculations	p. 36
3) Intermediate Energy Electron Cooling for the Fermilab Antiproton Source	p. 49
A) Antiproton Production and Stochastic Cooling	p. 49
B) Initial Velocity Distributions	p. 54
C) Expected Cooling Time -- Ideal Case	p. 57
4) Complete Simulation of the Expected Cooling Time	p. 61
A) Analytic Derivation of the Cooling Force	p. 61
B) Numerical Simulation of Ideal Case	p. 65
C) Electron Temperature Effect	p. 69
D) The Effect of Betatron Oscillations on the Cooling Time	p. 72
E) Intrabeam Scattering	p. 76

Table of Contents -- Continued

5) Expected Performance of the Device -- Final Antiproton Emittances p. 85

A) Focusing the Electron Beam -- Effective Temperature Increase p. 85

B) Cooling Force Near Equilibrium -- Electron Temperature Effect p. 89

C) Final Antiproton Emittances -- Equilibrium With Intrabeam Scattering p. 96

D) Final Antiproton Emittances -- Possible Instabilities p. 108

Appendix -- Computer Codes p. 113

Appendix 1 -- Electron Beam Optics in a Transport Line p. 113

Appendix 2 -- Complete Pelletron Optics Code Package p. 114

Appendix 3 -- Ideal Cooling Time Calculation p. 117

Appendix 4 -- Calculation of the Effect of Electron Temperature on the Electron Cooling Force p. 118

Appendix 5 -- The Effect of Betatron Oscillations on the Cooling Time p. 119

Appendix 6 -- The Effect of Intrabeam Scattering on the Cooling Time p. 120

Appendix 7 -- Calculation of the Ideal Electron Cooling Rates p. 122

Acknowledgments p. 123

References p.124

Where are the Pictures?

Figure 2.1 -- Emittance Measurement Device p. 19

Figures 2.2 through 2.13 -- Scope traces. (Data from the emittance measurement experiment.) pp. 20-25

Figure 2.14 -- Emittance measurement at $\gamma = 5$. Experimental fit to data. p. 26

Figure 2.15 -- Emittance measurement at $\gamma = 6$. Experimental fit to data. p. 27

Figure 2.16 -- Electron gun trajectory simulation. Current = 0.315 A. p. 30

Figure 2.17 -- Electron gun trajectory simulation. Current = 3.962 A. p. 31

Figure 2.18 -- Schematic of electron beam collector. p. 32

Figure 2.19 -- Electron collector trajectory simulation. Current = 3.962 A. p. 33

Figure 2.20 -- Pelletron electron optics simulation. Current = 0.315 A. p. 43

Figure 2.21 -- Pelletron electron optics simulation. Current = 3.962 A. p. 44

Figure 2.22 -- Schematic of the recirculation test set up. p. 45

Where are the Pictures? -- Continued

Figure 2.23 -- Pelletron electron optics simulation. Over-focused beam. p. 47

Figure 2.24 -- Pelletron electron optics simulation. Under-focused beam. p. 48

Figure 3.1 -- Stochastic cooling beam density profile as a function of time. p. 53

Figure 3.2 -- Initial velocity distributions of the antiproton and electron beams. p. 56

Figure 4.1 -- Electron cooling of the antiproton velocity distribution as a function of time. p. 68

Figure 4.2 -- Example of a single particle trajectory in phase space. p. 81

Figure 5.1 -- Electron beam expansion from a waist with and without space charge. p. 87

Figure 5.2 -- Antiproton density profile before and after electron cooling. p. 107

Figure 5.3 -- Regions of beam stability as a function of the complex impedance of a storage ring. p. 109

Table of Tables

Table 1.1 -- Main Parameters of the NAP-M Storage Ring p. 5

Table 1.2 -- Parameters of the Novosibirsk Electron-Beam Device p. 5

Table 1.3 -- Typical Experimental Parameters and Results of NAP-M p. 5

Table 1.4 -- Parameters of CERN's ICE Experiments p. 6

Table 1.5 -- Results of CERN's ICE Experiments p. 6

Table 1.6 -- Parameters of FNAL's Electron Cooling Experiment p. 6

Table 1.7 -- Results of FNAL's Electron Cooling Experiment p. 7

Table 1.8 -- European Electron Cooling Projects p. 8

Table 2.1 -- Experimental Results -- Sweep Rates at $\gamma = 5$ p. 17

Table 2.2 -- Experimental Results -- Beam Size at $\gamma = 5$ p. 17

Table 2.3 -- Experimental Results -- Sweep Rates at $\gamma = 6$ p. 17

Table 2.4 -- Experimental Results -- Beam Size at $\gamma = 6$ p. 17

Table 2.5 -- Ion and Electron Gyro-Radii p. 34

Table 2.6 -- Azimuthal Energy of Outer Electrons (in eV) p. 35

Table 3.1 -- Final Antiproton Stack Parameters -- Stochastic Cooling Only p. 52

Table of Tables -- Continued

Table 3.2 -- Intermediate Energy Electron Cooling Times p. 60

Table 4.1 -- Code Parameters -- Ideal Cooling Time Calculation p. 67

Table 4.2 -- $d\varepsilon/dt$ as a Function of Integration Step Size p. 70

Table 4.3 -- Code Parameters and Results -- Betatron Oscillation Transverse Cooling Time Improvement Factor p. 74

Table 4.4 -- Code Parameters and Results -- Betatron Oscillation Longitudinal Cooling Time Improvement Factor p. 75

Table 4.5 -- S. Mtingwa's Calculated x-x' Emittance Diffusion Rate Matrix p. 78

Table 4.6 -- x-x' Emittance Growth Rate Matrix Using Formula 4.20 p. 78

Table 4.7 -- S. Mtingwa's Calculated Longitudinal Diffusion Rate Matrix p. 79

Table 4.8 -- Longitudinal Growth Rate Matrix Using Formula 4.21 p. 79

Table 4.9 -- Code Parameters Used in Cooling Time Calculation Including IBS p. 82

Table 4.10 -- Results of Cooling Time Calculation Including IBS -- First Method p. 83

Table of Tables -- Continued

Table 4.11 -- Results of Cooling Time Calculation Including IBS -- Second Method p. 84

Table 5.1 -- Electron Beam Transverse Velocity Increase Due to Space Charge Expansion of the Beam p. 88

Table 5.2 -- Electron Beam Transverse Velocity Due to Emittance Alone p. 88

Table 5.3 -- The Transverse Electron Cooling Force as a Function of the Transverse Antiproton Velocity p. 92

Table 5.4 -- The Longitudinal Electron Cooling Force as a Function of the Longitudinal Antiproton Velocity p. 93

Table 5.5 -- Ratio of Transverse Cooling Force Including Electron Temperature to the Ideal Cooling Force p. 95

Table 5.6 -- Ratio of Longitudinal Cooling Force Including Electron Temperature to the Ideal Cooling Force p. 95

Table 5.7 -- Input Parameters for Calculating Electron Cooling Rates p. 99

Table 5.8 -- Ideal Electron Cooling Rates -- Electron Beam Radius = 6mm p. 99

Table 5.9 -- Intrabeam Scattering Longitudinal Heating Rates p. 99

Table 5.10 -- Intrabeam Scattering Transverse Heating Rates p. 100

Chapter One -- Introduction.

1A -- Overview

Electron cooling was originally proposed by Budker in 1966[1.1]. The basis for his proposal came from work done by Spitzer[1.2] (1956) who showed that warm ions come to an equilibrium with cooler electrons in a plasma. Due to the much larger mass of the ion, the final rms speed of the ions is much less than that of the electrons. Electron cooling experiments to date have been done at low energies -- electron energies less than 200 keV.

The purpose of the intermediate energy electron cooling project is to increase the phase space density of antiprotons for use in proton-antiproton colliders. Antiprotons are produced by bombarding a high Z material with protons. Increasing the incident energy of the protons results in much higher antiproton yields, but it also increases the resulting antiproton momenta. In order to collect the antiprotons the correct mixture of cooling techniques must be used. Stochastic cooling works best on beams with high emittance and low density, while electron cooling is most advantageous on low emittance beams and, in the region of parameters considered, is independent of the number of particles in the beam.

The present design for the Fermilab antiproton source uses stochastic cooling (originally proposed by Van der Meer[1.3]) in conjunction with R-F stacking to obtain the antiproton density required to operate the collider. Each new antiproton bunch is placed in the accumulator ring at an energy higher than that of the antiprotons already in the ring. R-F deceleration brings the antiprotons to the stack top where the stochastic cooling system pushes them into the stack core, increasing the density of the antiprotons and making room for the next bunch.

There are two stochastic cooling systems, one at the stack top (or tail) where the antiproton density is low and one for the stack core where the antiproton density is high. Two systems are needed since the gain of the feedback system should be proportional to the inverse of the antiproton density for optimum operation of the system. The noise of the tail system destroys the beam at the core if only one system is used. Sacherer[1,4] has shown that use of filters alone provokes instability. Stochastic cooling works well enough for accumulation of antiprotons in the intermediate energy range, but leads to final phase space densities which are lower than desired.

To match the antiproton velocity in the Fermilab accumulator ring an electron beam energy of 4.5 MeV is required. Construction of infrared Free Electron Lasers (FELs) also require low emittance electron beams of this energy. University of California-Santa Barbara researchers Luis Elias and Gerry Ramian were working on such an FEL at the time the intermediate energy electron cooling effort began. As a first step in the project a collaborative effort was formed between the electron cooling group at the UW and the FEL team from UCSB to measure the emittance of a two ampere electron beam from a 3MV Pelletron accelerator. The value obtained indicated no substantial increase in emittance above the thermal limit -- thus the device was ideally suited for electron cooling. The UCSB group decided to do FEL research using a pulsed electrostatic accelerator. Since electron cooling required a DC device, the collaboration ended after the emittance measurement.

This work begins with a review of electron cooling projects done to date, followed by a brief look at the parameters of intermediate energy electron cooling.

The high current beams used in this project require numerical treatments that incorporate the effect of space charge in the analysis. The program EGUN (written by Herrmannsfeldt) is used to simulate the electron gun operation. A Hamiltonian treatment is applied to the electrostatic accelerator optics that includes space charge, emittance and acceleration. A complete optics study of the system is presented, including designs of the gun, collector, and

solenoids. The collector design is similar to the successful FNAL model (which obtained recirculation of 99.99%). The electron gun design is an optical match to the one used by the UCSB group. The terminal electronics and beam line components of the system are designed by the National Electrostatics Corporation, originator and manufacturer of Pelletron accelerators.

The operation of the system as an electron cooler is simulated by doing a detailed study of the cooling force. Electron temperature, betatron oscillations and intrabeam scattering are included in determining the expected cooling time. The resulting prediction is that the antiproton beam should cool in 30 minutes. Equilibrium with intrabeam scattering is estimated, with an anticipated increase in the antiproton beam phase space density of about 5×10^3. The expected equilibrium emittances are a final $\Delta p/p$ of the antiproton beam of 1×10^{-5}, and transverse emittances of 0.12π mm-mr. (The final equilibrium obtainable with stochastic cooling is estimated to be a longitudinal emittance of 3×10^{-4} and a transverse emittance of 2π mm-mr.) The topic of instabilities is touched on briefly. Some instabilities will have to be overcome in order to reach the emittances made possible by electron cooling. The appendix contains the FORTRAN codes used in the analysis.

1B -- Review of Electron Cooling Experiments

The Early Experiments

NAP-M Electron cooling experiments were first carried out on the storage ring NAP-M at Novosibirsk in the Soviet Union[1.5]. NAP-M storage ring parameters are presented in Table 1.1, while Table 1.2 shows electron beam parameters. Tests were made on beams with small energy and momentum spread. No effects were observed when the relative velocity spread between the two beams was greater than 2×10^{-2}, however, within this range the main results obtained were the following:

i) betatron oscillation damping;

ii) existence of an equilibrium dimension for a proton beam;

iii) energy spread reduction and acceleration caused by the electron beam;

iv) a substantial increase of the proton beam lifetime.

A summary of typical experimental parameters and results is given in Table 1.3.

ICE Electron cooling was next demonstrated in Europe at CERN in the ICE ring[1.6]. The objective of this experiment was to cool a beam of much larger phase space than that in the NAP-M experiment, such as a secondary antiproton beam. This was to test the feasibility of a high luminosity $\bar{p}p$ collider. The parameters and results of this experiment are summarized in Tables 1.4 and 1.5.

FNAL The Fermilab electron cooling experiment[1.7] was the last of the major laboratory tests of electron cooling. This experiment cooled protons at a higher energy than that used in the other experiments and also experimented with the process of stacking hot protons during the cooling process. The nominal operating parameters for the system are presented in Table 1.6, while experimental results are shown in Table 1.7.

Table 1.1 -- Main Parameters of the NAP-M Storage Ring

Proton Energy	Up to 150 MeV
Injection Energy	1.5 MeV
Straight-section Length	7.1 m
Cooling Section Aperture	±5 cm
Betatron Wave Numbers	1.24, 1.34
Transition Energy	110 MeV
Acceleration Cycle Duration	30 sec
Average Pressure	5×10^{-10} Torr

Table 1.2 -- Parameters of the Novosibirsk Electron-Beam Device

Cooling Section Length	1 m
Electron Energy	Up to 100 keV
Electron Current	Up to 1 A
Electron Angular spread	2×10^{-3}
Longitudinal Magnetic Field	1 kg

Table 1.3 -- Typical Experimental Parameters and Results of NAP-M

Proton Energy	35-80 MeV
Electron Energy	19-43.6 keV
Electron Beam Diameter	10 mm
Electron Current	0.1-0.25 A
Proton Current	20-100 μA
Average Pressure	5×10^{-10} Torr
At an Energy of 65 MeV	
Equilibrium Proton Beam Dimensions	0.8 mm
Cooling Time (at Electron Current = 0.1 A)	5 sec
Lifetime With Cooling	5000 sec
Lifetime Without Cooling	900 sec
Effective Electron Temperature	0.2 eV
Neutral Hydrogen Flux	17 ±2 $A^{-1}A^{-1}sec^{-1}$

Table 1.4 -- Parameters of CERN's ICE Experiments

Proton Beam Energy	46.2 MeV
Initial $\Delta p/p$	2.5×10^{-3}
Emittances $\varepsilon_h, \varepsilon_v$	60,30 π mm-mr
Intensity of Proton Beam	3×10^{8}
Electron Beam High Voltage	25.9 kV
Electron Beam Current	1.3 A
Solenoidal Magnetic Field	500 G

Table 1.5 -- Results of CERN's ICE Experiments

Momentum Cooling Time	300-400 ms
Betatron Cooling Time	1.2 s
Average Pressure	2×10^{-9}Torr
Lifetime of Cooled Beam	140 min
Lifetime Gain Factor	40
Equilibrium Proton Momentum Spread	4×10^{-5}
Equilibrium Proton Beam Cross Section	0.5 mm
Neutral Beam Rate	650 H^0/s

Table 1.6 -- Parameters of FNAL's Electron Cooling Experiment

Proton Energy	200 MeV
Effective Ring Radius	21.56 m
Betatron Frequencies ν_h, ν_v	5.57.3.57
Transverse Ring Acceptance $\varepsilon_h, \varepsilon_v$	40,20 π mm-mr
Electron Cathode Potential	-111 kV
Electron Current	1-3 A
Electron Interaction Length	5 m
Electron Beam Radius	2.5 cm
Solenoidal Guide Field	0.93 kg
Cooling Region Vacuum	1×10^{-8} Torr

Table 1.7 -- Results of FNAL's Electron Cooling Experiment

Momentum Cooling Time	2 s
Betatron Cooling Time	5-10 s
Average Pressure	1×10^{-10}Torr
Lifetime of Cooled beam	4000 s
Lifetime Gain Factor	400
Equilibrium Proton Momentum Spread	1×10^{-4}

Experiments Planned for the Near Future

The LEAR Electron Cooler -- An electron cooler for LEAR is being pursued as a collaboration between CERN and KfK Karlsruhe. This will be a unique device in the aspect that it will cool antiprotons. The goals of the project are: i) to compliment stochastic cooling at low energies; ii) to allow internal target operation at low energies; iii) to improve understanding of the cooling process; and iv) to exploit that knowledge for physics experiments.

The Indiana Cooler -- Electron cooling will be a part of the Indiana synchrotron at some time in the near future. The scheduled startup date for the electron cooler is late 1986. Cooling of a wide variety of ions is planned. The cooling will be very important during internal target operation.

TARN II -- Beam cooling studies are one of the scheduled physics tests at the TARN II ring at INS -- Tokyo.

European Coolers -- It is not possible to include a review of all of the cooling projects for Europe because of the fast growing number of proposals. Table 1.8 shows a partial list of the proposed experiments.

Table 1.8 -- European Electron Cooling Projects

What	Where
LEAR -- ELENA	CERN
CELSIUS	Uppsala, Sweden
ESR	GSI, Dormstadt, Germany
HICE	Heidelberg MPI for Nuclear Physics
COSY	KFA, Julich, Germany

1C -- Parameters of Intermediate Energy Electron Cooling

Electron cooling works due to the simple principle of thermodynamic equilibrium. In the rest frame of the electrons the temperature of the electron gas is on the order of one tenth of an electron volt, while the temperature of the ion (or antiproton) gas is orders of magnitude higher. If the electron beam is constantly collected and regenerated the equilibrium temperature will be the temperature of the electron beam. The rate at which this process goes to equilibrium is characterized by what is traditionally called a friction force. A derivation of this term and the corresponding energy loss per unit time will now be presented using the assumption that the electron beam is perfectly cold. A more complete treatment of the problem will be presented later.

Friction Force -- The electron cooling friction force arises from the energy lost by the antiprotons as they pass through the electron cloud. As can be found in Jackson[1.8],

$$\vec{F} = \frac{dE}{dx}\hat{v} = \frac{4\pi n e^4 \Lambda \vec{v}}{m_e v^3}, \text{ where } \Lambda = \log(b_{max}/b_{min}) \approx 15 \ . \tag{1.1}$$

Energy Loss per Unit Time -- The energy loss per unit time will be evaluated in the moving frame first and then relativistically transformed to the lab frame. (The moving frame is defined to be the rest frame of the electron beam.) Defining η to be the fraction of the time the force acts on the (anti)protons the force in the moving frame is

$$\frac{dE}{dx}\hat{v} = \frac{4\pi n e^4 \Lambda \eta}{m_e} \cdot \frac{\vec{v}}{v^3} \ . \tag{1.2}$$

This yields an energy loss per unit time of

$$\frac{dE}{dt} = \frac{dE}{dx}\,\hat{v}\cdot\vec{v} = \frac{4\pi n e^4 \Lambda\eta}{m_e v}$$

$$= -\frac{4\pi n r_e^2 m_e c^4 \Lambda\eta}{v} \; . \qquad (1.3)$$

Estimate of the Cooling Time Using a Four Ampere Electron Beam -- The velocity of the antiprotons in the rest frame of the electrons will be shown to be primarily determined by the transverse velocity $\beta_\perp = \gamma\theta_\perp = 6.2\times10^{-3}$. The electron density is

$$n = \frac{I}{\gamma\pi r^2 \beta c e} . \qquad (1.4)$$

With $I = 4A$, $r = 6$ mm, $\Lambda = 15$, $\eta = .02$, and $\gamma = 10$,

$$\frac{dE}{dt} = 55\text{eV/s (in the electron rest frame)} \; . \qquad (1.5)$$

The energy of the antiprotons in the electron rest frame is $0.5 m_p v^2 = 18$ keV. A crude estimate of the cooling time is then

$$\tau = \frac{18{,}000\text{eV}}{55(\text{eV/s})} = 327 \text{ s} \; . \qquad (1.6)$$

Since this calculation was done in the moving frame, the cooling time will be 3270 s in the lab frame (time dilation). This rough

calculation of the cooling time demonstrates that intermediate energy electron cooling is quite promising.

Relativistic Scaling of the Problem -- Summary -- The process of electron cooling is scaled by a factor of γ^2 from relativistic effects. One factor of γ comes from electron density depletion due to length contraction, while the other comes from time dilation. Other factors of γ enter the cooling force equation through the Lorentz transformation of the antiproton velocity, but these come from the fact that adiabatic damping decreases the transverse beam emittance, and represent no actual gain in the cooling time.

Diffusion Times for the Antiproton Velocity Due to Finite Electron Beam Temperature -- As the antiproton beam passes through the finite temperature electron cloud it is subjected to diffusion as well cooling. The equations for the diffusion and slowing down of a particle beam in a plasma are found in the NRL Plasma Formulary. (Originally derived by Spitzer[1,2].)

$$\text{slowing down} -- \frac{d\vec{v}}{dt} = -\nu_s \vec{v} \tag{1.7}$$

$$\text{transverse diffusion} -- \frac{d}{dt}(\vec{v} - \langle\vec{v}\rangle)_\perp^2 = \nu_\perp v^2 \tag{1.8}$$

$$\text{parallel diffusion} -- \frac{d}{dt}(\vec{v} - \langle\vec{v}\rangle)_\parallel^2 = \nu_\parallel v^2 \tag{1.9}$$

For the case of intermediate energy electron cooling the initial antiproton mean velocity (in the moving system) is much larger than the electron mean velocity (in the moving system) and the following expressions are valid.

$$\frac{\nu_s}{n_e\lambda} = 1.7\times10^{-4}\times\varepsilon^{-3/2} \tag{1.10}$$

$$\frac{\nu_\perp}{n_e\lambda} = 1.8\times10^{-7}\times\varepsilon^{-3/2} \tag{1.11}$$

$$\frac{\nu_\parallel}{n_e\lambda} = 1.7\times10^{-4}\times T\varepsilon^{-5/2} \tag{1.12}$$

In the above formulas ε is the energy of the antiprotons in eV, T is the average energy of the electron beam in eV, n_e is the density of the electron beam in cm^{-3}, and λ is the Coulomb log (15). Substituting in the numbers the scaling times are: $\tau_s = 13$ s; $\tau_\perp = 1.20\times10^4$ s; and $\tau_\parallel = 2.30\times10^6$ s. All of these times have been evaluated in the moving frame. Transforming to the lab frame requires multiplication by gamma and $1/\eta$. Thus the cooling time in the lab frame is $13\times10\times50 = 6500$ s, well within an order of magnitude of the result obtained above. The diffusion times are so large that they do not affect the analysis until the antiproton velocity distribution is within the electron velocity distribution. This result is not surprising, we know where the diffusion due to electron beam temperature is equal to the cooling -- at thermal equilibrium.

Chapter Two -- Use of an Electrostatic Accelerator as an Electron Beam Source

2A -- Emittance Measurement

Note -- This section is a reproduction of a paper[2.1] presented at the 1981 Particle Accelerator Conference. (A few improvements have been made.)

Introduction -- As shown at FNAL, electron cooling of protons is a very efficient way to reach high luminosity in a proton beam.[2.2] The emittance of the 120 KeV electron beam used at Fermilab corresponds to a cathode temperature of 0.1 eV. In order to apply cooling techniques to GeV proton beams, MeV electron energies are required. In this section, the results of an emittance measurement on a 3-MV Pelletron electron accelerator are presented. The experiment shows that the emittance scales to a value appropriate for electron cooling. (The machine tested was jointly owned and operated by the University of California-Santa Barbara and National Electrostatics Corporation for research into free-electron lasers, which also require low emittance beams for operation.)

Thermal Emittance Estimate -- The thermal emittance ε of the beam is defined to be the area in phase space in which 90% of the beam trajectories lie. The only contribution to the perpendicular velocity of the particles is assumed to be the perpendicular thermal velocity of the electrons as they are emitted from the cathode. The area of the phase space ellipse is then

$$\varepsilon = \pi x_{max} \Theta_{90} \cdot \qquad (2.1)$$

In evaluating ε, it is assumed that the cathode emits electrons uniformly over its surface. Thus x_{max} is the radius of the cathode. In this case $x_{max} = 7.6\times10^{-3}$m. The quantity Θ_{90} is defined to be the angle with respect to the beam axis that contains 90% of the electron trajectory angles.

$$\Theta_{90} = P_\perp/P_{11} = MV_{\perp 90}/\gamma MC\beta \qquad (2.2)$$

$V_{\perp 90}$ is evaluated by assuming a one-dimensional Maxwell distribution with a cathode temperature of kT = 0.1eV. This yields $\varepsilon = 1.8\pi$mm-mrad for $\gamma = 5$ and $\varepsilon = 1.5\pi$ mm-mrad for $\gamma = 6$ as the estimates of thermal emittance.

(The evaluation goes as follows: For a Maxwellian velocity distribution the number of particles with velocity in the range between zero and any arbitrary velocity v_1 is:

$$\frac{N_1}{N} = \int_0^v \frac{4}{\pi^{1/2}}\frac{1}{v_m^3}\, v^2 \exp\left(-\frac{v^2}{v_m^2}\right) dv$$

where $v_m = (2kT/m)^{1/2}$.

Evaluating the above expression for $\frac{N_1}{N} = .9$ requires $v = 2v_m$, or $V_{\perp 90} = 2(.2/511{,}000)^{1/2}c = 3.75\times10^5$. So, using Eq. (2.2), $\theta_{90} = 2.08\times10^{-4}$ for $\gamma = 6$, and thus the thermal estimate for ε at $\gamma = 6$ is $\pi\theta_{90}x_{max} = \varepsilon = 1.58\pi$ mm-mr.)

<u>The Emittance-Measurement Method -- Theory</u> -- The radius of a beam of emittance area $\pi\varepsilon$ is $r = \sqrt{\beta_L\varepsilon}$ where β_L is one of the Twiss parameters[2.3] α_L, β_L and γ_L which satisfy the equations

$$\alpha_L' = K\beta_L,\ \beta_L' = -2\alpha_L,\ \gamma_L = (1+\alpha_L^2)/\beta_L\ . \qquad (2.3)$$

In Eqs. (2.3) the prime denotes differentiation with respect to distance in the beam direction and $K = B'/B\rho$ is determined by the transverse gradient of the magnetic field. Space charge adds defocusing in both transverse directions and can be represented for a circular uniform beam by an additional term

$$K_{S.C.} = 2I/I_0(\beta\gamma)^3\beta_L\varepsilon \text{ with } I_0 = MC^3/e = 17000\text{A}. \qquad (2.4)$$

The equations for the Twiss parameters can now be numerically integrated to give the beam radius as a function of distance, given the initial values of α_L, β_L and ε. This treatment then includes the effects of space charge and thermal velocity (emittance). Measurements of beam radius at several positions, including a waist, gives a unique value of the emittance. Calculations indicate that measurements downstream from the waist yield the initial values α_L and β_L and that given these initial values ε varies linearly with the radius of the waist.

Beam-Size Measurements -- Current flowing from the terminal of the Pelletron causes the terminal voltage to decrease, which in turn causes the particle energy to decrease during the pulse. In the constant magnetic field of a dipole, this decrease in energy causes the beam to sweep upward during the current pulse. This sweep acts as though it is swept from a single pivot point.

We can determine an effective length L for the distance from the exit edge of the dipole to the pivot point for the sweep. The equation of motion in the bending plane for a particle of momentum $p+\Delta p$ in a dipole of bending radius ρ is

$$x''+w^2x = \rho(\delta p/p). \qquad (2.5)$$

A solution for this differential equation, with $x' = x = 0$ at $\Theta = 0$, is

$$x = \frac{\rho}{w^2}\frac{\Delta p}{p}(1-\cos w\Theta) \ . \qquad (2.6)$$

Hence $x' = dx/ds = dx/d(\rho\Theta) = (\Delta p/pw)\sin w\Theta$. Therefore, since $x' = x/L$, $L = x'/x = \frac{\rho}{w}\frac{(1-\cos w\Theta)}{\sin w\Theta}$. For our dipole $\rho = 24.1$cm, $w = \sqrt{1-0.44}$, $\Theta = \pi/2$, so $L = 21.5$cm.

Multiple wires located parallel to each other were installed at several locations downstream from the dipole. (Figure 2.1 shows a diagram of the wire chamber installed). The electrical signals picked up as the beam crossed the wires were observed on an oscilloscope and photographed.

The beam was successively focused on each set of wires by adjusting a quadrupole in the beamline. This produced sharp signals from which a sweep rate could be calculated. The effective distances from the pivot point to the three wire sets were $r_1 = 39.5$cm, $r_2 = 79.5$cm and $r_3 = 109.5$cm. (See Figure 2.1). The distance between the two wires at r_2 was 3.0cm, while the distance between the wire at r_3 and its support frame was 4.5cm. (The beam hitting this support frame also generated an electrical signal.) Thus the angle the beam sweeps out between the two wires at r_2 was $\Delta\Theta_1 = 3.77\times10^{-2}$rad. Similarly the angular sweep made at r_3 was $\Delta\Theta_2 = 4.11\times10^{-2}$rad. (Sweep rates were obtained by dividing the appropriate angular separation by the time between pulses ΔT.)

To measure beam blow up from a waist, the quadrupole field strength was set near zero so that a waist was formed at r_1. (The expected temperature rise of the 25μ carbon filament was ~400C.) The quadrupole was then left at this setting for measurements at r_1, r_2 and r_3.

The "angular size" of the beam is $\Psi = \Delta\tau\cdot\overline{\Delta\Theta/\Delta T}$ where $\Delta\tau$ is the time duration of the beam hitting the wire and $\overline{\Delta\Theta/\Delta T}$ is the average measured sweep rate. The beam radius is then $R(r_i) = \frac{1}{2}r_i\Psi_i$ where r_i is the distance from the pivot point to the ith wire set. $(i = 1,2,3)$.

Table 2.1 -- Experimental Results -- Sweep Rates at $\gamma = 5$

	$\Delta T(\mu sec)$	$\Delta\Theta/\Delta T(rad/\mu sec)$	Scope trace shown in
r_2	19	1.98×10^{-3}	Figure 2.2
r_3	21.5	1.91×10^{-3}	Figure 2.3

These data yield an average sweep rate of $\overline{\Delta\Theta/\Delta T} = 1.95 \times 10^{-3} rad/\mu sec$.

Table 2.2 -- Experimental Results -- Beam Size at $\gamma = 5$

	$\Delta\tau(\mu sec)$	R(mm)	Scope trace shown in
r_1	0.7	0.27	Figure 2.4
r_2	10	7.75	Figure 2.5
r_3	13	13.9	Figure 2.6

Table 2.3 -- Experimental Results -- Sweep Rates at $\gamma = 6$

	$\Delta T(\mu sec)$	$\Delta\Theta/\Delta T(rad\ 1\mu sec)$	Scope trace shown in
r_2	12.5	3.01×10^{-3}	Figure 2.7
r_3	14	2.94×10^{-3}	Figure 2.8

These data indicate an average sweep rate of $\overline{\Delta\Theta/\Delta T} = 2.97 \times 19^{-3} rad/\mu sec$.

Table 2.4 -- Experimental Results -- Beam Size at $\gamma = 6$

	$\Delta\tau(\mu sec)$	R(mm)	Scope trace shown in
r_1	0.5	0.29	Figure 2.9
r_2	5	5.9	Figure 2.10
r_3	6	9.8	Figure 2.11

Electron beam current readings were taken by using a Faraday cup as a beam dump. Secondaries were suppressed by a 300 V battery. The voltage drop across a one ohm resistor was displayed on an

oscilloscope and photographed. Figure 2.12 displays the scope trace corresponding to the beam current of 0.8 A measured at $\gamma = 5$, while Figure 2.13 shows the scope trace corresponding to the current of 1.35 A at $\gamma = 6$.

Computer Simulation to Determine Emittance -- The computer code TRAN2 is used to calculate the growth of a beam from a waist including the effects of space charge and emittance. (The source code TRAN2 is presented in Appendix 1.) The emittance assumed for the beam is varied to get a best fit to the data. The calculated results are presented in Figure 2.14 for $\gamma = 5$, and in Figure 2.15 for $\gamma = 6$. The data points (shown with their respective errors) are included in the figures. The best fit to the data indicates that the emittance of the FEL test device is 5.3π mm-mr at $\gamma = 5$ and 4π mm-mr at $\gamma = 6$. This measurement indicates an emittance growth of about a factor of three at $\gamma = 5$ and slightly less than 3 at $\gamma = 6$. The better beam behavior at higher energy may be a result of the fact that all beam optics designs assumed $\gamma = 7$.

Error Analysis -- The major source of error in the data analysis is in reading the scope traces. Scope traces are readable to about one-half of one division. There is thus a relative error in scope trace readings of about half of a division divided by 15 divisions for the sweep rates or a 3.5% error in this value and a relative error in the wire pulse readings of about 25% (0.5/2) for the waist pulse readings. Thus the relative error is about 30% for the waist size. Since the beam emittance used in calculations is linearly dependent on the waist radius, the relative error in the emittance measurement is estimated at 30%.

Conclusion -- The emittance of the beam at $\gamma = 5$ is 5.3±1.6mm-mrad and at $\gamma = 6$ is 4.0±1.2mm-mrad. This implies an emittance growth of about a factor of three between cathode and measurement. The beam quality is adequate for electron cooling. (At the time of publication analysis showed no emittance growth from the

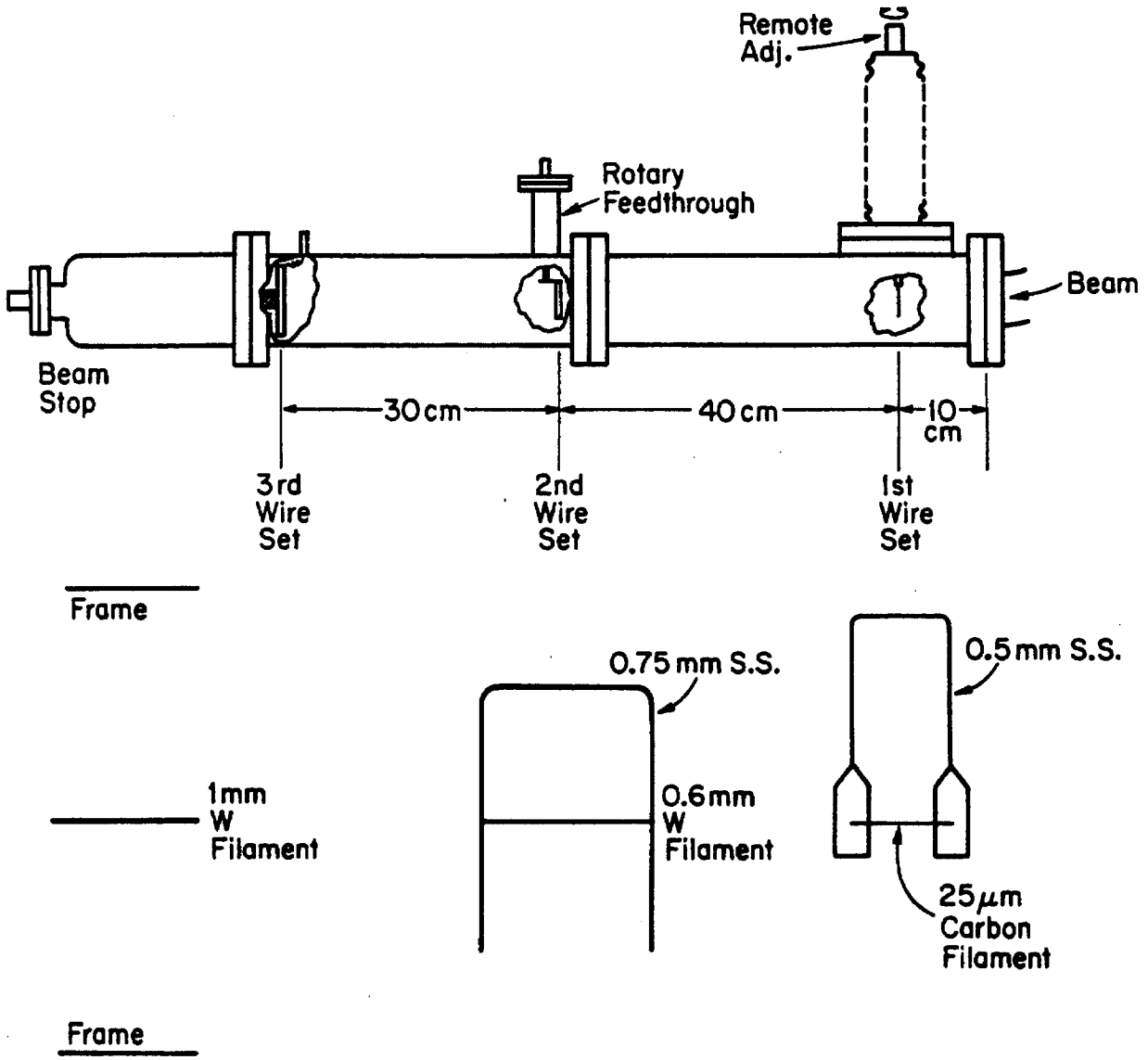

Figure 2.1 -- Emittance Measurement Device

cathode, subsequent investigation determined that there was emittance growth.)

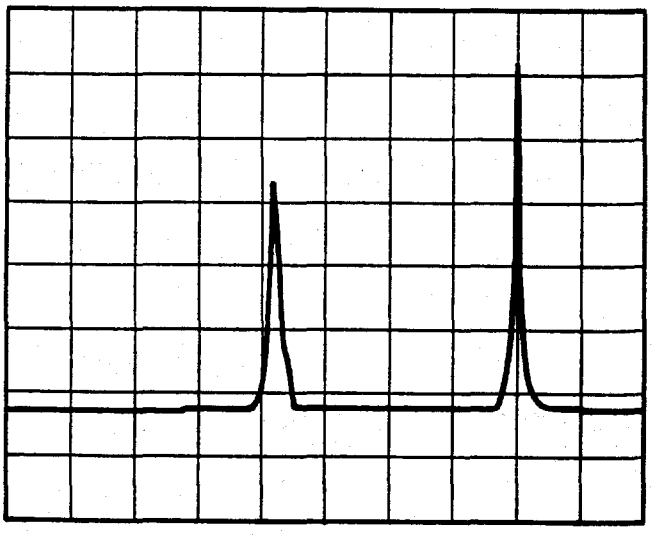

Figure 2.2 -- Scope trace. $\gamma = 5$, second wire set -- sweep rate. Vertical Scale 1 Volt/division, Horizontal Scale 5 μseconds/division.

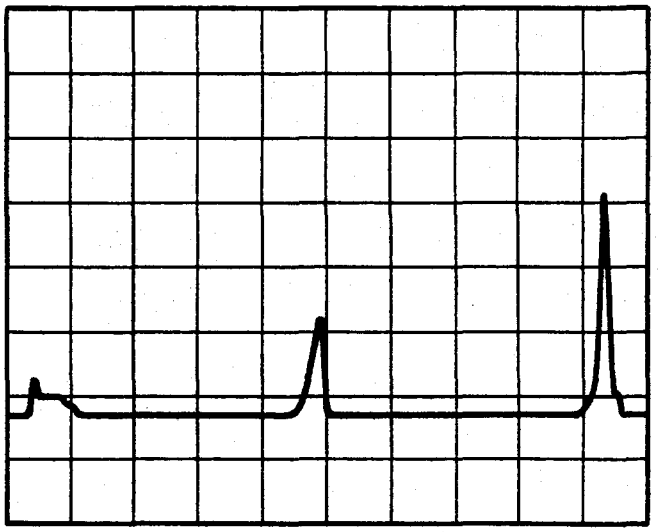

Figure 2.3 -- Scope trace. $\gamma = 5$, third wire and frame -- sweep rate. Vertical Scale 5 Volts/division, Horizontal Scale 5 μseconds/division.

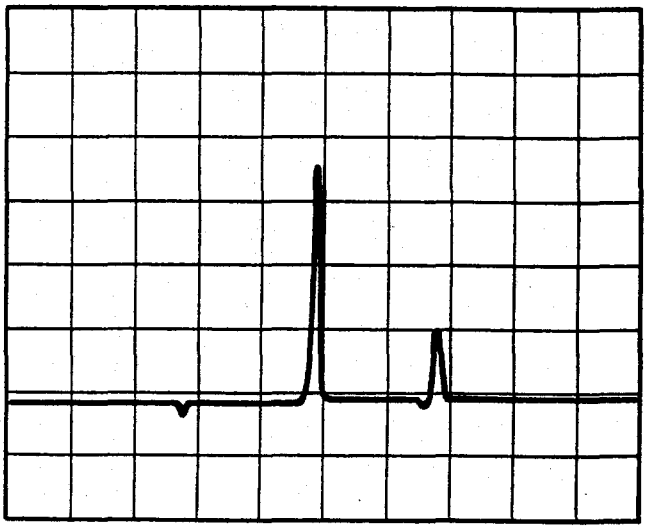

Figure 2.4 -- Scope trace. $\gamma = 5$, single carbon wire. Vertical Scale 50 mV/division, Horizontal Scale 2 μseconds/division.

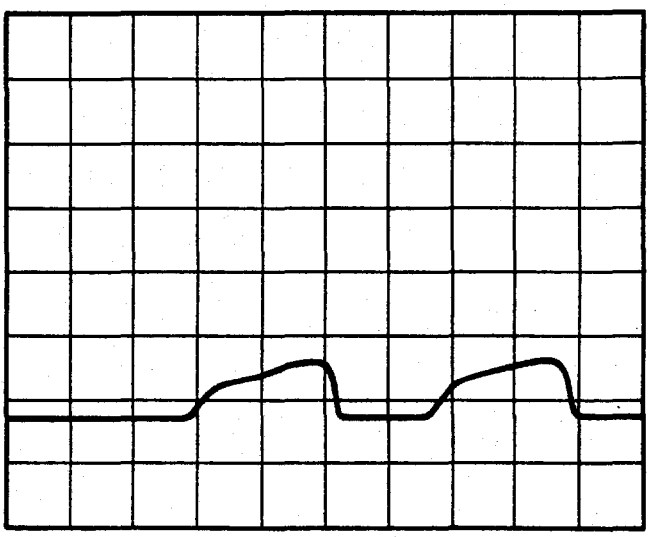

Figure 2.5 -- Scope trace. $\gamma = 5$, second wire set. Vertical Scale 1 Volt/division, Horizontal Scale 5 μseconds/division.

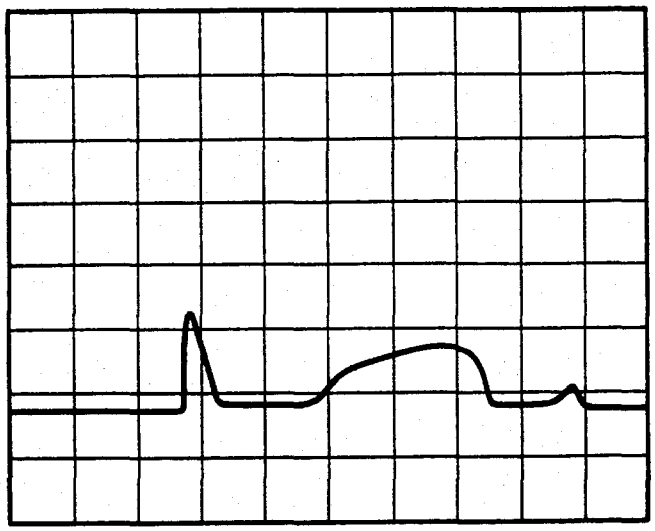

Figure 2.6 -- Scope trace. γ = 5, third wire. Vertical Scale 1 Volt/division, Horizontal Scale 5 μseconds/division.

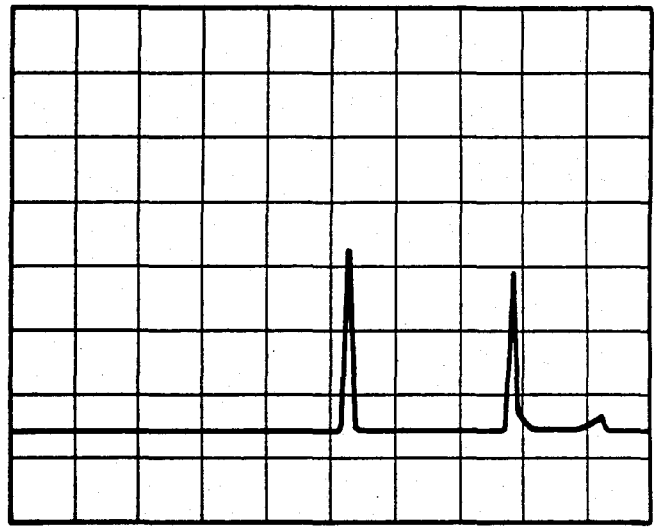

Figure 2.7 -- Scope trace. γ = 6, second wire set -- sweep rate. Vertical Scale 5 Volts/division, Horizontal Scale 5 μseconds/division.

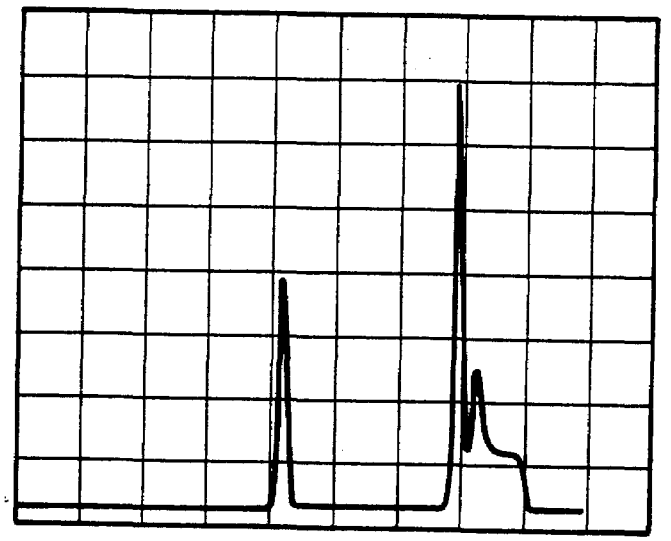

Figure 2.8 -- Scope trace. $\gamma = 6$, third wire and frame -- sweep rate. Vertical Scale 5 Volts/division, Horizontal Scale 5 μseconds/division.

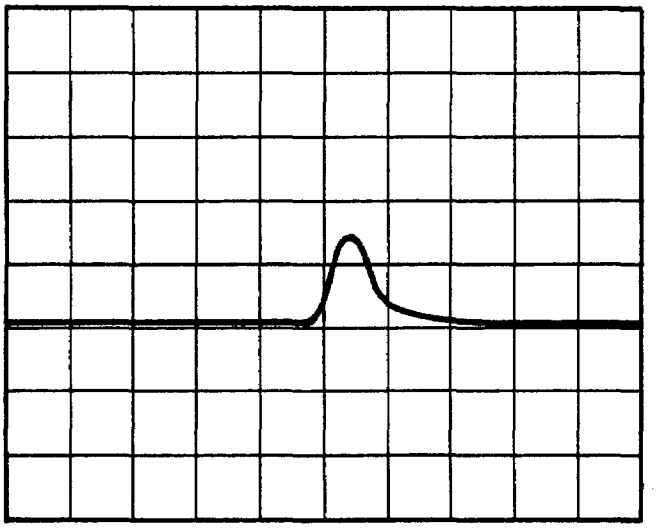

Figure 2.9 -- Scope trace. $\gamma = 6$, single carbon wire. Vertical Scale 0.1 Volts/division, Horizontal Scale 0.2 μseconds/division.

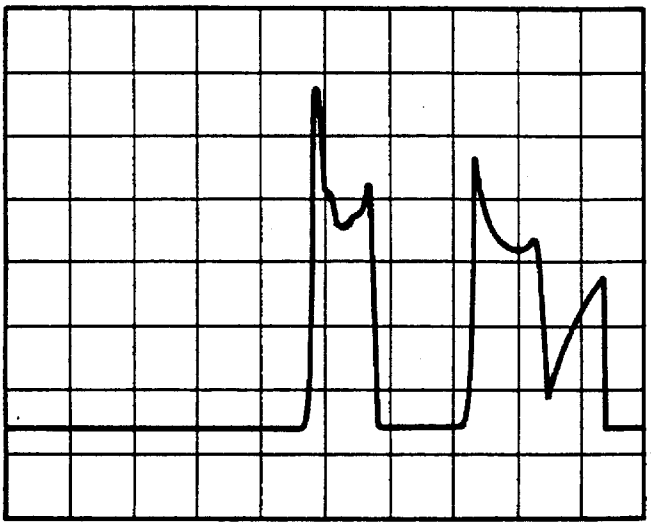

Figure 2.10 -- Scope trace. $\gamma = 6$, second wire set. Vertical Scale 5 Volts/division, Horizontal Scale 5 μseconds/division.

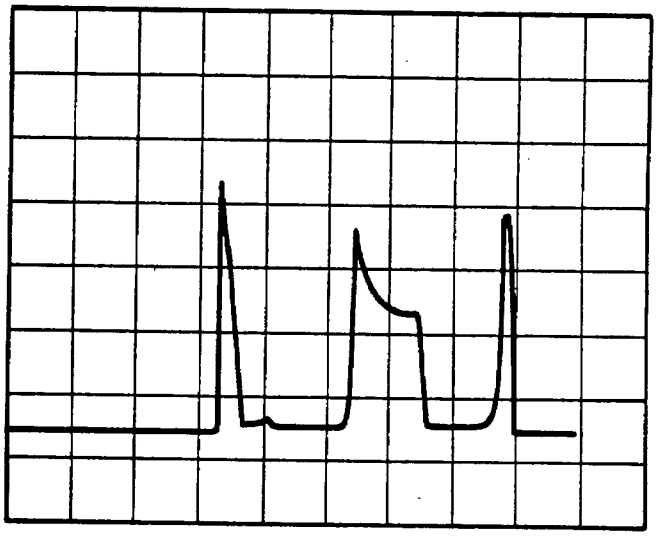

Figure 2.11 -- Scope trace. $\gamma = 6$, third wire and frame. Vertical Scale 1 Volt/division, Horizontal Scale 5 μseconds/division.

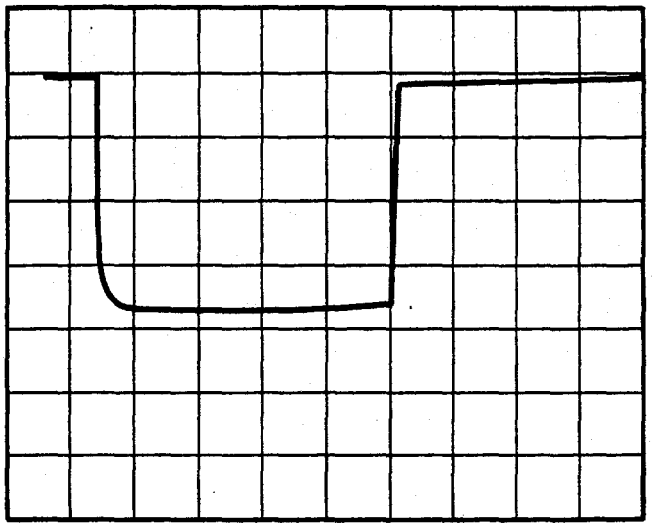

Figure 2.12 -- Scope trace. $\gamma = 5$, Faraday Cup. Vertical Scale 0.2 Volts/division, Horizontal Scale 5 μseconds/division.

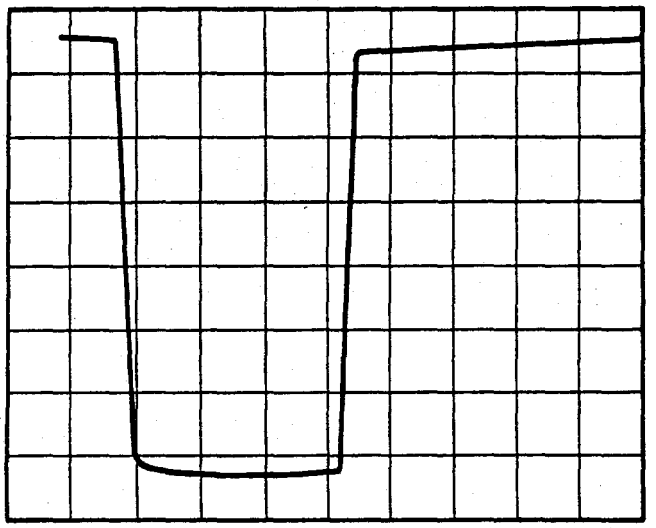

Figure 2.13 -- Scope trace. $\gamma = 6$, Faraday Cup. Vertical Scale 0.2 Volts/division, Horizontal Scale 5 μseconds/division.

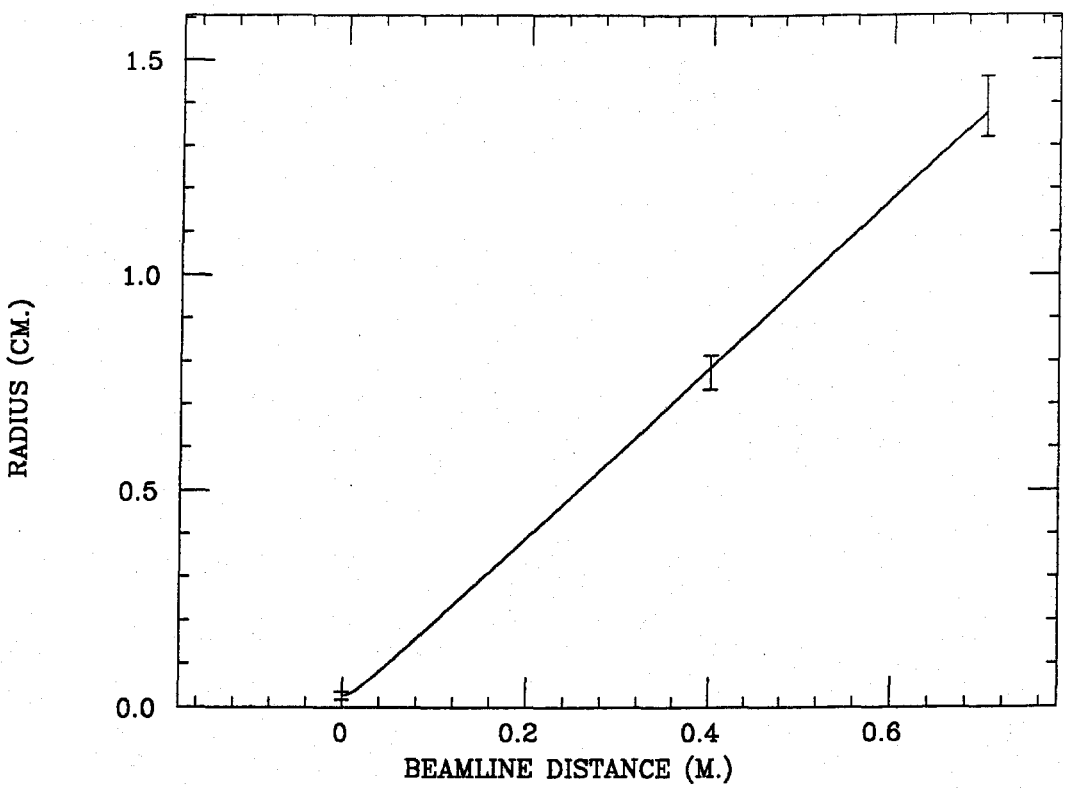

Figure 2.14 -- Emittance measurement at $\gamma = 5$. Experimental fit to data.

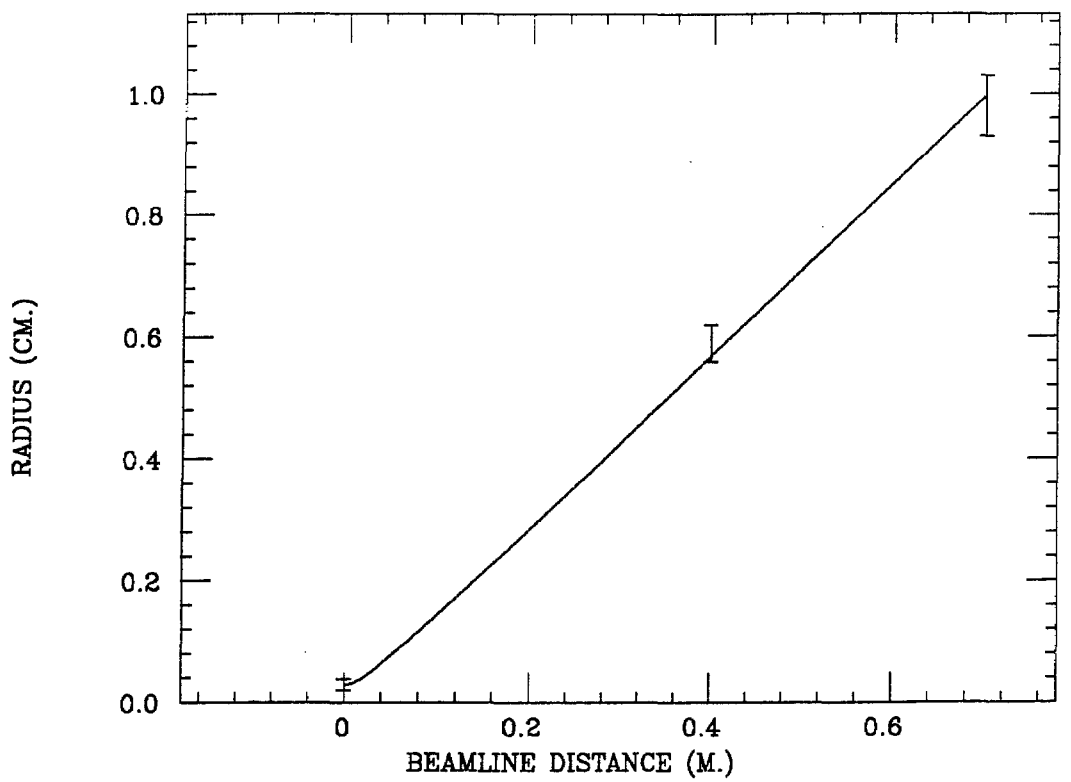

Figure 2.15 -- Emittance measurement at $\gamma = 6$. Experimental fit to data.

2B -- Collector and Gun Designs for the Pelletron

Introduction -- Since the charging capability of Pelletron accelerators is limited to about 500 microamps, operation in the ampere region requires highly efficient electron beam recovery. The collection of these nonmagnetized electron beams requires a highly efficient collector just above terminal potential as well as electron optics designed to keep the beam within apertures throughout the system.

Electron Gun Design -- The emittance measurement of the FEL test device indicated that there was little emittance growth throughout the system. For this reason the electron gun for the electron cooling effort has been designed to be optically identical to the UCSB gun. The original FEL gun was designed to be an optical match to the Pelletron by Bill Herrmannsfeldt of SLAC.

One major difference existed between the electron cooling effort and FEL operation, the electron cooler must operate DC, while the FEL was a pulsed device. Since the collector space charge neutralization region takes a time of about a second to respond the cathode must be made with the ability to slowly turn the current up. The design of the gun has a center spot and three concentric cathode rings, which can all be operated in both the thermal and space charge limited regimes. By turning on one ring after another the current can be ramped from one milliamp to 3.9 amperes.

The optics program used to investigate the gun behavior is EGUN written by Bill Herrmannsfeldt. This program uses the method of finite differences to numerically solve for the fields created by various potential surfaces, and then iteratively solves for the electron trajectories. Space charge of the electron beam is included in the problem, but as of yet the finite electron beam temperature is not. (Although EGUN allows this to be done.)

Due to the complicated electron optics problem at the start of the accelerating column, the first 120,000 volts of acceleration in the Pelletron is included in the gun optical study. From that point

on the electric field has no radial component and another optical treatment of the device is done. Two studies of the gun are presented. Figure 2.16 shows the electron trajectories calculated for a thermally limited current of 0.315 amperes, while Figure 2.17 shows the full space charge limited current of 3.962 amps as it is accelerated through the first 170,000 volts (the gun provides 50,000 volts of acceleration). These calculations were done with all cathodes heated, but due to the radial symmetry of both the space charge and emittance forces the calculations are valid for any cathode radius.

Collector Design -- The collector for the intermediate energy electron cooling effort is designed upon the principles which led to successful operation of the Fermilab Electron Cooling Experiment[2.4,2.5,2.6,2.7]. In that experiment electron beam recovery was found to be 99.99%. A schematic of the collector planned for this experiment is shown in Figure 2.18. Not shown in the figure is a solenoid just preceding the collector, which focuses the beam. The collector has a Pierce geometry which is used to decelerate the electrons to an energy of about 1 KeV without space charge blowup of the beam. After the final Pierce electrode the beam enters a solenoidal magnetic field region which is space charge neutralized by an ion cloud. The ion cloud is formed from ionization of the residual gas as the beam passes through this region. The ions are radially trapped by the solenoidal magnetic field, and longitudinally trapped by the electrostatic fields of the collector. After the beam leaves the solenoidal field it is accelerated to a collecting surface made of graphite brazed on copper. The fields which accelerate the beam to this surface suppress secondary electrons. Figure 2.19 shows an EGUN study done on the collector.

Ion and Electron Gyro-radii in the Solenoidal Field -- The formula for the gyro-radius of a particle in a magnetic field is given by the following equation.

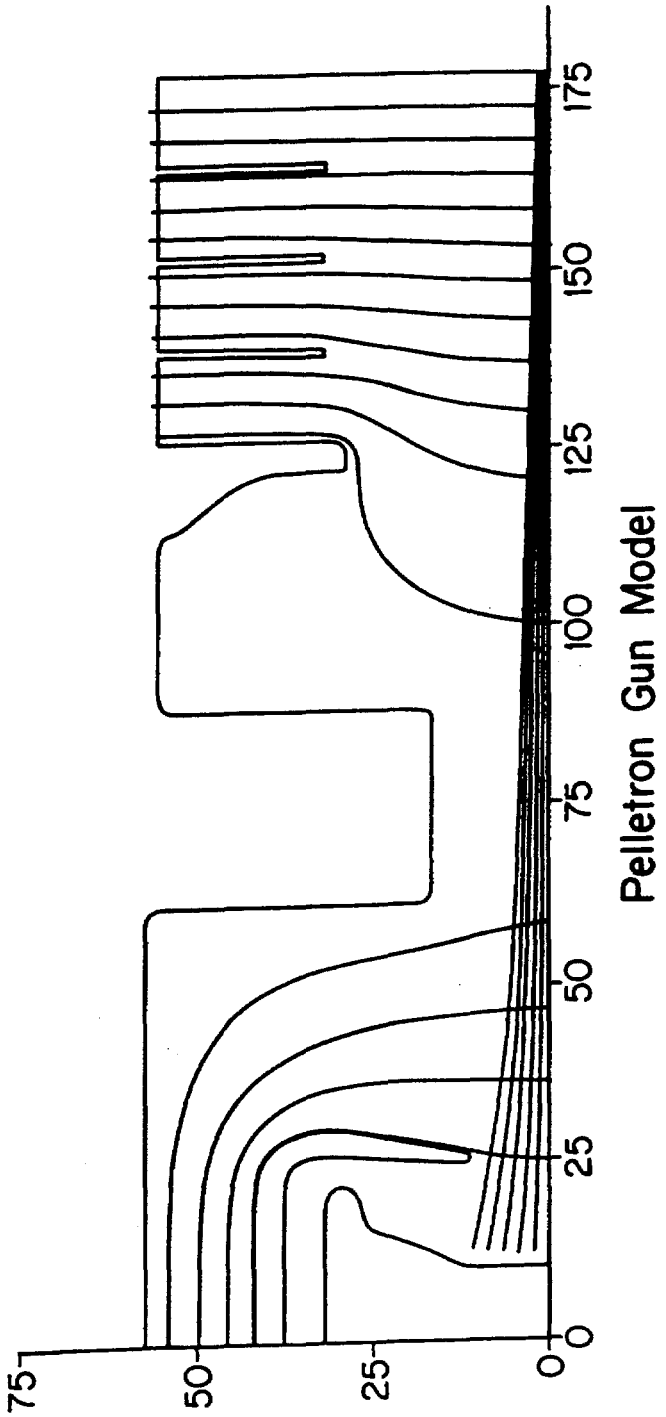

Figure 2.16 -- Electron gun trajectory simulation. Current = 0.315 A.

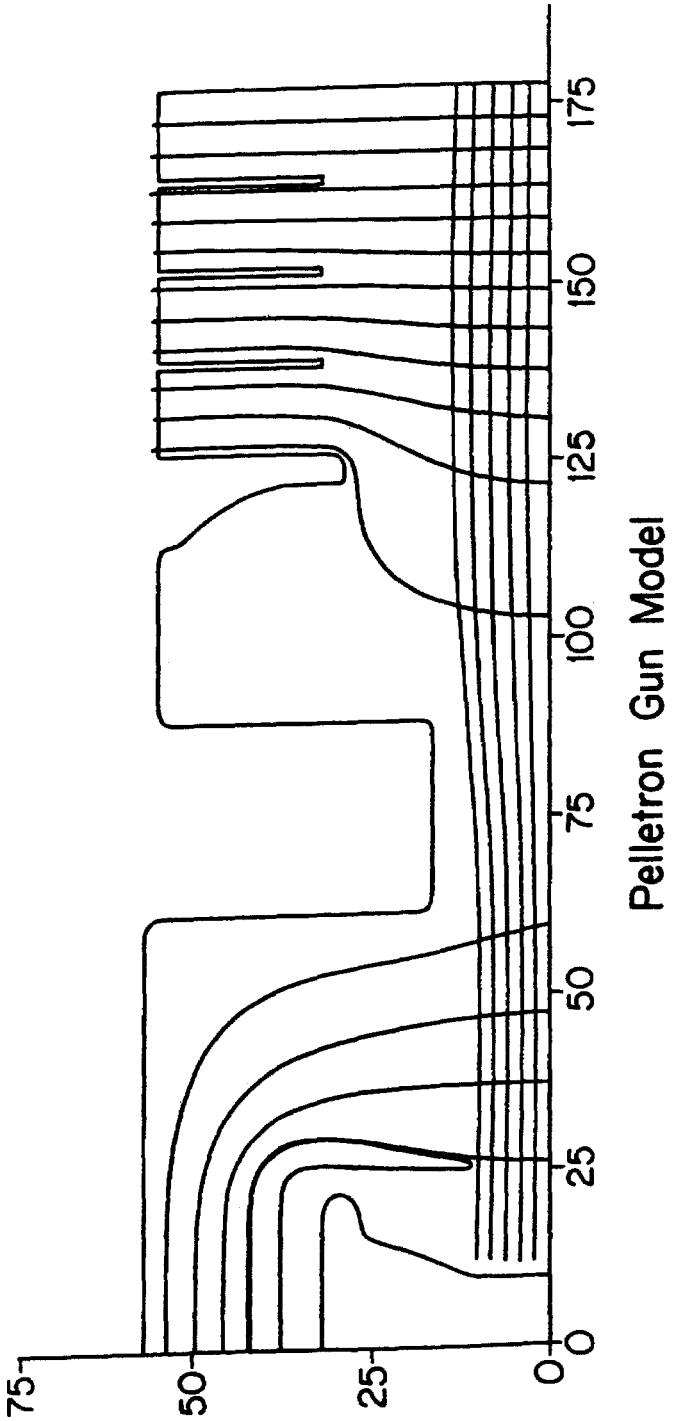

Figure 2.17 -- Electron gun trajectory simulation. Current = 3.962 A.

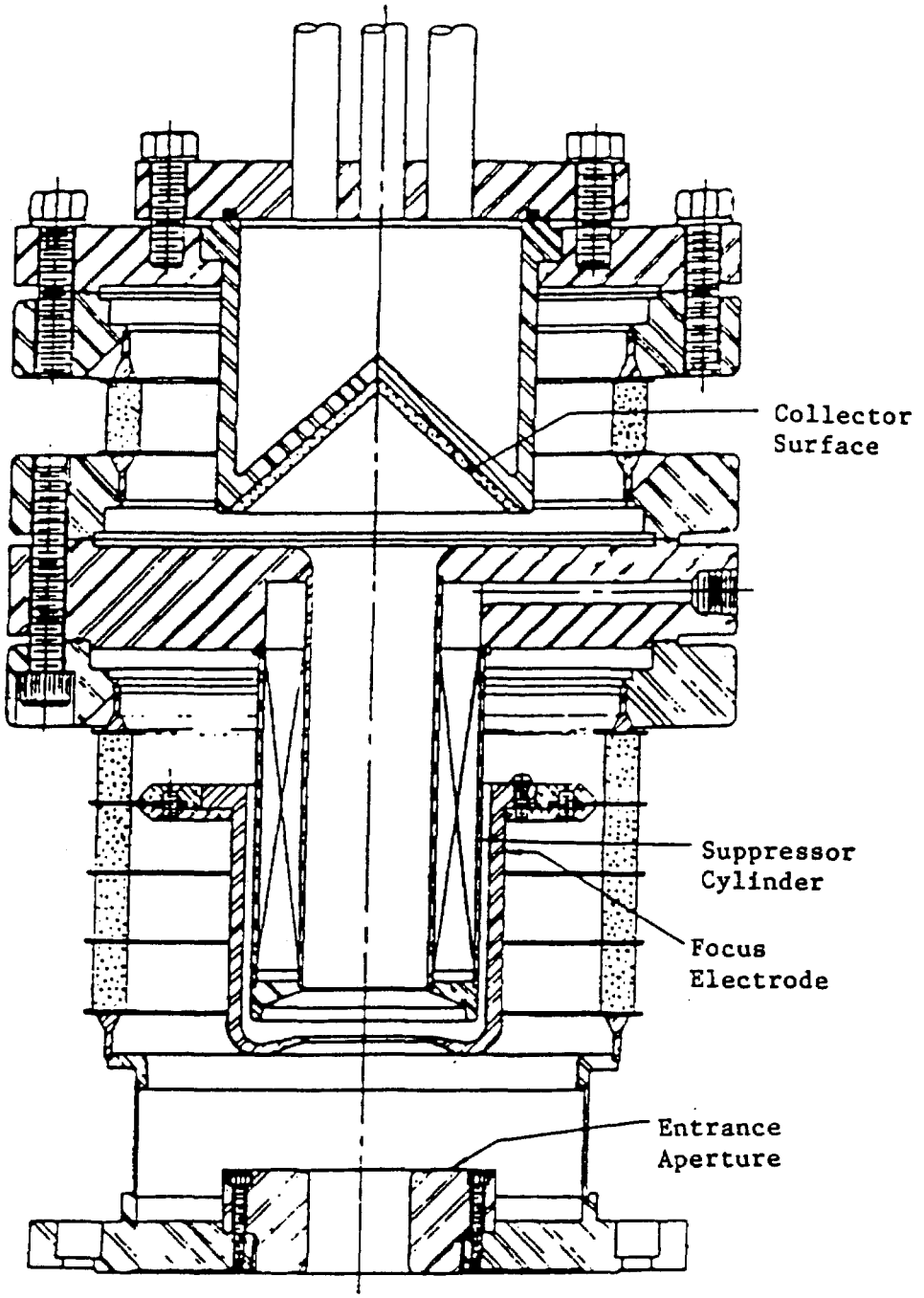

Figure 2.18 -- Schematic of electron beam collector.

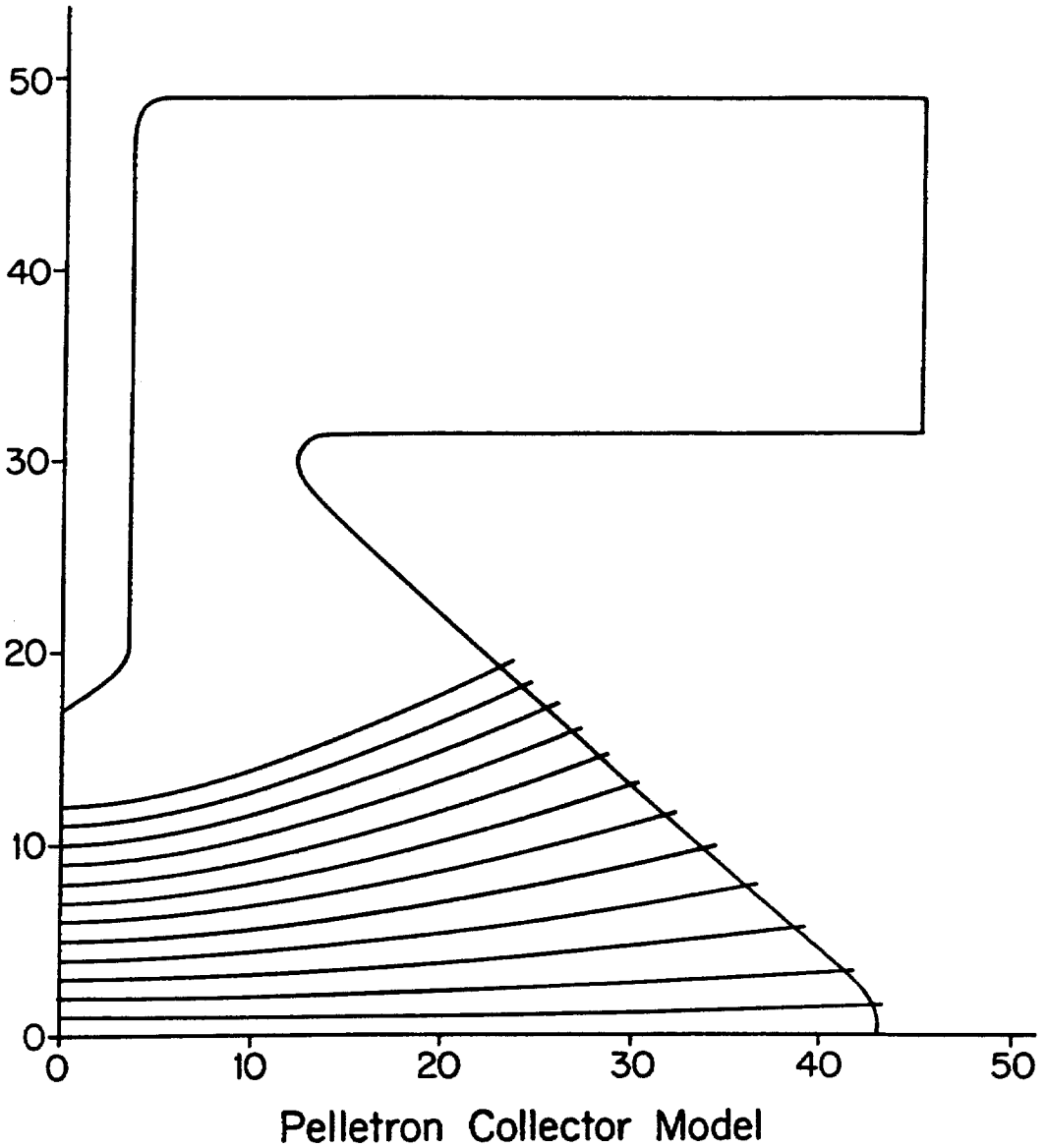

Figure 2.19 -- Electron collector trajectory simulation. Current = 3.962 A.

$$r_g = \frac{mv}{eB} \tag{2.7}$$

Values for the ion and electron gyro-radii are presented in Table 2.5. The electron gyro-radius varies strongly with the divergence of the electron beam prior to its entering the solenoidal region. For the values presented in Table 2.5 a beam divergence of 1% is assumed. (This is the electron gyro-radius of the electron at the extreme edge of the beam.)

Table 2.5 -- Ion and Electron Gyro-Radii

B(T)	r_{ion}(mm)	$r_{electron}$(mm)
.025	.289	.30
.015	.482	.50
.005	1.45	1.5

<u>Production Rate for Ion Cloud Formation</u> -- The rate for production of ions is given by the following equation.

$$R = \frac{n\ \sigma_i\ I}{\sigma_b} \tag{2.8}$$

In the above equation n is the number density of neutral hydrogen molecules in the collector due to residual gas, σ_i is the cross section for ionization of the gas, I is the electron beam current, and σ_b is the cross sectional area of the beam in the solenoidal region. Calculations for this design show that R = 2.11E-11 s^{-1}. This results in the time τ for complete space charge neutralization of $\tau = n_e/R = .8$ sec. This result is compatible with the experimentally obtained value in the Fermilab electron cooling experiment.

Effect of Solenoidal Field on Azimuthal Beam Momenta -- The electron beam will pick up azimuthal momentum as it enters the solenoidal field region of the collector -- Busch's Theorem. The amount of energy corresponding to that momentum is given in the following equation:

$$E_{az} = \frac{e^2 r^2 B^2}{2m} . \qquad (2.9)$$

Table 2.6 -- Azimuthal Energy of Outer Electrons (in eV)

r(m)	.012	.006	.003
B(T)			
.025	7910	1979	494
.015	2850	712	178
.005	316	79	20

The transverse electron beam energy in the solenoidal field can not exceed the energy of the beam as it enters that region or reflection of the beam will occur. In a bench test as well as in the first recirculation tests the collector parameters will be varied to determine optimum operating conditions.

2C -- Pelletron Optics Calculations

Note -- This section is a slight modification of a paper[2.8] presented at the 1985 Particle Accelerator Conference.

Introduction -- Because of the complicated problem of electron optics at the start of the Pelletron accelerating column, the first 120 kV of acceleration in the Pelletron is included in the gun optical study. At that point in the Pelletron, the electric field no longer has any significant radial component and the following optical treatment of the device is done.

Pelletron Optics -- The solution of the Pelletron optics is accomplished by the use of Hamiltonian mechanics combined with a treatment similar to that used by Courant, Livingston and Snyder in their classic treatment of strong-focusing synchrotrons[2.3]. Since the desired result is the beam radius as a function of distance z along the beamline, it is useful to use the coordinate z as the independent variable in the problem. The Hamiltonian, G, is then

$$G = -P_z c =$$

$$-([M_e c^2 + e\phi]^2 - P_r^2 c^2 - [M_e c^2]^2)^{1/2} + eA_z c \ . \qquad (2.10)$$

The space-charge electric potential ϕ can be calculated from Gauss' law; the potential at the beam edge is not a function of the size of the beam. The potential is thus given by the voltage of the Pelletron as

$$\phi = \phi_0 + E_0 z \ . \qquad (2.11)$$

The rate of change of the radial momentum with respect to the independent variable can be calculated from Hamilton's equations using the fact that A_z is much less than P_z.

$$\frac{dP_r c}{dz} = -\frac{\partial G}{\partial r} = \frac{M_e c^2 + e\phi}{P_z c} \cdot \frac{\partial}{\partial r}(e\phi) - e\frac{\partial}{\partial r}A_z c \ . \tag{2.12}$$

The partial derivative of the electrostatic potential is simply the radial electric field due to the space charge of the beam which for a beam of radius a is

$$\frac{\partial}{\partial r} e\phi = -eE_r = \frac{eIr}{2\pi\varepsilon_0 \beta c a^2} \ . \tag{2.13}$$

The last term of Eq. (2.12) is the azimuthal component of the magnetic field, which can be found from Amperes' law to be

$$\frac{\partial}{\partial r} eAc = -eB = \frac{eIr}{2\pi\varepsilon_0 c a^2} \ . \tag{2.14}$$

By noting that $\frac{M_e c^2 + e\phi}{P_z c} = \frac{1}{\beta_z}$, Eqs. (2.13) and (2.14) can be substituted into Eq. (2.12) to obtain a numerically integrable relation for P_r.

$$\Delta P_r c = \frac{eI\cdot(1-\beta_z^2)r}{2\pi\varepsilon_0 a^2 \beta^2 c}\cdot\Delta z = \frac{eIr}{2\pi\varepsilon_0 a^2 (\beta\gamma)^2 c}\cdot\Delta z \tag{2.15}$$

By updating the radial momentum with Eq. (2.15), it is possible to obtain the longitudinal momentum from Eqs. (2.15), (2.11), and (2.10).

Numerical integration shows that for space charge limited emission current density, the beam profile obtained is an adequate representation of the problem, but for low densities beam expansion due to beam emittance must be included. A differential equation for the radial coordinate along with equations for β and γ as functions of z can be derived. At $r = P_r = 0$ (neglecting transverse motion),

$$\gamma = \frac{eE_0 z}{M_e c^2} + 1 = \alpha z + 1 ,$$

$$\text{with } \alpha = \frac{eE_0}{M_e c^2} . \text{ Also,} \tag{2.16}$$

$$\beta = \left(1 - \frac{1}{(1 + \alpha z)^2}\right)^{1/2} .$$

The radial momentum can now be expressed as

$$P_r = \gamma m \beta r' c \tag{2.17}$$

where the primes denote derivatives with respect to z.

Eq. (2.17) can now be used with Eq. (2.15) to obtain a differential equation for r.

$$r'' + \frac{(\beta\gamma)'}{(\beta\gamma)}r' - \frac{K_0}{(\beta\gamma)^3}r = 0 \tag{2.18}$$

$$\left(K_0 = \frac{eI}{2\pi\varepsilon_0 a^2 mc^3}\right)$$

Now make a canonical transformation using the generating function

$$F_2 = f(z)P_x cr \ . \tag{2.19}$$

Applying this generating function to the Hamiltonian of Eq. (2.10), the conjugate coordinate and momentum pair and Hamiltonian are

$$G^* = G + f'P_x cr =$$

$$-\left[(H + e\phi)^2 - P_x{}^2 f^2 c^2 - (mc^2)^2\right]^{1/2} + eA_z c + \frac{f'P_x cx}{f}, \tag{2.20}$$

$$P_r = P_x f \ , \tag{2.21}$$

$$x = fr \ . \tag{2.22}$$

The equations of motion for the electrons in the new coordinates are

$$P_x{}'c = -\frac{\partial G^*}{\partial x} = \frac{mc^2 K_0 x}{(\beta\gamma)^2 f^2} - \frac{f'P_x c}{f}, \tag{2.23}$$

where K_0 is defined in Eq. (2.18), and

$$x' = \frac{\partial G^*}{\partial P_x c} = \frac{P_x f^2 c}{[(H + e\phi)^2 - P_x{}^2 f^2 c^2 - (mc^2)^2]^{1/2}} + \frac{f'x}{f} =$$

$$\frac{P_x f^2}{P_z} + \frac{f'x}{f} . \tag{2.24}$$

In the second of Eq. (2.24), we have neglected A_z compared with P_z in the denominator. Eqs. (2.23) and (2.24) can be combined to give

$$x'' = \frac{f''x}{f} + \frac{mc^2 K_0 x}{(\beta\gamma)^2 P_z c} + \frac{2f'fP_x}{P_z} - \frac{P_x P_z' f^2}{P_z{}^2} . \tag{2.25}$$

If f^2 is proportional to P_z, the last two terms in Eq. (2.25) cancel, leaving a differential equation for x with no first-derivative term. One obvious choice for the function f(z) is $f(z) = (\beta\gamma)^{1/2}$. By making this choice, Eq. (2.25) can be rewritten as

$$x'' + K(z)x = 0 . \tag{2.26}$$

Where $K(z) = -\frac{f''}{f} - \frac{K_0}{(\beta\gamma)^3}$

and $\frac{f''}{f} = -\frac{\alpha^2(\gamma^2 + 2)}{4(\beta\gamma)^4}$.

An analysis following the methods of Courant and Snyder[2.3] can now be made. The Twiss parameters of the beam obey the equations:

$$\alpha_L' = K\beta_L - \gamma_L,$$

$$\beta_L' = -2\alpha_L, \tag{2.27}$$

$$\gamma_L = (1+\alpha_L^2)/\beta_L \ .$$

Numerical integration of Eqs. (2.27) can now be done to determine the evolution of the function x, with $x = (\beta_L\varepsilon/\pi)^{1/2}$. Here ε is the Courant-Snyder invariant

$$\varepsilon = \frac{\pi}{\beta_L}(x^2 + (\alpha_L x + \beta_L x')^2) \ . \tag{2.28}$$

In this way the beam-envelope equation as a function of z can be obtained. The initial Twiss parameters for the numerical treatment are related to radius and divergence of the beam.

$$\beta_L = \frac{\pi x^2}{\varepsilon} = \frac{\pi\beta\gamma r^2}{\varepsilon} \tag{2.29a}$$

$$\alpha_L = -\frac{\pi x' x}{\varepsilon} = -\frac{\pi x}{\varepsilon}\times\left[(\beta\gamma)^{1/2} r' + \frac{\gamma\alpha r}{2(\beta\gamma)^{3/2}}\right] \tag{2.29b}$$

$$\gamma_L = \frac{1 + \alpha^2}{\beta} \tag{2.29c}$$

The initial value of the beam emittance is taken to be the thermal limit. Solenoidal focusing of the beam can be included in the program by changing the value of α. The divergence of the beam after passing through a focusing element of focal length f is given by:

$$r_2' = r_1' - \frac{r}{f} . \qquad (2.30)$$

Substituting the new value of r' into Eq. (2.29b) the updated value of α is obtained.

Once the beam leaves the Pelletron it is defocused by the change in the electric field. The focal length for this effect is 4V/E, where V is the beam energy and E is the electric field of the Pelletron.

The solution of the beam size as a function of position along the (non-accelerating) transport line is a numerical integration of Eqs. (2.27), with the difference that the equations now represent the variable r directly and $K(z) = K_0/(\beta\gamma)^3$.

The complete optics calculation for the Pelletron is shown in Figure 2.20 for a thermally limited current of 0.315 A. The space charge limited current of 3.962 A is shown in Figure 2.21. In each case the beam can be successfully recirculated. A schematic of the Pelletron set up used for the recirculation study is shown in Figure 2.22.

It can be seen Figures 2.20 and 2.21 that both the high-current and low-current beam envelopes are well within the two inch diameter aperture of the accelerating column. The beam envelopes also pass the periodic one inch diameter apertures of the Pelletron.

The is the end of the material contained in Reference 2.8.

The computer codes used to calculate the electron beam optics are presented in Appendix 2.

Solenoid Design -- The focal lengths of the solenoids needed for this system are determined by the Pelletron optics calculation just described. Figure 2.23 shows the electron optics obtained by assuming the angular convergence of the beam to be 50% more than the result of the EGUN study. Figure 2.24 assumes an input angular convergence of 50% less than the EGUN result. In each case it was determined that

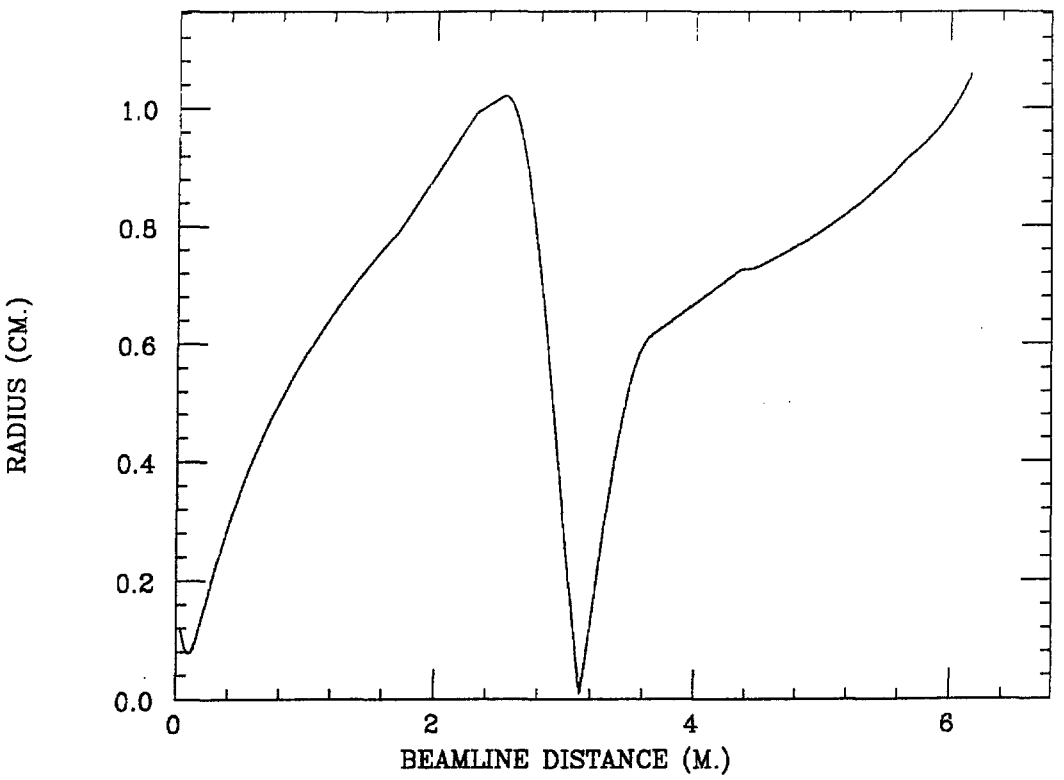

Figure 2.20 -- Pelletron electron optics simulation. Current = 0.315 A. (See Figure 2.22 for the beamline schematic.)

two 10 meter focal length solenoidal lenses at the one MeV level of the Pelletron and two five meter focal length lenses in the exterior beamline are sufficient to obtain recirculation.

The reference used for the design of these lenses was Septier[2.9], although any electron optics text would suffice. These solenoids are in the class of weakly converging lenses for which

$$\frac{f}{f_{1m}} = \frac{0.442}{(NI/NI_0)^2} \; . \qquad (2.31)$$

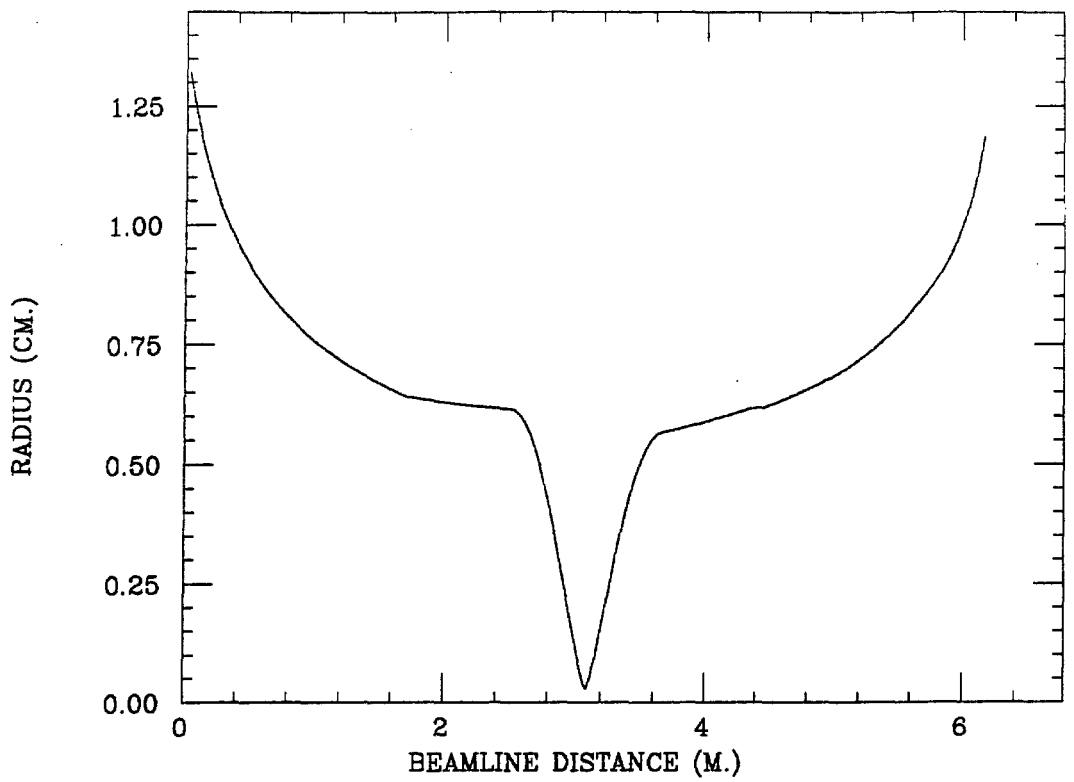

Figure 2.21 -- Pelletron electron optics simulation. Current = 3.962 A. (See Figure 2.22 for the beamline schematic.)

In Eq. (2.31) $f_{1m} = 0.5[s^2 + 0.45 \times D^2]^{1/2}$,

$NI_0 = 13.5(V^*)^{1/2}$, and

$$V^* = V\left(1 + \frac{eV}{2m_e c^2}\right) .$$

These expressions can now be solved for NI.

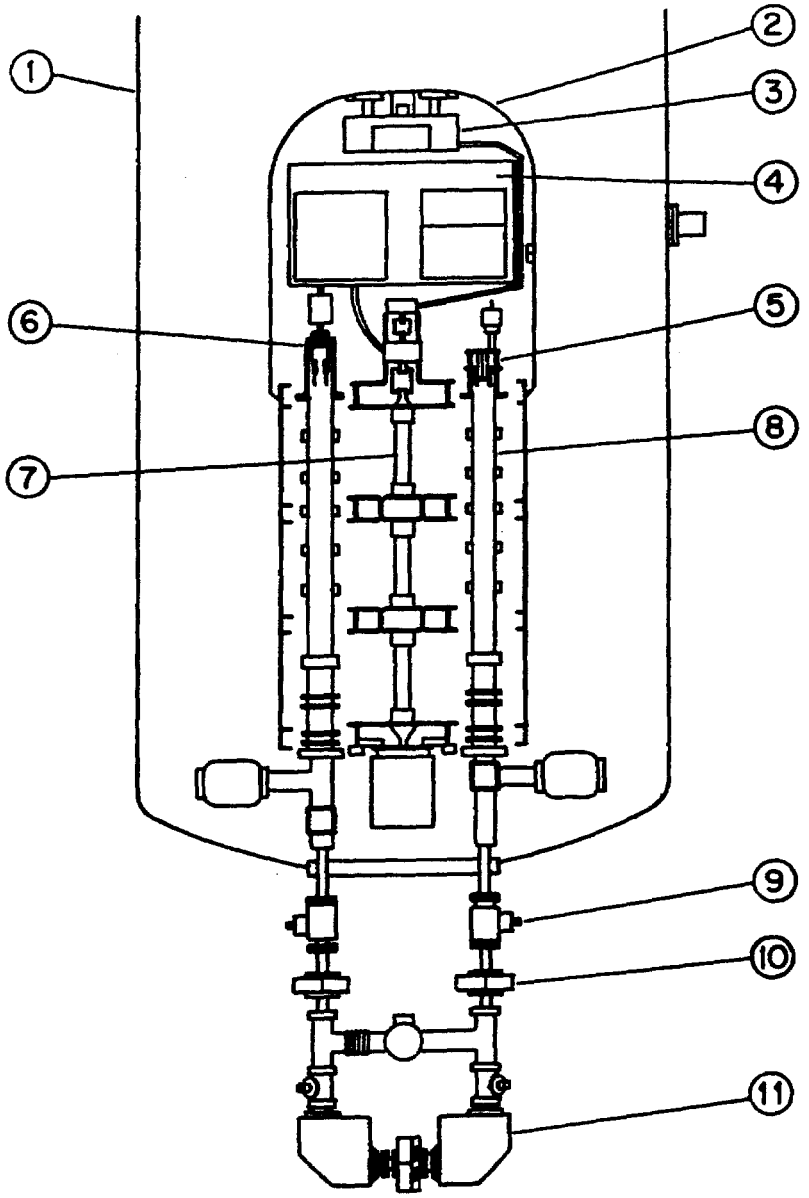

Figure 2.22 -- Schematic of the recirculation test set up: (1) Tank, (2) Terminal, (3) Terminal Potential Electronics, (4) Cathode Potential Electronics, (5) Electron Gun, (6) Collector, (7) Rotating Shaft, (8) Accelerating Tube, (9) Faraday Cup, (10) Quadrupole Singlet, (11) Bending Dipole.

$$NI = \left(\frac{40.3(S^2 + 0.45\ D^2)^{1/2}\ V\ (1 + \frac{eV}{2m_0c^2})}{f} \right)^{1/2} \qquad (2.32)$$

At the one MeV level of the machine we have an accelerating tube outside diameter (D) of 6.5 inches, and a possible solenoidal thickness (S) of two inches. With $V = 1.05\times10^6$ and $f = 10m \approx 380$ in. the solenoidal current must be 1040 A-turns. At 3MeV the beam pipe allows $D = S = 4$ in., with $V = 3.05\times10^6$ and $f = 190$ in. Eq. (2.32) requires a solenoidal current of 3,500 A-turns. The solenoidal designs are somewhat larger than these values.

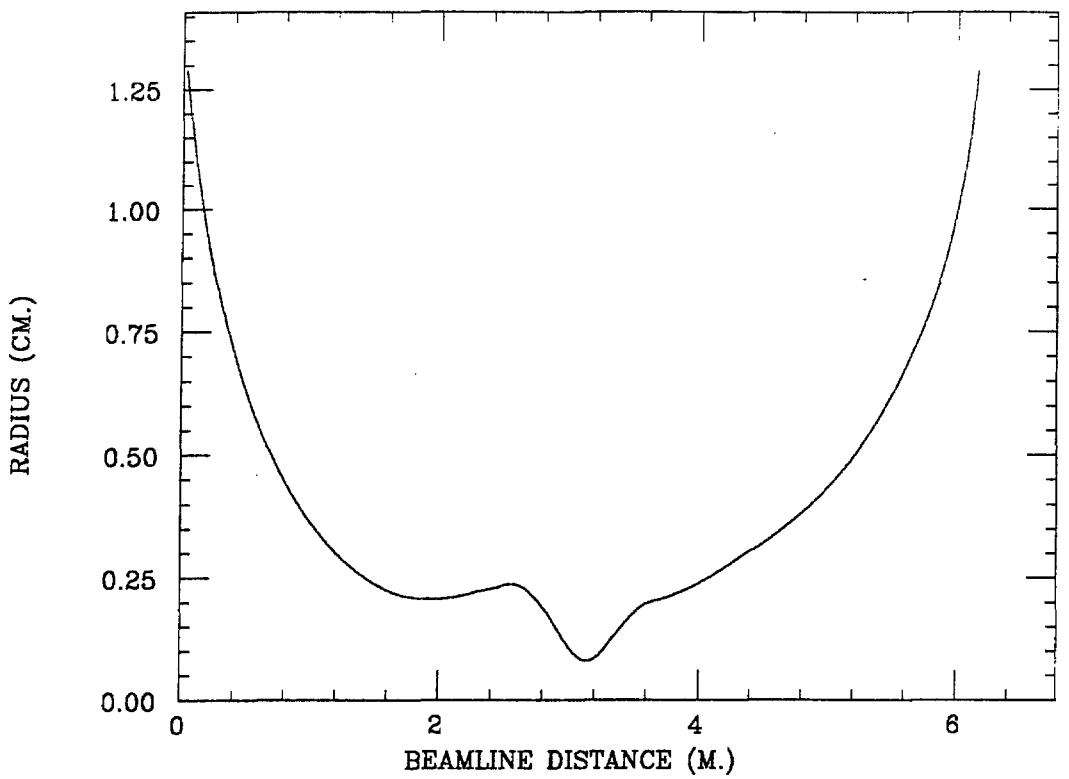

Figure 2.23 -- Pelletron electron optics simulation. Over-focused beam. (See Figure 2.22 for the beamline schematic.)

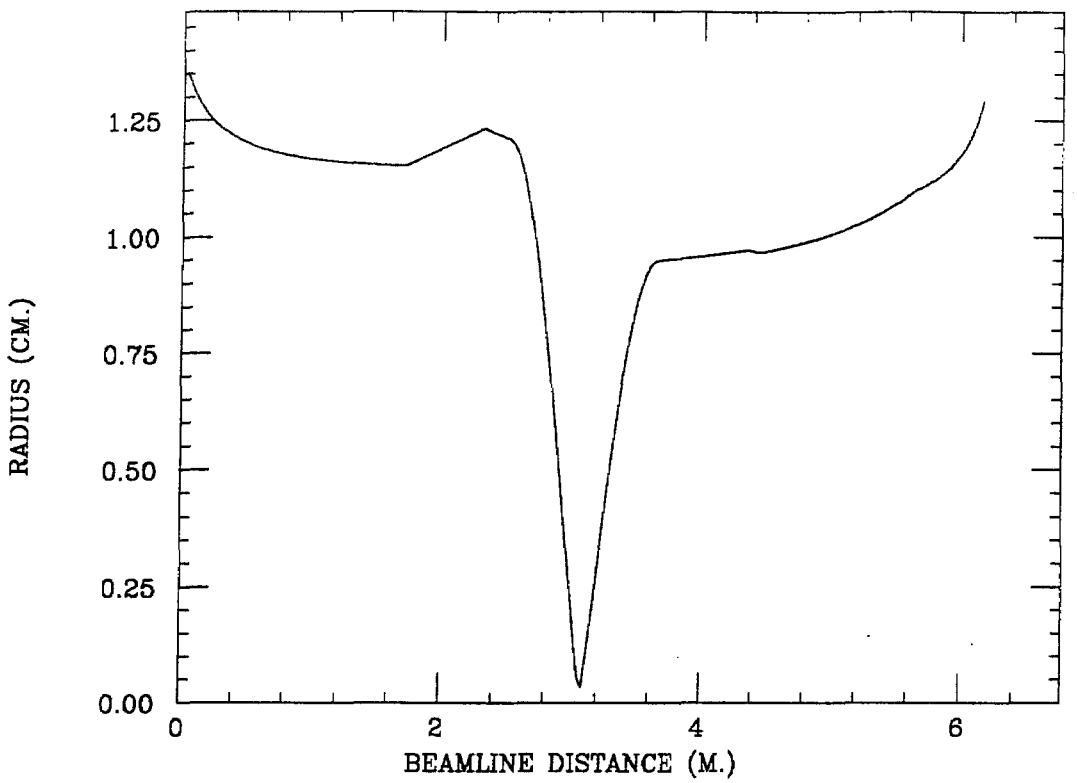

Figure 2.24 -- Pelletron electron optics simulation. Under-focused beam. (See Figure 2.22 for the beamline schematic.)

Chapter Three -- Intermediate Energy Electron Cooling for the Fermilab Antiproton Source

3A -- Antiproton Production and Stochastic Cooling

The intermediate energy electron cooler described in this document has been designed to be compatible with the Fermilab Tevatron's p-bar source. At this time it will be useful to review some of the design parameters and goals of the Tevatron.

The motivation for building the Tevatron comes from the fact that by providing a center of mass energy of two TeV the Tevatron will have the highest center of mass energy of any machine anywhere in the world up to the mid 1990's and will therefore provide enormous opportunities for exciting new physics.

As stated in the design report[3.1] there are three goals for the design of the Tevatron. After energy the most important parameter of any high energy machine is the luminosity, or interaction rate per unit cross section. The design goal for the Tevatron was set at $10^{30} cm^{-2} sec^{-1}$ which requires 1.8×10^{11} antiprotons of the appropriate phase space density. The second goal is to accumulate and cool the required number of antiprotons in five hours or less in order to minimize frustration of the users. The third goal of the design of the FNAL antiproton source is to provide for improvements in beam cooling as they come about. The four possibilities in this regard that have been left requisite aperture and straight section space are:

i) Momentum precooling in the debuncher.

ii) Improved stochastic cooling in the accumulator.

iii) Improved main ring extraction for antiproton production.

iv) Intermediate energy electron cooling in the accumulator.

The design chosen to achieve the goals is based on the method of stochastic cooling developed by Van der Meer et al.[3.2] The source has been designed to accumulate 4.3×10^{11} antiprotons in four hours, with 1.8×10^{11} antiprotons in the core being suitable for injection into the

collider. The remaining antiprotons will be used in subsequent cooling periods and the time for the next injection can be considerably shorter than the first.

The final density is more easily reached if the initial density is large. The only ways to increase the phase space density of the antiprotons produced are to decrease the spot size and time spread of the production. It has been determined that the smallest effective spot size is 0.38 mm, as any smaller beam will defocus within the length of the target. The protons are focused to this size by standard quadrupole magnetic lenses. At the exit of the target the antiproton divergence is too large for the acceptance of the beam transport system and thus requires strong focusing made possible by a lithium lens developed by the INP at Novosibirsk[3.3]. The time spread is minimized by rf manipulation just prior to targeting. Since the time spread of the antiprotons is small it is possible to increase the time spread while decreasing the momentum spread. This is done with the debuncher. The smaller momentum spread of the beam greatly simplifies the design of the magnets and cooling system of the accumulator.

Continuing with the introduction in the design report the sequence leading to colliding beams involves seven steps:

1) Proton Acceleration for Antiproton Production. Every two seconds 2×10^{12} protons are accelerated in one booster batch to 120 GeV.

2) Preparation of the Protons for Targeting. The rf voltage is decreased to allow the protons to spread to a time width of nine ns. Then the rf is suddenly stepped up to rotate the proton bunch to a time width of less than one ns. This in turn raises the energy spread to 0.4%. As soon as the bunch rotation is complete the protons leave the main ring at F17.

3) Antiproton Production and Transport. The short proton bunches hit a tungsten target and produce equally short bunches of antiprotons. A lithium lens then focuses this beam of 7×10^{7} 8.9 GeV antiprotons into the transport line which sends them into the

debuncher. At this point the beam has a momentum spread of 3% and transverse emittances of 20π mm-mr.

4) Bunch Rotation in the Debuncher. The bunch is now rotated 90 degrees in rf phase space in the debuncher and the rf voltage is stepped down to match the bunch height at that point. Following this the rf is adiabatically lowered to reduce the momentum spread to 0.2%.

5) Transverse Cooling in the Debuncher. In the debuncher the beam is stochastically cooled from 20π to 7π mm-mr in the two seconds it takes for the operation to begin again.

6) Antiproton Accumulation and Cooling. The antiprotons are injected into the accumulator from the debuncher. They are then rf stacked at the tail of the antiproton distribution already in the accumulator. The stack tail stochastic cooling system subjects these antiprotons to stochastic cooling forces which decay exponentially from the tail toward the core causing the density to increase. During the two seconds it takes for the next bunch to arrive the stochastic system moves most of the antiprotons out of the way.

The core stochastic cooling system builds up the core density to about 10^5 antiprotons per eV. Diffusion from the Schottky noise of the antiprotons and the thermal noise from the amplifiers cause particles to move to the low density regions of the stack. It is the core stochastic cooling system which is responsible for reducing the transverse emittances from 7π to 2π mm-mr.

7) Filling the Tevatron. The antiprotons are then injected into the Main Ring, accelerated to 150 GeV, and injected into the Tevatron. Protons are injected into the Tevatron from the main ring, and together the protons and antiprotons are accelerated in the Tevatron to 1 TeV.

The process of stochastic cooling has been simulated by Jim Simpson of Argonne National Lab.[3.4] His codes have been modified to be run on the UW Vax computers. Figure 3.1 shows the beam density as a function of time as the stochastic system operates in the accumulator. It is at the end of the stochastic cooling process that the beam will be subject to electron cooling in this analysis. The properties of

the beam upon completion of the stochastic cooling are summarized in the design report, and presented here in Table 3.1.

Table 3.1 -- Final Antiproton Stack Parameters
-- Stochastic Cooling Only

Number of Antiprotons	5×10^{11}
$\Delta p/p$	0.05%
Horizontal and Vertical Emittances	2π mm-mr
Peak Density	1×10^{5} eV^{-1}
Core Width (Gaussian part)	1.7 MeV (rms)
Total Stacking Time	5 Hours

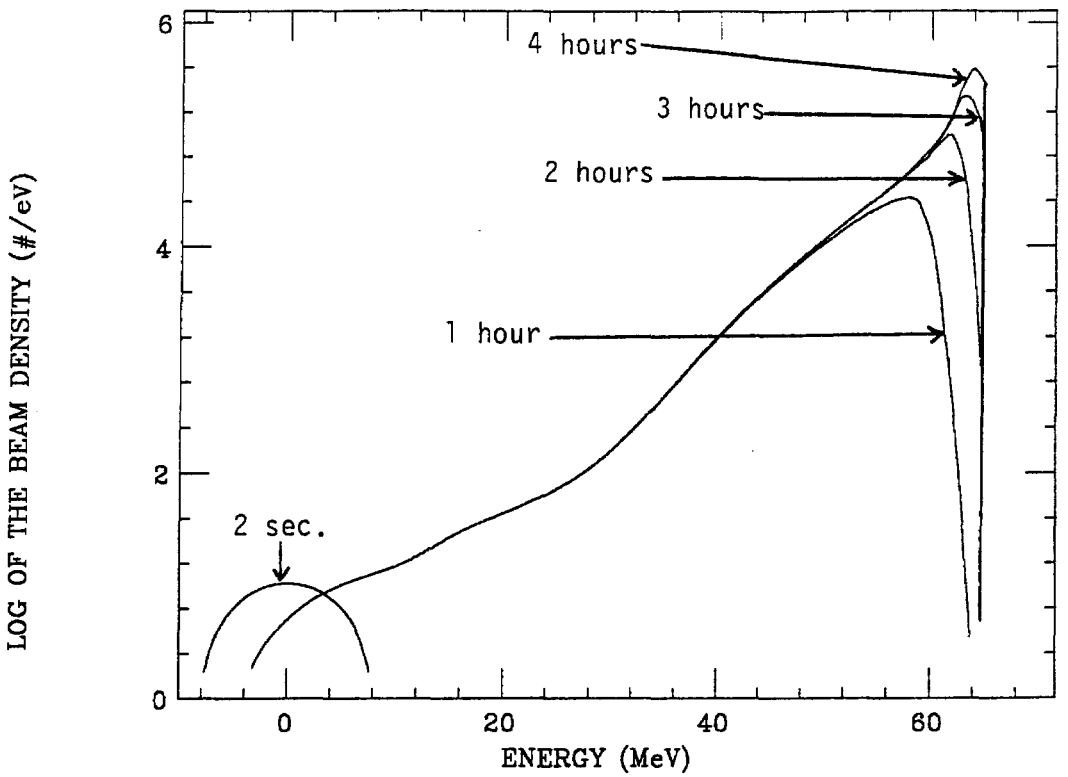

Figure 3.1 -- Stochastic cooling beam density profile as a function of time.

3B -- Initial Velocity Distributions

In order to analyze the effect of intermediate energy electron cooling one must first obtain the initial velocity distributions of both the antiprotons and the electrons in a frame moving at the rms electron velocity. To do this a relativistic transformation must be done from the lab frame to the moving frame. The equations of transformation for the energy-momentum four vector are

$$
\begin{aligned}
P_y' &= \gamma P_y + \beta\gamma \frac{E}{c} , \\
P_x' &= P_x , \\
P_z' &= P_z , \\
E' &= \gamma E + \beta\gamma P_y c .
\end{aligned}
\tag{3.1}
$$

The resonant particle is defined to be that particle with $P_x = P_y = P_z = 0$ and $E = mc^2$ in the moving frame. In the lab frame

$$
\begin{aligned}
P_{yr}' &= \beta\gamma mc , \\
P_{xr}' &= 0 , \\
P_{zr}' &= 0 , \\
E_r' &= \gamma mc^2 .
\end{aligned}
\tag{3.2}
$$

The nonresonant particle is defined to have $P_x = dp_x$, $P_y = dp_y$, $P_z = dp_z$, and $E = (dp^2c^2 + m^2c^4)^{1/2}$ in the moving frame, where $dp^2 = dp_x{}^2 + dp_y{}^2 + dp_z{}^2$. In the lab frame

$$P_y' = \gamma dp_y + \beta\gamma(dp^2 + m^2c^2)^{1/2} ,$$

$$P_x' = dp_x ,$$

$$P_z' = dp_z \ , \tag{3.3}$$

$$E' = \gamma(dp^2c^2 + m^2c^4)^{1/2} + \beta c\gamma dp_y \ .$$

The energy in the moving frame can be expanded to obtain

$$E = mc^2(1 + \frac{dp^2c^2}{2m^2c^4}) \ . \tag{3.4}$$

Using this expansion $\Delta p = Py' - P_{yr}' = \beta\gamma\frac{dp^2c}{2mc^2} + \gamma dp_y$. Neglecting terms of order $(dp/mc)^2$:

$$\frac{\Delta p}{P} = \frac{dp_y}{\beta mc} \ . \tag{3.5}$$

Using $dp_y = m\beta_{\parallel}c$ leaves

$$\beta_{\parallel} = \beta\frac{\Delta p}{P} \tag{3.6}$$

as the parallel velocity of the off resonant particle in the moving frame.

To find the perpendicular velocity the divergence of the beam, $\theta_{\perp} \equiv (P_x'/P_y')$, is used. Substituting the appropriate expressions and throwing out second order terms leaves the following expression:

$$\beta_{\perp} = \theta_{\perp}\beta\gamma \ . \tag{3.7}$$

Using these expressions one may now evaluate the initial velocity distributions of the two beams. The electron beam generated by the NEC Pelletron has an ideal transverse temperature of 0.1 eV.[3.5] This corresponds to a perpendicular velocity of $\beta_{\perp}c = 6\times10^{-4}c$. The Pelletron can be kept to a constant voltage to within ±100 V, and so

$\beta_{\parallel} = 3\times10^{-5}$. For the antiproton beam the design parameters state that $\Delta p/p$ is 5×10^{-4} yielding a $\beta_{\parallel}$ of 5×10^{-4}, and with the lattice beta function of the ring equal to 10m and $\varepsilon = 2\pi$mm-mr, $\Theta_{\perp} = 4.4\times10^{-4}$ and thus $\beta_{\perp} = 4.4\times10^{-3}$. Figure 3.2 shows the initial velocity distributions of the two beams.

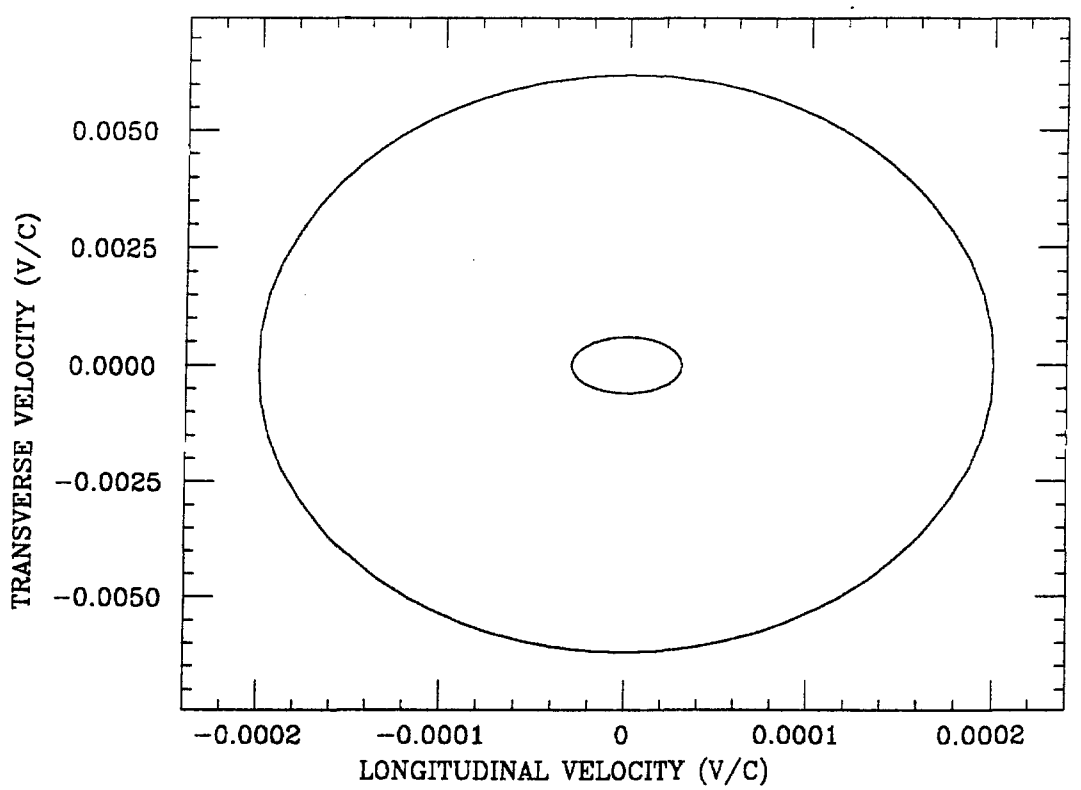

Figure 3.2 -- Initial velocity distributions of the antiproton and electron beams. (The antiproton distribution has the larger area.)

3C -- Expected Cooling Time -- Ideal Case

The electron cooling will be evaluated in the rest frame of the electrons. This is the frame moving with respect to the lab system. The electron cooling friction force arises from the energy loss experienced by the antiprotons as they move through the electron cloud. The energy loss of a charged particle moving through a stationary electron cloud is found in Jackson[3.6] to be

$$\frac{dE}{dx} = \frac{4\pi Ne^4\Lambda}{m_e v^2} \ . \tag{3.8}$$

For the situation here we assume that the velocity distribution of the electron cloud is a delta function. (Initial simulations indicate that this assumption does not affect the cooling time calculation.) Including the fact that the electron cooling system is operating over a fraction of the accumulator ring η, and setting the friction force equal to $dp/dt = m_p dv/dt$, we arrive at the following equation for the rate of change of the antiproton velocity:

$$\frac{dv}{dt} = \frac{4\pi Ne^4\Lambda\eta}{m_e m_p v^2} \ . \tag{3.9}$$

Integrating out Eq. (3.9) leaves

$$v_i^3 - v_f^3 = 3K(t_f - t_i) \ , \tag{3.10}$$

where $K = \dfrac{4\pi Ne^4\Lambda\eta}{m_e m_p}$.

The parameter K will now be evaluated. The number density of electrons in the electron beam is

$$N = \frac{I}{\gamma \pi a^2 \beta c e} , \tag{3.11}$$

$$\text{thus, } K = \frac{4 I r_e r_p \Lambda \eta c^3}{\gamma \beta a^2 e} . \tag{3.12}$$

In the above equation the Gaussian unit relations $r_e = \frac{e^2}{m_e c^2}$ and $r_p = \frac{e^2}{m_p c^2}$ have been used. The values of the parameters are $I = 4A$, $r_e = 2.82\times10^{-15}m$, $r_p = 1.53\times10^{-18}m$, $\Lambda = 15$ (the Coulomb log), $\eta = .02$ (the percent of the accumulator ring making use of electron cooling), $\gamma = 10$, $\beta = .995$, and $a = 0.01$ m . The value of the beam radius (a) will be a point of later discussion so a good form to leave K in is

$$K = \frac{3.5\times10^{11}}{a^2} , \text{ a in meters .} \tag{3.13}$$

In Section 3b of this work the initial velocity distribution of the antiproton beam is determined. The Fermilab design report states that $\Delta p/p$ is 5×10^{-4} yielding $\beta_{\parallel} = 5\times10^{-4}$. With the lattice beta function (β_1) of the ring equal to 10m and $\varepsilon = 2\pi$mm-mr, $\Theta_x = \Theta_z = (\frac{\varepsilon}{\pi\beta_1})^{1/2}$ leads to $\Theta_\perp = (\frac{2\varepsilon}{\pi\beta_1})^{1/2}$ which leaves $\beta_\perp = 6.2\times10^{-3}$. Note that as a function of the emittance we have $\beta_\perp = 10(\frac{2\varepsilon}{10\pi})^{1/2} = (\frac{20\varepsilon}{\pi})^{1/2}$.

We see that the initial antiproton velocity is primarily determined by the initial transverse velocity. Introducing this

initial velocity into Eq. (3.10), with the final velocity equal to zero, and also using Eq. (3.13) leaves

$$t_f = \frac{c^3 a^2 (\frac{20\varepsilon}{\pi})^{3/2}}{3\times 3.5\times 10^{11}} . \tag{3.14}$$

As stated earlier, this is the time in the moving system. In order to obtain the time in the lab system multiplication by γ must be done. Lastly, the effect of betatron oscillations on the cooling time should be included. Betatron oscillations have the effect of lowering the cooling time. The physical reason is that since the cooling rate is inversely proportional to the square of the velocity, smaller velocities cool faster. Betatron oscillations cause the velocity of the antiprotons in the cooling straight to have the form $v = v_{max}\sin\phi$. Since we have plugged in $v = v_{max}$ into the expression for the cooling time, we have overestimated the cooling time. Initial simulations (see section 4d) estimate the magnitude of this effect to be about 1.7. Including the effects of betatron oscillations and γ leaves:

$$t_f = \frac{c^3 a^2 (\frac{20\varepsilon}{\pi})^{3/2}}{1.8\times 10^{11}} . \tag{3.15}$$

In order to have optimum cooling the radius of the electron beam should be matched to the radius of the antiproton beam. The radius of the antiproton beam is given by $r = (\beta\varepsilon/\pi)^{1/2}$. In Table 3.2 the expected cooling times are presented for the case where the beam sizes are matched, and for the case where the electron beam is $2^{1/2}$ larger than the antiproton beam. Due to the fact that the antiproton beam will expand from its waist, it will not remain as small as its waist size throughout the cooling straight. For this reason the best possible cooling time will be somewhere between the matched and unmatched times shown in the table. Since the cooling time is

proportional to beam current, a .4A electron beam will take 10 times longer to cool, while a 40A beam will cool in 1/10 the time indicated.

Table 3.2 -- Intermediate Energy Electron Cooling Times

ε(mm-mr)	$.2\pi$	2π(design)	20π
a(mm)			
Matched	2.4 sec.	13 min.	66 hours
Unmatched	4.8 sec.	26 min.	133 hours

Chapter Four -- Complete Simulation of the Expected Cooling Time

4A -- Analytic Derivation of the Cooling Force

The electron cooling friction force arises from the energy loss experienced by the antiprotons as they move through the electron cloud. The energy loss by a charged particle moving through a stationary electron cloud is found in Jackson[4.1] to be

$$\frac{dE}{dx} = \frac{4\pi N e^4 \Lambda}{m_e v^2} \ . \tag{4.1}$$

For the situation here we must integrate over the velocity distribution of the electron cloud, $g(v_e)$, and also include the fact that the electron cooling system is operating over a fraction of the accumulator ring η. The friction force can then be set equal to $dp/dt = m_p dv/dt$ to arrive at the following equation for the rate of change of the antiproton velocity.

$$\frac{dv_p}{dt} = 4\pi N r_e r_p \Lambda \eta c^4 \int_{\vec{v}_e} \frac{g(v_e)dv_e}{(v_p - v_e)^3}(\vec{v}_p - \vec{v}_e) \ . \tag{4.2}$$

Now the equation will be transformed into an equation for β. The notation used will be that antiproton velocities will appear as β, while electron velocities will be given the notation β'.

$$\frac{d\beta_\parallel}{dt} = 4\pi N r_e r_p \Lambda \eta c \int_{\vec{v}_e} \frac{g(v_e)dv_e(\beta_\parallel-\beta'_\parallel)}{[(\beta_\perp-\beta'_\perp)^2 + (\beta_\parallel-\beta'_\parallel)^2]^{3/2}}$$

and (4.3)

$$\frac{d\beta_\perp}{dt} = K \int_{\vec{v}_e} \frac{g(v_e)dv_e(\beta_\perp-\beta'_\perp)}{[(\beta_\perp-\beta'_\perp)^2 + (\beta_\parallel-\beta'_\parallel)^2]^{3/2}}$$

where $K = 4\pi N r_e r_p \Lambda \eta c$.

The equations which make the relativistic transformation from the lab frame to the moving frame are derived in Section 3b.

$$\beta_\parallel = \beta\frac{\Delta p}{P} , \tag{3.6}$$

$$\beta_\perp = \theta_\perp \beta\gamma . \tag{3.7}$$

(In all of the calculations involving the averaging over the initial electron velocities, integration is over the three dimensional velocity distribution $g(\vec{v}_e)$. In the analysis $\beta_\perp$ and $\theta_\perp$ are two dimensional vector functions:

$$\beta_\perp \equiv (\beta_x{}^2 + \beta_z{}^2)^{1/2}$$

$$\theta_\perp \equiv (\theta_x{}^2 + \theta_z{}^2)^{1/2}) .$$

Use of these equations leaves Eq. (4.3) in the following form: (β and γ without subscripts are the relativistic quantities.)

$$\frac{d(\frac{\Delta p}{p})}{dt} = \frac{K}{(\beta\gamma)^3} \int_{\vec{v}_e} \frac{g(v_e)dv_e \; (\frac{\Delta p}{p} - \frac{\Delta p'}{p'})}{[(\theta_\perp - \theta_\perp')^2 + (\frac{\Delta p}{\gamma p} - \frac{\Delta p'}{\gamma p'})^2]^{3/2}} ,$$

and (4.4)

$$\frac{d\theta_\perp}{dt} = \frac{K}{(\beta\gamma)^3} \int_{\vec{v}_e} \frac{g(v_e)dv_e \; (\theta_\perp - \theta_\perp')}{[(\theta_\perp - \theta_\perp')^2 + (\frac{\Delta p}{\gamma p} - \frac{\Delta p'}{\gamma p'})^2]^{3/2}} .$$

The above equations are satisfactory for the change in antiproton velocity due to electron cooling, but what is really desired is an equation for the change in emittance. The equation for the emittance of a single particle can be defined as the CLS invariant W[4.2] times π,

$$\pi W = \pi(\gamma x^2 + 2\alpha x\theta + \beta\theta^2) \tag{4.5}$$

(α, β, γ are the Twiss parameters at the point of evaluation).

For a waist, $\alpha = 0$, and in the case where the beam divergence within the cooling section can be neglected the change in the emittance is

$$\pi\Delta W = \pi W(x + \Delta x, \; \theta + \Delta\theta) - W(x, \; \theta) =$$

$$= \pi\beta(\theta + \Delta\theta)^2 - \pi\beta\theta^2 \simeq 2\pi\beta\theta\Delta\theta \; . \tag{4.6}$$

The equation for the rate of change of the emittance is thus

$$\frac{d\varepsilon}{dt} = \frac{2\pi\beta_{twiss}K\theta_\perp}{\beta^3\gamma^3} \int_{\vec{v}_e} \frac{g(v_e)dv_e \; (\theta_\perp - \theta_\perp')}{[(\theta_\perp - \theta_\perp')^2 + (\frac{\Delta p}{\gamma p} - \frac{\Delta p'}{\gamma p'})^2]^{3/2}} \tag{4.7}$$

But this equation must be averaged over the betatron oscillations which obey the equations $\theta_x = \theta_x \sin(\psi_x)$, $\theta_z = \theta_z \sin(\psi_z)$. The equations for electron cooling are then

$$\frac{d\varepsilon_x}{dt} = K' \int\int \theta_x \sin(\psi_x) \int_{\vec{v}_e} \frac{g(v_e)dv_e d\psi_x d\psi_z \; (\theta_x \sin(\psi_x) - \theta_x')}{[(\theta_\perp - \theta_\perp')^2 + (\frac{\Delta p}{\gamma p} - \frac{\Delta p'}{\gamma p'})^2]^{3/2}} , \qquad (4.8)$$

$$\frac{d\varepsilon_z}{dt} = K' \int\int \theta_z \sin(\psi_z) \int_{\vec{v}_e} \frac{g(v_e)dv_e d\psi_x d\psi_z \; (\theta_z \sin(\psi_z) - \theta_z')}{[(\theta_\perp - \theta_\perp')^2 + (\frac{\Delta p}{\gamma p} - \frac{\Delta p'}{\gamma p'})^2]^{3/2}} , \qquad (4.9)$$

$$\frac{d(\frac{\Delta p}{p})}{dt} = \frac{K}{4\pi^2(\beta\gamma)^3} \int\int\int_{\vec{v}_e} \frac{g(v_e)dv_e d\psi_x d\psi_z \; (\frac{\Delta p}{p} - \frac{\Delta p'}{p'})}{[(\theta_\perp - \theta_\perp')^2 + (\frac{\Delta p}{\gamma p} - \frac{\Delta p'}{\gamma p'})^2]^{3/2}} , \qquad (4.10)$$

where $K' = \frac{2\pi\beta_{twiss}K}{\beta^3\gamma^3 4\pi^2}$,

and $(\theta_\perp - \theta_\perp')^2 = (\theta_x \sin(\psi_x) - \theta_x')^2 + (\theta_z \sin(\psi_z) - \theta_z')^2$.

4B -- Numerical Simulation of the Ideal Case

The equations given in section 4a (4.8-4.10) are an exact formulation of the cooling process but do not contain the effect of intrabeam scattering (IBS). In order to determine the cooling time one could, in principle, solve Eqs. 4.8, 4.9 and 4.10 along with the effect of IBS numerically. Initial computer simulations indicated that this approach to the problem would be prohibitively costly however, and so the treatment of the problem will be to isolate the various effects one by one and investigate their contribution to the cooling time. This will justify the assumptions made in Section 3c.

The first simulation is done on the ideal case where we have no IBS, no betatron oscillations, and no electron temperature. The cooling time for this case can be determined exactly, as is done in Section 3c, and the purpose of doing this analysis is to obtain an estimate on the costs of, and convergence parameters needed for, future codes, as well as to check on the accuracy of the result.

Definition of the Cooling Time -- The cooling time will now be defined to be the time it takes the antiproton velocity distribution to cool to a value where it is within the electron velocity distribution. For the ideal case this is obtained by rearranging Eq. (3.10) and including the time dilation factor of gamma.

$$t_f = \gamma \frac{v_{pbar0}^3 - v_{e0}^3}{3K} \tag{4.11}$$

where $K = \dfrac{4\pi N e^4 \Lambda \eta}{m_e m_p}$.

For the non-ideal case such a simple formula will not apply and the cooling time will have to be evaluated numerically.

The definition of the cooling time must also include a definition of the initial beam that is to be cooled. The beam is defined to consist of those particles which constitute 95% of all the particles

in the ring. This definition is used in the Fermilab design report to set the x and z emittances at 2π mm-mr. The particle that takes the most time to cool is that particle with maximum x and z velocities of the defined beam. The maximum x velocity is proportional to $(\varepsilon_x)^{1/2}$, while the maximum z velocity is proportional to $(\varepsilon_z)^{1/2}$. Adding the maximum x velocity to the maximum z velocity yields a velocity $2^{1/2}$ greater than the maximum one dimensional velocity. By calculating the cooling of a particle of initial emittance of 4π mm-mr the maximum cooling time will be obtained.

Numerical Treatment of the Ideal Case -- The computer code used for the numerical evaluation of the cooling time for the ideal case is shown in Appendix 3. The code evaluates the ideal expression

$$\frac{d\varepsilon_x}{dt} = K' \frac{\theta_x^2}{(\theta_x^2 + \theta_z^2 + (\Delta p/p)^2)^{3/2}} \tag{4.12}$$

where $K' = \dfrac{2\pi\beta_{twiss}K}{\beta^3\gamma^3}$, K as in (4.11).

The code calculates the amount of time required for the antiproton emittances to cool to a value less than or equal to the emittance that the antiproton beam would have if the antiproton velocity was just inside the electron velocity distribution. The result of the program can be compared with the analytic result of Eq. (4.11). Eq. (4.11) gives the final cooling time to be 6160 seconds. The cooling time obtained by the code converged toward just under 6100 seconds. Using double precision convergence to 6160 seconds is obtained -- indicating that double precision is more important than step size for much of this analysis. Transferring from velocity as the variable (in Eq. (4.11)) to emittance as the variable (as done in the code) created no ambiguity in the results. The parameters used in the analysis are given in Table 4.1. Especially note that the electron beam radius

used in the analysis was one cm. This is actually larger than the ideal value and is why the cooling times obtained here are larger than those presented in Section 3c.

Table 4.1 -- Code Parameters -- Ideal Cooling Time Calculation

parameter	value
initial $\beta_\perp$ (v/c)	6.22×10^{-3}
γ (relativistic)	10.0
β (relativistic)	0.995
β_{twiss}	10 m.
electron beam radius	1.0 cm.
electron current	4.0 A
Coulomb log	15
ratio of cooling length to ring length, η	.02
integration time step, run one	.5 sec.
cooling time, run one	6160 sec.
integration time step, run one	.01 sec.
cooling time, run two	6120 sec.
integration time step, run three	.003 sec.
cooling time, run three	6100 sec.

The output of the code shows the cooling of the antiproton beam as a function of time and is presented graphically in Figure 4.1. (Note that the cooling time indicated in Figure 4.1 is not 6100 s. -- Figure 4.1 shows the expected cooling time including the effects of betatron oscillations, finite temperature, and intrabeam scattering, and uses a smaller beam size than the one used in Table 4.1. The calculations leading to the times represented in Figure 4.1 are discussed in the remainder of Chapter Four.) From the figure we see that the longitudinal part of the antiproton distribution is cooled very rapidly and that the cooling time is entirely dominated by the transverse cooling time. For this reason the discussion in the

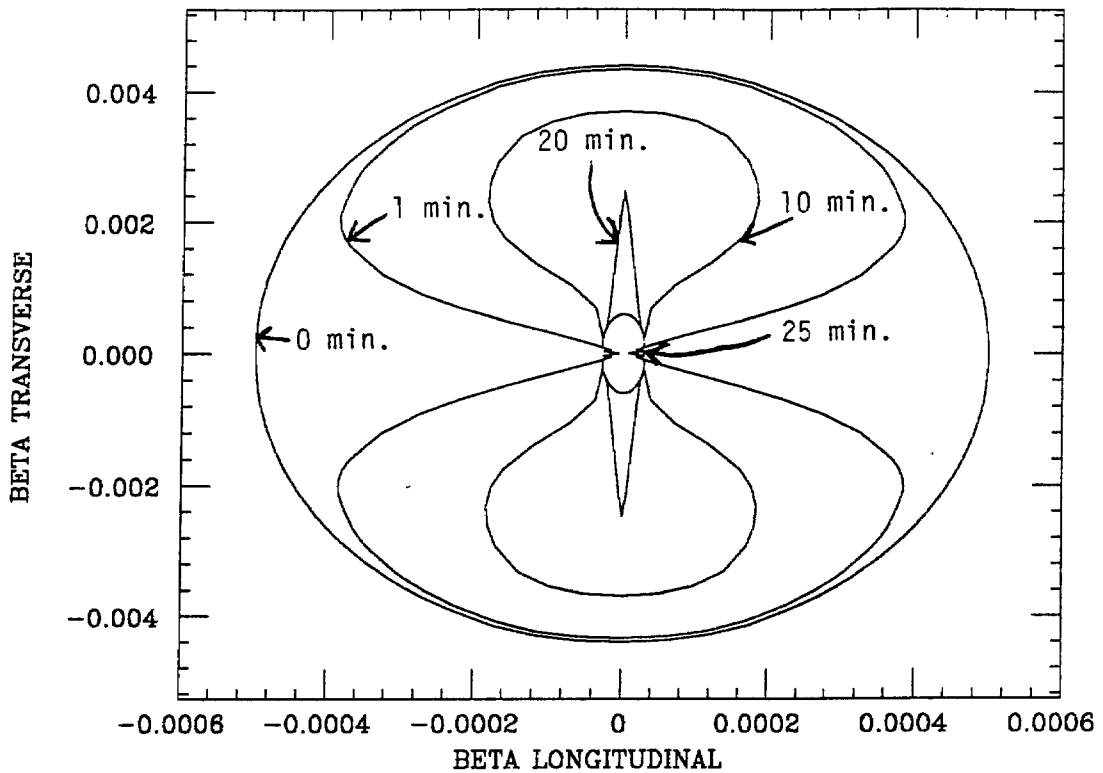

Figure 4.1 -- Electron cooling of the antiproton velocity distribution as a function of time.

following sections will calculate the cooling time of the transverse emittances.

4C -- Electron Temperature Effect

The effect of the finite temperature of the electron beam on the cooling time requires two investigations. The first calculation is the diffusion caused by the electron beam temperature. This effect was discussed in the introduction and was seen to be unimportant. The final value of the antiproton temperature may be determined by thermal equilibrium between the two beams (should intrabeam scattering not be the limiting factor). (As has been shown in Figure 4.1, the dominant contribution to the cooling time occurs when the antiproton velocity is the largest. Since we are far from equilibrium when the antiproton velocity is large, diffusion due to the finite temperature will not influence the cooling time calculation.)

The second effect that finite temperature has on the cooling time is that we must now integrate over the electron velocity distribution. To do this Eq. (4.8) must be used with the integrals over the betatron oscillations taken out.

The value of the force assuming no electron velocities is given by the following formula:

$$\frac{d\varepsilon_x}{dt} = K' \frac{(\theta_x)^2}{[(\theta_x)^2 + (\theta_z)^2 + (\frac{\Delta p}{\gamma p})^2]^{3/2}} \text{ (ideal case)} \tag{4.13}$$

where $K' = \frac{2\pi\beta_{twiss}K}{\beta^3\gamma^3}$ and $K = 4\pi N r_e r_p \Lambda\eta c$.

Inclusion of the electron velocity distribution can be accomplished with integration over the distribution.

$$\frac{d\varepsilon_x}{dt} = K' \theta_x \int_{\vec{v}_e} \frac{g(v_e)dv_e\ (\theta_x - \theta_x')}{[(\theta_x - \theta_x')^2 + (\theta_z - \theta_z')^2 + (\frac{\Delta p}{\gamma p} - \frac{\Delta p'}{\gamma p'})^2]^{3/2}} \tag{4.14}$$

As was seen in the last section, the cooling time is entirely dependent on the cooling time of the transverse emittance. An initial computer run to determine the cooling time including the temperature effect was very costly, but the effect can be investigated by looking at the effect the velocity distribution has on the force.

The computer code used in this analysis is presented in Appendix 4. The code replaces the delta function electron velocity distribution of the first code by a uniform distribution of velocity delta functions within an ellipsoid. The axes of the ellipsoid correspond to the limiting values of the electron velocity distribution. The force parameter K' is then renormalized by dividing by the number of delta functions used. The number of delta functions is increased and the change in the force noted. Table 4.2 gives a summary of results of the code using a value of antiproton velocity corresponding to the beginning of the cooling, at the midpoint of the cooling, and at the point where the antiproton velocity is just outside the electron velocity. The values corresponding to one delta function are calculated from Eq. (4.13), while the rest are computer generated.

Table 4.2 -- $d\varepsilon/dt$ as a Function of Integration Step Size

θ_x	number of delta functions	the force, $d\varepsilon/dt$
	The onset of cooling	
6.251E-04	1	1.327E-08
6.251E-04	8	1.331E-08
6.251E-04	4094112	1.330E-08
	The midpoint of cooling	
3.125E-04	1	2.655E-08
3.125E-04	8	2.688E-08
3.125E-04	4094112	2.683E-08
	Just about done	
6.633E-05	1	1.251E-07
6.633E-05	8	1.208E-07
6.633E-05	29752	1.815E-07
6.633E-05	4094112	1.884E-07
6.633E-05	112247560	1.894E-07

From Table 4.2 we see that the finite velocity of the electron beam will have no noticeable effect on the cooling time. The last force evaluated was close to the distribution function, hence convergence was much slower than for the other evaluated points.

4D -- The Effect of Betatron Oscillations on the Cooling Time

The effect of the finite temperature of the electron beam can now be removed from Eqs. 4.8, 4.9, and 4.10.

$$\frac{d\varepsilon_x}{dt} = K' \int\int \theta_x \sin(\phi_x) \frac{d\phi_x d\phi_z \; \theta_x \sin(\phi_x)}{[(\theta_\perp)^2 + (\frac{\Delta p}{\gamma p})^2]^{3/2}} \tag{4.15}$$

$$\frac{d\varepsilon_z}{dt} = K' \int\int \theta_z \sin(\phi_z) \frac{d\phi_x d\phi_z \; \theta_z \sin(\phi_z)}{[(\theta_\perp)^2 + (\frac{\Delta p}{\gamma p})^2]^{3/2}} \tag{4.16}$$

$$\frac{d(\frac{\Delta p}{p})}{dt} = \frac{K}{4\pi^2(\beta\gamma)^3} \int\int d\phi_x d\phi_z \frac{(\frac{\Delta p}{p})}{[(\theta_\perp)^2 + (\frac{\Delta p}{\gamma p})^2]^{3/2}} \tag{4.17}$$

Where $K' = \frac{2\pi\beta_{twiss}K}{\beta^3\gamma^3 4\pi^2}$,

and $(\theta_\perp)^2 = (\theta_x \sin(\phi_x))^2 + ((\theta_z \sin(\phi_z))^2$.

The effect that the betatron oscillations have on the cooling can be determined by forming the following ratio:

$$\frac{\text{(the equation for the force including betatron oscillations)}}{\text{(the equation for the force excluding betatron oscillations)}}$$

By using the symmetry of the integrals, equations for the betatron oscillation transverse cooling improvement factor (BOTCIF) and the betatron oscillation longitudinal cooling improvement factor (BOLCIF) are found.

BOTCIF =

$$\frac{\int\int d\phi_x\, d\phi_z \dfrac{(\theta_x \sin(\phi_x))^2}{[(\theta_x \sin(\phi_x))^2 + (\theta_z \sin(\phi_z))^2 + (\frac{\Delta p}{\gamma p})^2]^{3/2}}}{4\pi^2 \dfrac{\theta_x^2}{(\theta_x^2 + \theta_z^2 + (\frac{\Delta p}{\gamma p})^2)^{3/2}}} . \tag{4.18}$$

(With a similar equation for the z component.)

BOLCIF =

$$\frac{\int\int d\phi_x\, d\phi_z \dfrac{\frac{\Delta p}{p}}{[(\theta_x \sin(\phi_x))^2 + (\theta_z \sin(\phi_z))^2 + (\frac{\Delta p}{\gamma p})^2]^{3/2}}}{4\pi^2 \dfrac{\frac{\Delta p}{p}}{(\theta_x^2 + \theta_z^2 + (\frac{\Delta p}{\gamma p})^2)^{3/2}}} . \tag{4.19}$$

These equations are valid during the part of the trajectory when the antiproton velocity is outside the electron velocity distribution. Inside the electron velocity distribution the cooling force drops to zero as the velocity vanishes. This effect can be simulated by replacing $\theta \sin\phi$ in the denominator of the integrand with $\theta_{electron}$ when the antiproton velocity is within the electron velocity distribution.

Since the transverse cooling time determines the total cooling time, the effect of betatron oscillations on the transverse cooling will be investigated first. Two cases of interest should be looked at. The first is when the initial antiproton velocity has no z component. The other is when the z component of the initial

antiproton velocity equals the x component. The code used to calculate the effect of betatron oscillations is presented in Appendix 5. The results of the code are presented in Table 4.3.

Table 4.3 -- Code Parameters and Results -- Betatron Oscillation Transverse Cooling Improvement Factor

θ_{x0}	θ_{z0}	$d\phi_x$	$d\phi_z$	BOTCIF
6.2e-4	0.0e-4	.01	.01	1.68
6.2e-4	0.0e-4	.001	.001	1.68
4.5e-4	0.0e-4	.01	.01	1.49
3.1e-4	0.0e-4	.01	.01	1.22
4.4e-4	4.4e-4	.1	.1	1.55
4.4e-4	4.4e-4	.01	.01	1.65
4.4e-4	4.4e-4	.001	.001	1.64
3.3e-4	3.3e-4	.001	.001	1.59
2.2e-4	2.2e-4	.01	.01	1.46

The code shows that betatron oscillations initially improve the transverse cooling force by a factor of about 1.65. The enlargement of the cooling force arises from the periodic decrease in the transverse antiproton velocity caused by the betatron oscillations. (The cooling force is proportional to the inverse cube of the antiproton velocity.) As the cooling progresses the cooling force enhancement decreases since the finite electron beam temperature effect becomes more important. After 60% of the cooling time has passed the transverse cooling force enhancement drops to a factor of about 1.5. This factor of 1.5 is thus the approximate improvement in the cooling time due to betatron oscillations.

There should be an even more dramatic improvement in the cooling of the longitudinal component of the antiproton velocities, since this component is usually quite small compared to the transverse component. Table 4.4 gives the calculated estimate of the longitudinal cooling improvement for antiprotons with the maximum longitudinal velocity.

The result is that the longitudinal component of velocity is cooled at a much higher rate when betatron oscillations are taken into account.

Table 4.4 -- Code Parameters and Results -- Betatron Oscillation Longitudinal Cooling Improvement Factor

$\Delta p/p = 5 \times 10^{-4}$

θ_{x0}	θ_{z0}	$d\phi_x$	$d\phi_z$	BOLCIF
4.4e-4	4.4e-4	.1	.1	13.1
4.4e-4	4.4e-4	.01	.01	13.1
4.4e-4	4.4e-4	.001	.001	13.2
3.3e-4	3.3e-4	.01	.01	9.84
2.2e-4	2.2e-4	.01	.01	6.51
6.2e-4	0.0e-4	.01	.01	44.5
0.0e-4	6.2e-4	.01	.01	44.5
4.5e-4	0.0e-4	.01	.01	23.7
3.1e-4	0.0e-4	.01	.01	11.4

4E -- Intrabeam Scattering

In order to do a complete simulation of the electron cooling process some manner of including the effect of intrabeam scattering (IBS) must be done. IBS is a process that heats the antiproton beam due to the coulomb collisions between antiprotons within the antiproton beam. The strong focusing magnets in a storage ring continually distort the antiproton velocity distribution and it is this mechanism which is responsible for allowing a momentum transfer from the longitudinal beam momentum to the transverse beam momentum thereby heating the beam.

The most complete work on IBS that has been done to date is presented in a paper by Bjorken and Mtingwa[4.3]. (While earlier work on IBS has been done by Piwinski[4.4].) By fitting their predicted IBS heating rates (given as functions of emittance and $\Delta p/p$) to simple functions one can include the effect of IBS over the region of interest.

Definition of Emittance -- The question of what is meant by emittance must now be dealt with. In Reference 4.3 emittance is defined to be σ^2/β_{Twiss}, where the antiproton beam velocity distribution is assumed to be a gaussian distribution with standard deviation σ, and β_{Twiss} is the beta function of the lattice at the point where σ is determined. The Fermilab design report defines the emittance of the antiproton beam to be $6\pi\sigma^2/\beta_{Twiss}$. The FNAL definition of emittance includes 95% of the antiproton trajectories, while Reference 4.3 includes one standard deviation. This work uses the FNAL definition of emittance.

The cooling time calculation begins with the antiproton beam emittance of 2π mm-mr and ends somewhere near 0.037π mm-mr. (An antiproton beam emittance of 0.037π mm-mr corresponds to an antiproton velocity distribution which is just inside the electron velocity distribution, while the initial emittance of 2π mm-mr is the value expected after stochastic cooling is completed.) These values correspond to 3.3×10^{-7}m and 6.2×10^{-9}m in Reference 4.3. The values of $\Delta p/p$ during the cooling range from 2×10^{-4} to 3×10^{-5} and there is no

ambiguity in the notation since both Reference 4.3 and this analysis use the definition that $\Delta p/p$ of the antiproton beam contains one standard deviation of the antiproton trajectories.

IBS Growth Rates -- Empirically derived formulas which approximate the emittance and $\Delta p/p$ growth rates of the antiproton beam due to intrabeam scattering as given in Reference 4.3 are now presented. (The empirical derivation is done on computer generated data.)

$$\tau_x^{-1} = \frac{1}{\varepsilon_x}\frac{d\varepsilon_x}{dt} = 1.28\times10^{-2}\varepsilon'^{-2.48}(1 + 2.5\varepsilon'\sigma')(\sigma'^{-.24} - .4\sigma'^{.3}) \qquad (4.20)$$

$$\tau_1^{-1} = \frac{1}{\sigma_1^2}\frac{d\sigma_1^2}{dt} = .42\sigma'^{-2.24}\varepsilon'^{-1.47} \qquad (4.21)$$

In eq. (4.20) $\varepsilon' = 10^6\varepsilon$ and $\sigma' = 10^4\sigma$.

(Also note that $\frac{d\sigma_1^2}{dt} = 2\sigma_1\frac{d\sigma_1}{dt}$)

As can be seen in the defining equations (Eqs. (4.20) and (4.21)) the emittance growth rates are given as the inverse of the time required for the beam emittance to grow by a factor of 1/e. Results of S. Mtingwa's calculations[4.5] for the emittance growth rate in the x-x' plane due to IBS are presented in Table 4.5. The corresponding rates as determined by Eq. (4.20) are presented in Table 4.6. Similarly, S. Mtingwa's calculations for longitudinal beam size increase due to IBS are given in Table 4.7, while the rates obtained from Eq. (4.21) are presented in Table 4.8. In all tables the numbers given are in inverse hours. In almost all cases the formulas overestimate the extent of the IBS blowup and therefore overestimate its effect on the increase in cooling time. All calculations are done

with the parameters expected upon completion of the stochastic cooling of the antiproton beam.

Table 4.5 -- S. Mtingwa's Calculated x-x' Emittance Diffusion Rate Matrix
(The inverse time, in hours, required for a 1/e emittance growth.)

ε/π	.1e-7	.1e-6	.2e-6	.3e-6	.5e-6	.7e-6	.1e-5
$\Delta p/p$							
.1e-4	.128e4	.441e1	.789e0	.288e0	.806e-1	.348e-1	.143e-1
.5e-4	.745e3	.371e1	.702e0	.262e0	.752e-1	.329e-1	.136e-1
.9e-4	.507e3	.310e1	.616e0	.236e0	.694e-1	.308e-1	.129e-1
.12e-3	.407e3	.273e1	.560e0	.218e0	.653e-1	.293e-1	.124e-1
.18e-3	.293e3	.218e1	.468e0	.187e0	.578e-1	.264e-1	.114e-1
.28e-3	.201e3	.162e1	.363e0	.149e0	.478e-1	.223e-1	.985e-2

Table 4.6 -- x-x' Emittance Growth Rate Matrix Using Formula 4.20
(The inverse time, in hours, required for a 1/e emittance growth.)

ε/π	.1e-7	.1e-6	.2e-6	.3e-6	.5e-6	.7e-6	.1e-5
$\Delta p/p$							
.1e-4	.180e+4	.609e+1	.112e+1	.419e+0	.124e+0	.560e-1	.246e-1
.5e-4	.101e+4	.372e+1	.741e+0	.298e+0	.993e-1	.498e-1	.247e-1
.9e-4	.762e+3	.302e+1	.641e+0	.271e+0	.968e-1	.509e-1	.265e-1
.12e-3	.643e+3	.269e+1	.593e+0	.258e+0	.955e-1	.514e-1	.274e-1
.18e-3	.477e+3	.219e+1	.515e+0	.233e+0	.908e-1	.503e-1	.275e-1
.28e-3	.295e+3	.155e+1	.393e+0	.186e+0	.759e-1	.432e-1	.242e-1

Table 4.7 -- S. Mtingwa's Calculated Longitudinal Diffusion Rate Matrix
(The inverse time, in hours, required for a 1/e emittance growth.)

ε/π	.1e-7	.1e-6	.2e-6	.3e-6	.5e-6	.7e-6	.1e-5
$\Delta p/p$							
.1e-4	.462e5	.157e4	.561e3	.307e3	.143e3	.866e2	.508e2
.5e-4	.121e4	.548e2	.204e2	.114e2	.540e1	.330e1	.195e1
.9e-4	.259e3	.147e2	.570e1	.323e1	.156e1	.966e0	.577e0
.12e-3	.114e3	.749e1	.298e1	.171e1	.840e0	.522e0	.314e0
.18e-3	.320e2	.276e1	.115e1	.675e0	.340e0	.214e0	.130e0
.28e-3	.642e1	.856e0	.382e0	.232e0	.121e0	.778e-1	.483e-1

Table 4.8 -- Longitudinal Growth Rate Matrix Using Formula 4.21
(The inverse time, in hours, required for a 1/e emittance growth.)

ε/π	.1e-7	.1e-6	.2e-6	.3e-6	.5e-6	.7e-6	.1e-5
$\Delta p/p$							
.1e-4	.636e+5	.215e+4	.778e+3	.428e+3	.202e+3	.123e+3	.730e+2
.5e-4	.173e+4	.586e+2	.211e+2	.116e+2	.550e+1	.335e+1	.198e+1
.9e-4	.463e+3	.157e+2	.567e+1	.312e+1	.147e+1	.898e+0	.532e+0
.12e-3	.243e+3	.824e+1	.297e+1	.164e+1	.773e+0	.472e+0	.279e+0
.18e-3	.980e+2	.332e+1	.120e+1	.661e+0	.312e+0	.190e+0	.113e+0
.28e-3	.364e+2	.123e+1	.446e+0	.246e+0	.116e+0	.707e-1	.418e-1

How is the Effect of IBS Determined? -- The growth rates of the emittance and longitudinal standard deviation of the antiproton velocity distribution due to IBS are growth rates that indicate what is happening to the antiproton velocity distribution and not what is happening to individual trajectories within that distribution. The electron cooling friction force gives the rate of change of individual antiproton velocities within the distribution, and does not give the rate of change of the emittance and longitudinal standard deviation of the distribution. The correct way to do the problem would be to calculate the cooling of an ensemble of points in phase space individually, determine the emittance of the ensemble, calculate the

effect IBS has on the distribution and let the system evolve to equilibrium. This approach would be prohibitively costly however, and so some other estimate must be made.

The initial longitudinal and transverse emittances are determined by the semi-minor and semi-major axes of the velocity distribution ellipsoid. During electron cooling (as has been shown) the cool particles cool first, leaving the beam in the hourglass shape shown in Figure 4.1. Since the antiproton that has no transverse component of velocity cools very quickly, the first attempt at determining the effect IBS has on the cooling time is to assume that the distribution function reaches its equilibrium longitudinal emittance immediately. (The equilibrium longitudinal emittance is the final value of $\Delta p/p$ obtained.) Since particles with both longitudinal and transverse velocity will cool more slowly than particles with longitudinal velocity only, longitudinal equilibrium will not be established so quickly. The smaller value of longitudinal emittance being used in the analysis (the equilibrium value will be the smallest value possible) will simulate a larger IBS heating than actually exists, overestimating the cooling time. Since the equilibrium value of the longitudinal emittance has yet to be found, many values will be investigated and the effect on the cooling time noted.

Emittance of a Single Particle -- As the antiprotons traverse the storage ring they undergo betatron oscillations. If we plot the particle velocity and position at a given point in the ring each time they recirculate the points will lie on an ellipse. An example of such an ellipse in phase space is shown in Figure 4.2, where point 1 is the initial velocity and position of the particle at an arbitrary point in the ring where the measurement is being made. Point 2 is the point corresponding to the velocity and position of the particle after it has gone around the ring once. The area of this ellipse, the Courant Livingston Snyder (CLS) invariant[4.2], can interpreted as the emittance of the particle.

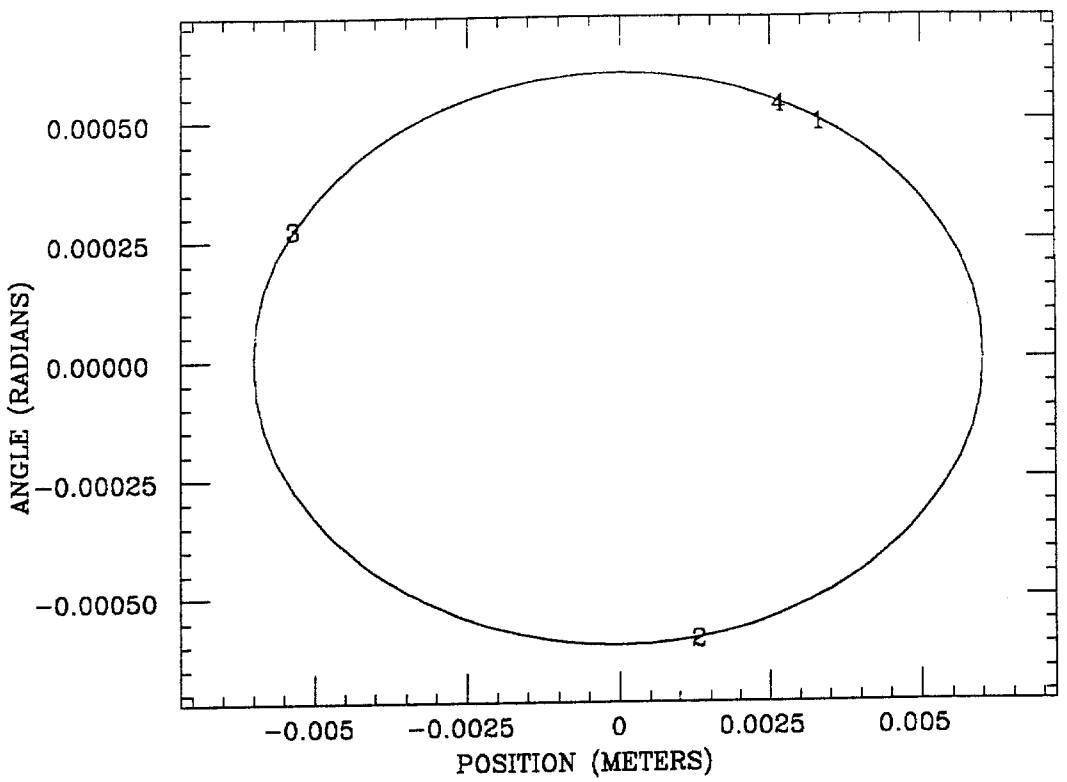

Figure 4.2 -- Example of a single particle trajectory in phase space.

$$\varepsilon_{\perp} = \pi\beta_{Twiss}\theta_{\perp}^{2} \ . \tag{4.22}$$

In Eq. (4.22) $\theta_{\perp}$ is determined by the antiproton's maximum transverse velocity at the point where the emittance is being measured, and β_{Twiss} is the lattice beta function at the point where the emittance is being measured.

Including IBS in the Cooling Time Calculation -- Simulation One -- The computer code EMIT2 (presented in Appendix 6) calculates the electron cooling of one antiproton, that antiproton with a transverse CLS invariant equal to the transverse emittance of the antiproton beam. The change in the velocity of the antiproton due to electron

cooling is calculated first. Then the increase in the beam emittance due to IBS is calculated. The increase in emittance due to IBS is then equated to an increase in the antiproton velocity by the inverse of Eq. (4.22). The change in the antiproton velocity is set equal to the increase in velocity due to IBS minus the decrease in velocity due to electron cooling. The velocity is then adjusted by this change, a new emittance is calculated for the beam using Eq. (4.22), and the process is repeated until the cooling stops. The increase in antiproton velocity due to IBS slows down the electron cooling, and the cooling is stopped when the decrease in velocity due to electron cooling equals the increase in velocity due to IBS.

The parameters used in the simulation are presented in Table 4.9, while the results are given in Table 4.10. The enhancement of the cooling force due to betatron oscillations is incorporated into the code.

Table 4.9 -- Code Parameters Used in Cooling Time Calculation Including IBS

Parameter	Value
Initial $\beta_\perp$ (v/c)	6.22×10^{-3}
γ (Relativistic)	10.0
β (Relativistic)	0.995
β_{Twiss}	10 m.
Electron Beam Radius	.63 cm.
Electron Current (Including Factor of 1.5 Betatron Oscillation Enhancement)	4.0 A
Coulomb Log	15
Ratio of Cooling Length to Ring Length, η	.02
BOLCIF (Eq. (4.19))	10.0
BOTCIF (Eq. (4.18))	1.5

Table 4.10 -- Results of Cooling Time Calculation Including IBS

First Method

Integration Time Step	$\Delta p/p$ at Equilibrium	Cooling Time	Final ε Achieved
.01 sec	7.5×10^{-7}	2291 sec	0.294 π mm-mr
.05 sec	7.5×10^{-7}	2373 sec	0.294 π mm-mr
.05 sec	1.0×10^{-6}	2311 sec	0.272 π mm-mr
.05 sec	1.0×10^{-5}	1968 sec	0.142 π mm-mr
.05 sec	3.0×10^{-5}	1865 sec	0.0976 π mm-mr
.05 sec	1.0×10^{-4}	1789 sec	0.0554 π mm-mr
.05 sec	2.0×10^{-4}	1726 sec	Inside Electron Distribution
		No IBS	
.05 sec		1631 sec	

Program EMIT2 indicates that IBS will increase the cooling time. The program has been run assuming several values of $\Delta p/p$. At the beginning of the electron cooling process $\Delta p/p = 2.0 \times 10^{-4}$, while at thermal equilibrium $\Delta p/p = 7.5 \times 10^{-7}$. The convergence of the code is such that the cooling time decreases as the integration step size is decreased, so in no possible case is the cooling time greater than 2300 sec. Also, an attempt has been made to overestimate the effect of IBS everywhere in this analysis -- this result represents an upper bound on the cooling time. The final values of emittance reached by this code are also arrived at by overestimating IBS, and the real emittance achievable will be lower than the values presented.

Including IBS in the Cooling Time Calculation -- Simulation Two -- A second computer simulation of the effect of IBS on the cooling uses that particle which cools the slowest, the particle with transverse and longitudinal velocities equal to the maximum of the defined beam. The emittance of the beam is then defined by this particle's transverse velocity using Eq. (4.22), and the $\Delta p/p$ of the beam is defined by this particle's longitudinal velocity by Eq. 3.6.

IBS is then calculated from these quantities and the particle is cooled to equilibrium. The results of this program are given in Table 4.11. (This code is a modification of the one presented in Appendix 6.)

Table 4.11 -- Results of Cooling Time Calculation Including IBS

Second Method

Integration Time Step	Final $\Delta p/p$ Achieved	Final ε Achieved	Cooling Time
.05 sec	1.70×10^{-4}	0.043 π mm-mr	1764 sec
.01 sec	1.70×10^{-4}	0.043 π mm-mr	1760 sec

Conclusion -- The two programs show that in no case should the cooling time exceed 35 minutes, and that in all probability the upper bound is actually around 30 minutes. No conclusion should be reached about the final equilibrium value of emittances from this analysis, as it overestimated the effect of IBS in order to get an upper bound on the cooling time and was not intended to predict the final equilibrium.

Chapter Five -- Expected Performance of the Device -- Final Antiproton Emittances

5A -- Focusing the Electron Beam -- Effective Temperature Increase

To determine the final equilibrium obtained between electron cooling and intrabeam scattering a different investigation of the cooling force must be done. In Chapter Four all effects are investigated for the case where the antiproton velocity is well outside the electron velocity distribution, since it is in this region that the dominant contribution to the cooling time is made. It will be shown in section 5c that equilibrium between the two beams will take place with the antiproton velocity distribution very near the electron velocity distribution and so the cooling force will need an accurate assessment in a new range of possible velocities.

Focusing the electron beam increases the number density of the electrons, but also increases the electron beam temperature. The increase in temperature comes from two effects -- space charge and emittance expansion. Focusing the beam to a small waist increases the space charge forces, which increases the beam divergence. Focusing the beam also increases the angular divergence of the beam due to conservation of phase space area.

Emittance Expansion of the Beam -- The transverse emittance of a beam is given by the following expression:

$$\varepsilon = \pi \cdot x \cdot x' \tag{5.1}$$

Since this quantity is an invariant of the electron beam, focusing the electron beam to increase the number density of electrons will increase the angular divergence of the beam. The angular divergence (and therefore the temperature) of the electron beam is easily

calculated by Eq. (5.1) for any waist radius once the beam emittance is known. The temperature of the electron beam is the temperature of the beam at the cathode times the radius of the beam at the cathode divided by the radius of the waist:

$$T_{eff} = T_{cathode} \times \frac{R_{cathode}}{R_{waist}} \tag{5.2}$$

Space Charge Expansion of the Beam -- The fact that the electron beam interacts with itself due to space charge leads to beam size expansion. This expansion causes the electron velocity distribution to have an increase in rms transverse velocity over that of a beam expanding due to emittance alone.

The angular divergence from a waist can be calculated for the Pelletron electron beam by using the program TRAN2. (This code is used in the emittance measurement and presented in Appendix 1. The code is a numerical integration of the beam Twiss parameters.) Figure 5.1 presents the results of simulations for two beam expansions from a waist of 6 mm. The lower of the two curves is a calculation which does not include the space charge force, while the upper curve includes both space charge and emittance in the simulation. While Figure 5.1 indicates that the expansion of the beam is much larger when space charge expansion is taken into account, this does not mean that the temperature of the beam due to space charge expansion is much larger than the temperature of the beam due to emittance alone. The increase in the angular divergence of the beam caused by the space charge force must be compared with the known angular divergence of the beam due to emittance. (Given by Eq. (5.1).)

During electron cooling, solenoids keep the electron beam focused to an appropriate radius. The electron beam will be focused to a waist 0.5 meters after each solenoid and expand from that waist for another 0.5 meters before it is again refocused. The program TRAN2 will find the average value of the divergence of the beam envelope as

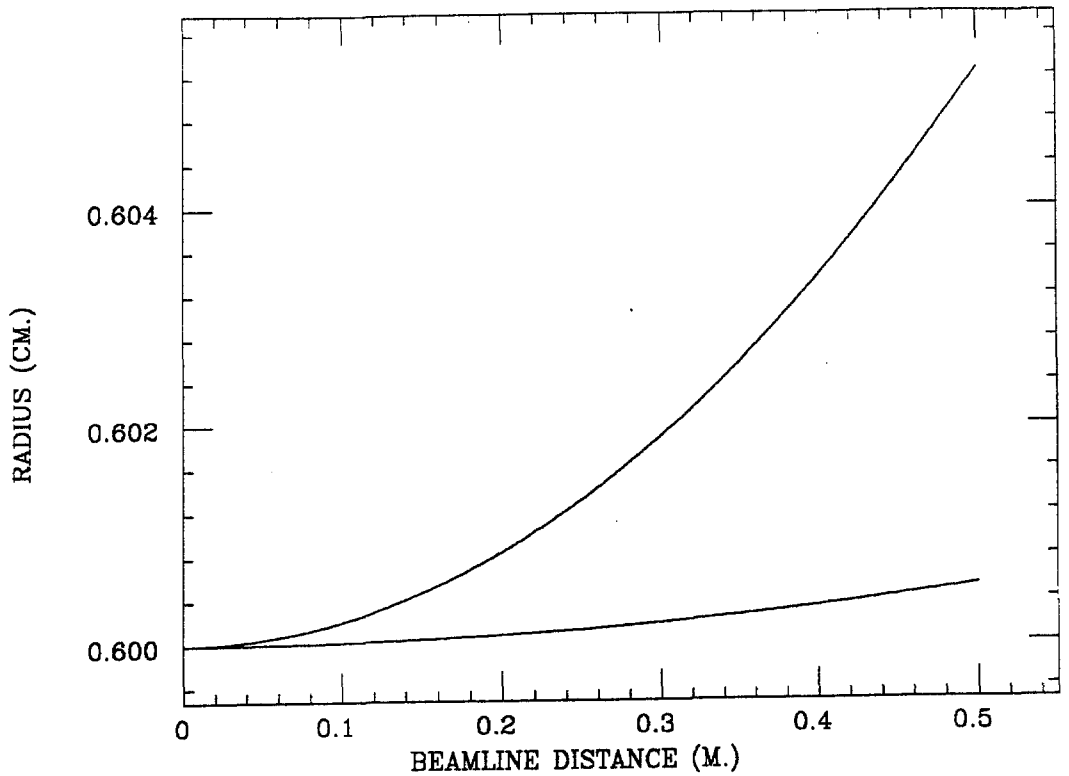

Figure 5.1 -- Electron beam expansion from a waist with and without space charge.

it expands from such a waist. Since this is the average divergence of the beam edge, the divergence averaged over all electrons within the beam is the square root of two less. The results of the code are presented in Table 5.1 for varying values of the assumed waist size. (For the table the expansion of the beam due to emittance is eliminated from the analysis by setting the input emittance to a very small value.) Table 5.2 presents the angular velocity of the electrons due to emittance alone for various values of waist radius. (Calculated from Eq. (5.1).) The angular divergence presented in Table 5.1 is an average over all the electrons of the beam, while the angular divergences presented in Table 5.2 are the angular divergences

of that electron which represents the outer edge of the velocity distribution.

Conclusion -- As can be seen from Tables 5.1 and 5.2 the increase of the electron temperature due to space charge expansion of the beam is a negligible effect. Much more serious is the effect focusing has on the electron temperature due to the invariant emittance.

Table 5.1 -- Electron Beam Transverse Velocity Increase Due to Space Charge Expansion of the Beam

Waist Radius(mm)	Simulated Beam Emittance (m)	Angular Divergence (radians)
10.0	4.04e-10	8.34e-6
6.0	4.04e-6	2.73e-5
6.0	4.04e-8	1.39e-5
6.0	4.04e-10	1.39e-5
1.0	4.04e-10	8.25e-5
0.5	4.04e-12	1.60e-4
0.1	4.04e-8	6.29e-4
0.1	4.04e-10	5.52e-4
0.1	4.04e-12	5.52e-4

Table 5.2 -- Electron Beam Transverse Velocity Due to Emittance Alone

Waist radius (mm)	Angular Divergence (radians)
10.0	1.25e-4
6.0	2.08e-4
1.0	1.25e-3
0.5	2.50e-3
0.1	1.25e-2

5B -- Cooling Force Near Equilibrium -- Electron Temperature Effect

Since the cooling force must now be investigated near (and possibly within) the electron velocity distribution, it is now necessary to present and use the 'Coulomb Analogy' of the electron cooling process.

The Coulomb Analogy -- The electron cooling friction force exerted on an antiproton traversing an electron cloud,

$$F_{cooling} = m_p \frac{dv_p}{dt} = m_p 4\pi N r_e r_p \Lambda \eta c^4 \int_{\vec{v}_e} \frac{g(v_e)dv_e}{(v_p - v_e)^3}(\vec{v}_p - \vec{v}_e) \ , \qquad (5.3)$$

is identical in form to the coulomb force exerted on a charged particle from a cloud of oppositely charged particles,

$$F_{coulomb} = m_p \frac{dv_p}{dt} = K_{coulomb} \int_{\vec{r}_e} \frac{g(r_e)dr_e}{(r_p - r_e)^3}(\vec{r}_p - \vec{r}_e) \ , \qquad (5.4)$$

where $K_{coulomb}$ is a constant which depends on choice of units.

The fact that the two processes are identical mathematically (except for a constant) allows a simplification in some of the analysis by treating the analogous coulomb problem. The force of a cloud of charge attracting an oppositely charged particle depends on variables in coordinate space, while the electron cooling force is a function of variables in velocity space.

In the case of intermediate energy electron cooling there exists an ellipsoidal electron velocity distribution with one of the axes much smaller than the other two. In the limit where the smaller axis is zero, the distribution becomes a disc. Far away from the disc (the antiproton velocity is much larger than the maximum electron velocity) the attraction of the disc will the same as that of a 'point charge'.

(A point charge corresponds to a delta function in velocity, that is, a perfectly cold electron beam.) In the large distance limit the attraction to the disc is only a function of distance from the disc and does not depend on the angle formed between the antiproton velocity vector and the axis of the disc.

Near the disc the force is no longer independent of the angle made between the axis of the disc and the direction of the particle's velocity vector. Those particles with velocity vector on the axis of the disc will experience a much smaller force than what they would have had the electron distribution been a delta function at the origin. Very near the disc, the attraction to the disc will be the same as that of a sheet of charge, that is, the force will tend toward a maximum value and not increase indefinitely as it would for a point charge.

Those particles near the edge of the disc (those particles with velocity vector perpendicular to the axis of the disc) will experience a force larger than the force caused by a delta function -- a larger 'charge' is now on average closer to the particle.

Calculation of the Temperature Effect -- In Section 4c the effect of the electron temperature is investigated and is found to have no influence on the cooling time. The finite velocity spread enhances the force felt by an antiproton that has a transverse velocity near that of the maximum electron velocity, agreeing with the qualitative prediction of the coulomb analogy.

For the calculations presented in Section 4c the electron beam velocity distribution is assumed to be uniform over a three dimensional ellipsoid in velocity space. The axes of the ellipsoid are set equal to the standard deviations of the expected gaussian distribution. Outside this ellipsoid the electron density is assumed to be zero. In the cooling time calculation electron temperature has no important effect, and so this model for the electron velocity distribution is valid. In the present analysis the same uniform density model will be used to determine the approximate equilibrium.

Table 5.3 repeats the results of Section 4c for the effect that finite electron beam temperature has on the transverse cooling force, while Table 5.4 presents the longitudinal results. The code used in this analysis is again the code EMIT2 presented in Appendix 4 (used in the analysis of Section 4c). Table 5.4 shows that the use of the coulomb analogy gives the correct qualitative result for the effect of finite electron beam temperature on the longitudinal force -- the force approaches a constant as the antiproton gets closer to the electron disc. The code simulates a cloud of electron velocities by dividing up the total 'charge' into a number of delta functions. The convergence of the code is checked as the number of delta functions is increased. (This is a three dimensional numerical integration done by the method of Riemann sum.)

For a single delta function electron velocity distribution the longitudinal cooling force may be obtained analytically.

$$\frac{d\left(\frac{\Delta p}{p}\right)}{dt} = \frac{K}{(\beta)^3\left(\frac{\Delta p}{p}\right)^2} \tag{5.5}$$

where $K = 4\pi N r_e r_p \Lambda \eta c$.

The ideal transverse cooling force may also be found analytically.

$$\frac{d\varepsilon_x}{dt} = K' \frac{(\theta_x)^2}{[(\theta_x)^2 + (\theta_z)^2 + (\frac{\Delta p}{\gamma p})^2]^{3/2}} \text{ (ideally)} \tag{5.6}$$

where $K' = \frac{2\pi\beta_{twiss}K}{\beta^3\gamma^3}$.

Tabulation of the Computed Effect of the Finite Temperature -- In the mass of data that follows a few words may help to clarify the situation. Tables 5.3 and 5.4 present the force as a function of antiproton velocity and integration step size. The convergence of the program is noted as the number of points used in the integration is increased (the step size is decreased). The values of the force associated with one delta function are calculated analytically from Eqs. (5.5) and (5.6). The effect of the finite temperature can be noted by comparing the converging value to the analytic value.

Table 5.3 -- The Transverse Electron Cooling Force as a Function of the Transverse Antiproton Velocity

θ_x	Number of Delta Functions	The Force, $d\varepsilon/dt$
	The Onset of Cooling	
6.251E-04	1	1.327E-08
6.251E-04	8	1.331E-08
6.251E-04	4094112	1.330E-08
	The Midpoint of Cooling	
3.125E-04	1	2.655E-08
3.125E-04	8	2.688E-08
3.125E-04	4094112	2.683E-08
	Just About Done	
6.633E-05	1	1.251E-07
6.633E-05	8	1.208E-07
6.633E-05	29752	1.815E-07
6.633E-05	4094112	1.884E-07
6.633E-05	112247560	1.894E-07

Table 5.4 -- The Longitudinal Electron Cooling Force as a Function of the Longitudinal Antiproton Velocity

$\Delta p/p$	The Force, $\frac{d(\Delta p/p)}{dt}$	Number of Delta Functions
	The Onset of Cooling	
2.00e-4	3.269E-03	1
2.00e-4	6.344E-04	112247560
2.00e-4	6.290E-04	4094112
2.00e-4	5.538E-04	3280
2.00e-4	2.526E-04	8
	The Midpoint of Cooling	
1.00e-4	1.308E-02	1
1.00e-4	8.089E-04	4094112
1.00e-4	5.820E-04	3280
1.00e-4	1.571E-04	8
	Near Equilibrium?	
5.00e-5	5.230E-02	1
5.00e-5	8.794E-04	4094112
5.00e-5	4.302E-04	3280
5.00e-5	8.339E-05	8
	Just About -- Or Maybe Past -- Done	
4.00e-5	8.172E-02	1
4.00e-5	9.4394E-04	112247560
4.00e-5	8.7104E-04	4094112
4.00e-5	3.668E-04	3280
4.00e-5	6.721E-05	8
3.00e-5	1.453E-01	1
3.00e-5	8.018E-04	4094112
3.00e-5	2.900E-04	3280
3.00e-5	5.069E-05	8

Electron Cooling of Antiprotons Within the Electron Velocity Distribution -- When the antiproton beam has been cooled to the point that the antiproton velocities are within the electron velocity distribution the cooling force will begin to drop off. At this point the coulomb analogy becomes useful. For the case of a uniform sphere of charge, the force drops off linearly to zero as the particle's position moves toward the center of the distribution. For the case of an infinite slab of charge, the force drops to zero as the particle's position moves to the central plane of the distribution. In the case of intermediate energy electron cooling the ellipsoidal velocity cloud is somewhat in between these two cases, but the assumption will be made that the force drops linearly to zero as the antiproton velocity goes to zero. (The force on a particle at the center of the distribution will be zero). The force will be evaluated near the edge of the electron velocity distribution and then scaled in this fashion. Since a rough estimate of the result is desired, this treatment should be adequate.

Effect of Electron Beam Focusing -- The analysis of the problem done in this section calculates the effect of an electron beam velocity of $v/c = 6.6\times10^{-4}$. This velocity is somewhat greater than one standard deviation of the transverse velocity of the electrons at the cathode. It is shown in Section 5a that focusing the beam to match the antiproton beam size of 6mm. will increase the standard deviation of the electron transverse velocity distribution up to $v/c = 1\times10^{-3}$. This increase in transverse velocity increases the size of the velocity disc. Using the coulomb analogy this will decrease the density of the effective sheet of charge, and the longitudinal cooling force (near the disc) will be decreased in direct proportion to the increase in the area of the disc. This scaling law is used to calculate the force under different possible electron temperatures.

In the next section ideal cooling rates will be derived for the case of a perfectly cold electron beam. The effect of finite temperature will be included by multiplying the ideal cooling rates by an appropriate ratio. Table 5.6 presents the ratio of the

longitudinal cooling force including electron temperature to the longitudinal force of a perfectly cold electron beam for the cases of 6 and 10 mm. beam sizes (as determined from Table 5.4). Table 5.5 gives the same ratio for the transverse cooling force.(as determined from Table 5.3). The values presented in Tables 5.5 and 5.6 are somewhat arbitrary in that I have chosen a value to which the calculation seems to be converging, I do not use the last computational run in forming the ratios.

Table 5.5 -- Ratio of Transverse Cooling Force Including Electron Temperature to the Ideal Cooling Force

$\beta_\perp$	ratio
6.251E-04	1.0
3.125E-04	1.0
6.333E-05	1.5

Table 5.6 -- Ratio of Longitudinal Cooling Force Including Electron Temperature to the Ideal Cooling Force

$\Delta p/p$	Ratio 1 (10mm. Electron Beam)	Ratio 2 (6mm. Electron Beam)
2.00E-04	0.2	.072
1.00E-04	0.073	0.026
5.00E-05	0.019	0.007
3.00E-05	1/135	1/330

5C -- Final Antiproton Emittances -- Equilibrium With Intrabeam Scattering

In this section the equilibrium between the competing processes of electron cooling and intrabeam scattering (IBS) will be investigated. The definition of equilibrium is presented first, followed by a derivation of electron cooling rates in a form which allows comparison with the predicted IBS rates. The initial assumption will be that the electron beam used for electron cooling will be a perfectly cold beam. These ideal electron cooling rates will be presented in a table along side the growth rates predicted for IBS. Next, the assumption of a perfectly cold electron beam is examined. This is followed by a semiquantitative analysis of where equilibrium will take place. The analysis uses the coulomb analogy presented in the last section. A few comments are given as to the form of the final distribution function and the effect that electron cooling and IBS have on the different parts of that distribution. Lastly, the scaling of the equilibrium with various beam parameters is discussed.

Definition of Equilibrium -- The IBS calculations of Bjorken and Mtingwa (BM)[5.1] have been done under the assumption of a gaussian distribution of antiproton velocities. The fact that the emittance of the beam grows in time is evidence that IBS is heating the beam. The assumption of BM is that the beam remains gaussian in shape after the heating. The work done on IBS gives the emittance growth rates of an antiproton beam, and says nothing about what is happening to the individual particles during the heating. Electron cooling, on the other hand, is calculated for the cooling of individual particles within the beam but does not infer what is happening to the velocity distribution function. In order to find equilibrium the two processes must be put on similar footing.

The same dilemma is encountered in the cooling time calculation presented in Section 4e, and a similar tack will now be applied in this section. 1) The emittance of a particle is defined by its CLS invariant[5.2]. 2) The emittance of a single reference particle is set

equal to the emittance of the beam (here the BM definition of emittance is used, $\varepsilon = \sigma^2/\beta_{Twiss}$). 3) Equilibrium is defined to exist when the electron cooling rate of the reference particle equals the IBS heating rate of the beam. 4) Equilibrium will be found separately for the transverse and longitudinal emittances. 5) A self consistent calculation between the two cases will determine where equilibrium exists.

Ideal Electron Cooling Rates -- In the work of BM the growth rates due to intrabeam scattering are given as functions of the transverse and longitudinal emittances of the antiproton beam. The beam velocity distribution is assumed to be gaussian in all three dimensions, with the standard deviations of the gaussians defined to be the emittances of the beam. The transverse velocity distribution function is then:

$$f(v) = \exp\left[-\left(\frac{v_\perp^2}{\varepsilon_\perp} + \frac{v_\parallel^2}{\sigma^2}\right)\right] . \tag{5.7}$$

Where $\varepsilon_\perp$ is the transverse beam emittance and σ is the longitudinal beam emittance.

The IBS growth rates are defined by the inverse of the time it takes for the beam emittance to grow by a factor of 1/e.

$$\frac{1}{\varepsilon}\cdot\frac{d\varepsilon}{dt} = K1(\varepsilon,\sigma) , \tag{5.8}$$

$$\frac{1}{\sigma^2}\cdot\frac{d\sigma^2}{dt} = K2(\varepsilon,\sigma) , \tag{5.9}$$

$(\sigma \equiv \Delta p/p)$.

The electron cooling rate equation should be in a similar form if it is to be compared with IBS. For the ideal case we use Eq. (4.8) along with the definition of ε to arrive at a formula which expresses the transverse electron cooling rate as a function of ε and σ.

$$\frac{d\varepsilon_x}{dt} = K' \frac{\theta_x^2}{(\theta_x^2 + \theta_z^2 + (\Delta p/\gamma p)^2)^{3/2}} , \tag{5.10}$$

where $K' = \dfrac{2\pi\beta_{Twiss}K}{4\pi^2\beta^3\gamma^3}$, and $K = \dfrac{4\pi N e^4 \Lambda\eta}{m_e m_p}$.

$$\frac{1}{\varepsilon}\cdot\frac{d\varepsilon}{dt} = \frac{2K}{4\pi^2\beta^3\gamma^3(\theta_x^2 + \theta_z^2 + (\Delta p/\gamma p)^2)^{3/2}} \tag{5.11}$$

Eq. (4.10) is used to obtain the longitudinal electron cooling rate as a function of ε and σ.

$$\frac{1}{\sigma^2}\cdot\frac{d\sigma^2}{dt} = \frac{2}{\sigma}\cdot\frac{d\sigma}{dt} = \frac{2K}{4\pi^2\beta^3\gamma^3(\theta_x^2 + \theta_z^2 + (\Delta p/\gamma p)^2)^{3/2}} \tag{5.12}$$

The equation for the cooling rate of the transverse emittance is the same as the equation for the cooling rate of the longitudinal emittance in the ideal case. The code COOLTIMEE (presented in Appendix 7) is used to evaluate the ideal electron cooling rates (using Eq. (5.11)). The input parameters for the code are presented in Table 5.7 and the matrix of the results is presented in Table 5.8. The transverse and longitudinal IBS heating rates are presented in Tables 5.9 and 5.10.[5.3]

Table 5.7 -- Input Parameters for Calculating Electron Cooling Rates

Electron Current	4.0 A.
Antiproton Current	0.041 A.
Electron Beam Radius	.006 m.
Gamma (Relativistic)	10.
Coulomb Log	15.
Eta	.02
Beta(Twiss)	10.

Table 5.8 -- Ideal Electron Cooling Rates -- Electron Beam Radius = 6mm

ε/π	2.27e-11	1e-10	1e-9	1e-8	3.63e-8	1e-7	1e-6
$\Delta p/p$							
7.5e-7	.242E9	.262E8	.829E6	.262E5	.379E4	.829E3	.262E2
1e-6	.241E9	.262E8	.829E6	.262E5	.379E4	.829E3	.262E2
1e-5	.140E9	.227E8	.817E6	.262E5	.379E4	.829E3	.262E2
3e-5	.219E8	.100E8	.729E6	.259E5	.378E4	.828E3	.262E2
5e-5	.582E7	.401E7	.593E6	.253E5	.375E4	.826E3	.262E2
1e-4	.802E6	.719E6	.293E6	.227E5	.364E4	.817E3	.262E2

Table 5.9 -- Intrabeam Scattering Longitudinal Heating Rates

ε/π	.23e-10	.1e-9	.1e-8	.1e-7	.36e-7	.1e-6	.1e-5
$\Delta p/p$							
.75e-6	.562e11	.761e10	.273e9	.897e7	.131e7	.287e6	.911e4
.1e-5	.308e11	.423e10	.153e9	.504e7	.735e6	.161e6	.512e4
.1e-4	.740e8	.191e8	.115e7	.462e5	.703e4	.157e4	.508e2
.3e-4	-.698e6	.479e6	.706e5	.412e4	.696e3	.163e3	.553e1
.5e-4	-.703e6	.188e5	.154e5	.121e4	.223e3	.548e2	.195e1
.1e-3	-.194e6	-.179e5	.121e4	.193e3	.426e2	.115e2	.462e0

Table 5.10 -- Intrabeam Scattering Transverse Heating Rates

ε/π	.23e-10	.1e-9	.1e-8	.1e-7	.36e-7	.1e-6	.1e-5
$\Delta p/p$							
.75e-6	.372e10	.118e9	.432e6	.142e4	.571e2	.455e1	.144e-1
.1e-5	.354e10	.116e9	.430e6	.142e4	.570e2	.455e1	.144e-1
.1e-4	.950e9	.469e8	.296e6	.128e4	.542e2	.441e1	.143e-1
.3e-4	.369e9	.187e8	.154e6	.958e3	.468e2	.406e1	.140e-1
.5e-4	.233e9	.120e8	.103e6	.745e3	.402e2	.371e1	.136e-1
.1e-3	.123e9	.640e7	.573e5	.468e3	.289e2	.296e1	.128e-1

<u>Where Finite Electron Beam Temperature Becomes Important</u> -- Assuming no emittance growth of the electron beam from the cathode, and also assuming an electron beam waist radius of 6mm., the standard deviation of the electron beam transverse velocity distribution is $\beta_\perp = 1\times10^{-3}$. (An antiproton beam of emittance 0.1π mm-mr has a standard deviation of the antiproton velocity distribution equal to $\beta_\perp = 1\times10^{-3}$.) Longitudinally the electron beam emittance is $\Delta p/p = 3\times10^{-5}$. The effect that the electron beam temperature has on the cooling rates is presented in Section 5b for these electron beam parameters.

The results presented in Table 5.8 for the rate of decrease of the transverse and longitudinal emittances of an antiproton are arrived at by making the assumption that the electron beam is perfectly cold. As is shown in Section 5b, this assumption fails in two respects: 1) The effect of the electron beam temperature is very strongly felt on an antiproton with longitudinal velocity only, reducing the force by a factor of 140 when $\Delta p/p = 5\times10^{-5}$. 2) Once the antiproton velocity is within the electron velocity distribution the force drops to zero as the antiproton velocity goes to zero.

The diffusion caused by the finite electron beam temperature becomes important only when the two beams are close to thermal equilibrium. Since (as will be shown) the beams do not get close to thermal equilibrium this effect is unimportant.

Equilibrium Transverse Emittance -- a Rough Estimate -- In order to account for the effect of the finite electron beam temperature an analysis will be done using the model presented in Section 5b. (Section 5b defines the electron beam to be a four ampere beam with a uniform velocity distribution over a three-dimensional ellipsoid in velocity space. The axes of the ellipsoid are defined to be equal to one standard deviation of the expected gaussian electron velocity distribution.)

At a transverse emittance of 0.1π mm-mr the standard deviation of the antiproton beam transverse velocity distribution matches the standard deviation of the electron beam transverse velocity distribution. Using the coulomb analogy (presented in Section 5b) the transverse cooling rate should decrease linearly to zero with the antiproton velocity once the antiproton velocity is within the electron distribution. Since the emittance is a function of the square of the velocity, the transverse cooling rate will decrease as the square root of the transverse emittance. In Table 5.5 the result is stated that the ellipsoidal velocity distribution enhanced the transverse cooling force by a factor of 1.5. Combining the factor of 1.5 with the result tabulated in Table 5.8 for the ideal cooling rate yields an equation for the cooling rate of antiprotons with emittances less than 0.1π mm-mr.

$$\text{Transverse Cooling Rate } (\text{hr}^{-1}) = \left(\frac{\varepsilon}{0.1\pi \text{ mm-mr}}\right)^{1/2} \times .125\times10^{4} \qquad (5.13)$$

(The above equation holds only for $\varepsilon < 0.1\pi$ mm-mr.)

By using Eq. (5.13) it is seen that the cooling rate for a antiproton of emittance 0.01π mm-mr is $.395\times10^{3}\text{hr}^{-1}$. For an antiproton of emittance 0.036π mm-mr the cooling rate will be $.750\times10^{3}$. By comparing the IBS heating rates as given in Table 5.10 with these cooling rates an estimate for the transverse equilibrium is determined.

The transverse equilibrium emittances should be about $\pi\sigma^2/\beta_{Twiss}$ = 0.02π mm-mr, or by the FNAL definition, $\varepsilon = 0.12\pi$ mm-mr.

Equilibrium Longitudinal Emittance -- a Rough Estimate -- At a longitudinal emittance of $\Delta p/p = 3\times10^{-5}$ the standard deviation of the antiproton beam longitudinal velocity distribution matches the standard deviation of the electron beam longitudinal velocity distribution. By once again making use of the coulomb analogy it is clear that the longitudinal cooling rate should decrease linearly to zero with the antiproton velocity once the antiproton velocity is within the electron distribution. The longitudinal velocity scales linearly with $\Delta p/p$, so the longitudinal cooling force will decrease linearly with $\Delta p/p$ once the antiproton is within the electron longitudinal velocity distribution. In Table 5.6 the result is stated that the ellipsoidal velocity distribution reduced the longitudinal cooling force of an antiproton with $\Delta p/p = 3\times10^{-5}$ by a factor of 330. Combining the factor of 330 with the result tabulated in Table 5.8 for the ideal cooling rate yields an equation for the cooling rate of antiprotons with $\Delta p/p$ less than 3×10^{-5}. (The ideal cooling rate is the rate corresponding to $\Delta p/p = 3\times10^{-5}$ and no transverse emittance.)

$$\text{Longitudinal Cooling Rate } (\text{hr}^{-1}) = \frac{\Delta p/p}{3\times10^{-5}}\times.930\times10^{5} \qquad (5.14)$$

(The above equation holds only for $\Delta p/p < 3\times10^{-5}$.)

By using Eq. (5.14) it is seen that the cooling rate for a antiproton of $\Delta p/p = 1\times10^{-5}$ is $.310\times10^{5}\text{hr}^{-1}$. For an antiproton of $\Delta p/p = 1\times10^{-6}$ the cooling rate will be $.310\times10^{4}\text{hr}^{-1}$. By comparing the IBS heating rates as given in Table 5.9 with these cooling rates an estimate for the transverse equilibrium is determined.

The longitudinal equilibrium emittance should be about 1×10^{-5}.

Comments About the Shapes of the Velocity Distribution Functions -- For the rough estimates arrived at in the above analysis the electron velocity distribution function is assumed to be uniform over an ellipsoid. Using this model the effect of electron cooling and IBS on several points within the antiproton velocity distribution can be investigated. For IBS heating the following equation is used:

$$\frac{1}{\varepsilon}\times\frac{d\varepsilon}{dt} = K(\varepsilon,\sigma) \tag{5.15}$$

The emittance of a single particle is proportional to the square of the particle velocity.

$$\frac{1}{v}\times\frac{dv}{dt} = K'(\varepsilon,\sigma) \tag{5.16}$$

Since the work done on IBS was not intended to be applied to individual antiproton trajectories, it is not obvious that Eq. (5.15) should hold for all of the trajectories within the antiproton beam. However, it will now be demonstrated that while each trajectory may not directly obey the growth formula given by Eq. (5.16), there does exist a one to one mapping of trajectories which do obey Eq. (5.16).

Random diffusive properties leave a distribution function in a gaussian. We start at time t = 0 with a gaussian transverse velocity distribution with standard deviation σ.

$$f(v) = \exp\left\{\frac{-v^2}{2\sigma^2}\right\} \tag{5.17}$$

If the emittance of the particle is defined to be $\varepsilon_p = \beta_{Twiss}\times\theta^2$, Eq. 5.17 can be written in terms of emittance.

$$f(\varepsilon_p) = \exp\{\frac{-\varepsilon_p}{\varepsilon_b}\}, \text{ where } \varepsilon_b \text{ is the beam emittance} \tag{5.18}$$

After some time dt the emittance of the beam expands by Eq. (5.15), leaving the beam in a new gaussian with $\varepsilon_b' = \varepsilon_b + \Delta\varepsilon$. If we map that antiproton trajectory which is at one standard deviation before the heating to that antiproton trajectory at one standard deviation after the heating, it has increased in emittance by $\Delta\varepsilon$. Similarly, that antiproton at two standard deviations before the heating can be mapped to that antiproton at two standard deviations after the heating and its emittance has increased by $2\times\Delta\varepsilon$. This mapping can be done for the entire distribution with the result that $\Delta\varepsilon = K\times\varepsilon$, that is, Eq. (5.15), leading to Eq. (5.16).

Using the coulomb analogy the electron cooling force on an antiproton with a velocity within the electron velocity distribution increases linearly with the antiproton velocity.

$$\frac{dv}{dt} = K2\times v \tag{5.19}$$

or

$$\frac{1}{v}\times\frac{dv}{dt} = K2$$

In the rough estimate on where equilibrium exists, equilibrium is defined to exist when the cooling rate of an antiproton with velocity equal to one standard deviation of the antiproton velocity distribution equals the IBS heating rate of that beam. In terms of Eqs. (5.16) and (5.17) this is equivalent to the statement that $K' = K2$. By looking at the form of both Eqs. (5.16) and (5.17) it is clear that the equilibrium will exist for all antiproton trajectories which have a velocity within the electron velocity distribution.

(The above statement applies for the case where each antiproton trajectory is individually heated due to IBS by the amount given in Eq. (5.16). Since diffusion is a random process this does not actually occur. However, on average the individual particles will be scattered by the amount given by Eq.(5.16).)

Outside the electron velocity distribution Eq. (5.19) is no longer valid, and the 'equilibrium' will no longer exist. The antiproton velocity distribution function outside the electron velocity distribution will not be gaussian. Since the electron velocity distribution has a standard deviation three times larger than the standard deviation of the antiproton velocity distribution function most of the antiprotons will be inside the electron distribution. The effect is a longer tail of the antiproton distribution. (The longer tail is a result of the cooling force falling off as the velocity increases once the antiproton velocity is outside the electron velocity distribution.)

Another problem with the above analysis is that the electron velocity distribution function is not uniform over an ellipsoid, it is gaussian. The effect that this should have on the distribution function should be to make the core of the antiproton distribution function a bit steeper than a gaussian and the tail a bit longer than a gaussian. This is a result of the higher density of electrons near the core of the electron distribution function causing a higher force at the core than the uniform distribution model would indicate. The fact that some electrons exist outside the ellipse used in the uniform density model will cause some shortening in the far end of the distribution's tail over that expected by the uniform density model.

All of these effects should not greatly change the expected equilibrium from the value estimated by the rough calculation above.

Effect of Parameter Changes on the Equilibrium -- The electron cooling force (and therefore the electron cooling rate) scales linearly with the current of the electron beam. For electron beam currents other than 4A a new cooling rate can be determined by multiplying the cooling rates given in Table 5.8 by the ratio of the

new current to 4A. The new rate can then be compared to the IBS rates to determine the new equilibrium.

The longitudinal cooling rate depends linearly upon the transverse emittance of the electron beam. This can be most easily seen by invoking the coulomb analogy. Increasing the transverse velocity of the electron distribution increases the radius of the velocity disc. The force scales with the square of the radius of the disc, since the charge density of the disc scales as the inverse of the area of the disc. Since the emittance of the electron beam also scales as the square of the electron velocity, the electron cooling rate will scale linearly with the electron beam emittance. The increase in the transverse temperature of the electron beam will cause the transverse cooling rate to fall as well, since the antiproton velocity will now enter the electron velocity distribution sooner, and the force will drop linearly to zero with the antiproton velocity from there.

An emittance growth of the electron beam by a factor of two to three will not have much effect on the final equilibrium. Since the cooling forces scale linearly with the antiproton velocity within the electron distribution, any enlargement of the equilibrium antiproton emittance causes an increase in the cooling rate. This helps to mitigate against any large changes in the equilibrium values from the values stated above.

The IBS heating rates are linearly dependent on the number of particles in the antiproton beam. Values of antiproton current different than 0.041A (the value assumed here) can be handled by arriving at new IBS rates and comparing them to the cooling rates.

Conclusion -- Intermediate energy electron cooling should reduce the three-dimensional phase space area of the accumulator antiproton beam by a factor of 5.5×10^3. The transverse emittances (x and z) should be reduced from 2π mm-mr to about 0.12π mm-mr. The longitudinal emittance should be reduced from $\Delta p/p = 2\times10^{-4}$ to about 1×10^{-5}. Figure 5.2 shows the effect of electron cooling on the longitudinal velocity distribution. The stochastic cooling profile

shown represents the situation with both the stack tail and core cooling systems operating. If the beam is allowed to be cooled with the core cooling system only, the long stack tail will be pulled into the core of the distribution with no significant increase in longitudinal phase space density.

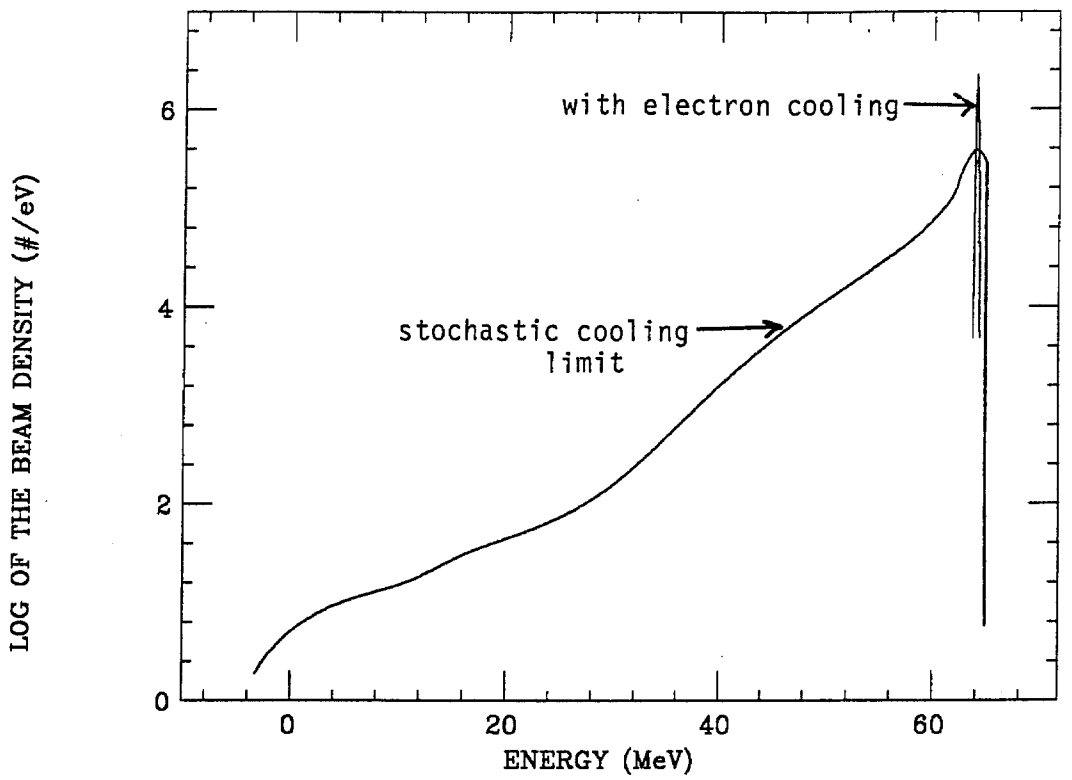

Figure 5.2 -- Antiproton density profile before and after electron cooling.

5D -- Final Antiproton Emittances -- Possible Instabilities

In high density beams many instabilities may arise. The resistive wall instability, otherwise known as the Z/n instability, is the self bunching of the beam caused by the voltage induced on the vacuum walls by image charges. Although much of the science of the origin of instabilities is still incomplete, knowledge of where the instabilities occur has been acquired. This section looks at what the resistance of the accumulator ring must be in order to store an antiproton beam with the emittances estimated in Section 5c.

Longitudinal Stability -- The Keil-Schnell Criterion -- Good references on the problem of longitudinal instabilities are Schnell[5.4] and Hofmann[5.5]. Beams become susceptible to longitudinal instability when the impedance of the storage ring gives rise to voltages large enough to bunch the beam. The larger the ring impedance, the larger will be the voltage generated by a given image current. Bunching occurs more readily for beams with low longitudinal emittance. In low $\Delta p/p$ beams, the particles have frequencies of revolution that are nearly the same and the image forces can constructively interfere causing instability. Figure 5.3 (found in Reference 5.4) shows which regions of impedance are stable for various forms of the antiproton velocity distribution function. The scale of the figure is given by a circle of stability common to all possible distributions. The radius of this circle is given by the Keil-Schnell[5.6] criterion. The Keil-Schnell criterion:

$$\frac{Z}{n} = F\frac{m_p c^2 \beta^2 \gamma \eta (\Delta p/p)^2}{eI_0} \tag{5.20}$$

For the accumulator $\gamma = 10$, $\eta = 0.0245$, $I_0 = 0.041$ A, and $\Delta p/p = 1\times10^{-5}$. This yields a value for Z/n of 0.5 Ohms. From Figure 5.3 it can be noted that the purely resistive component of the impedance can be about twice this size, or about one ohm. Thus the

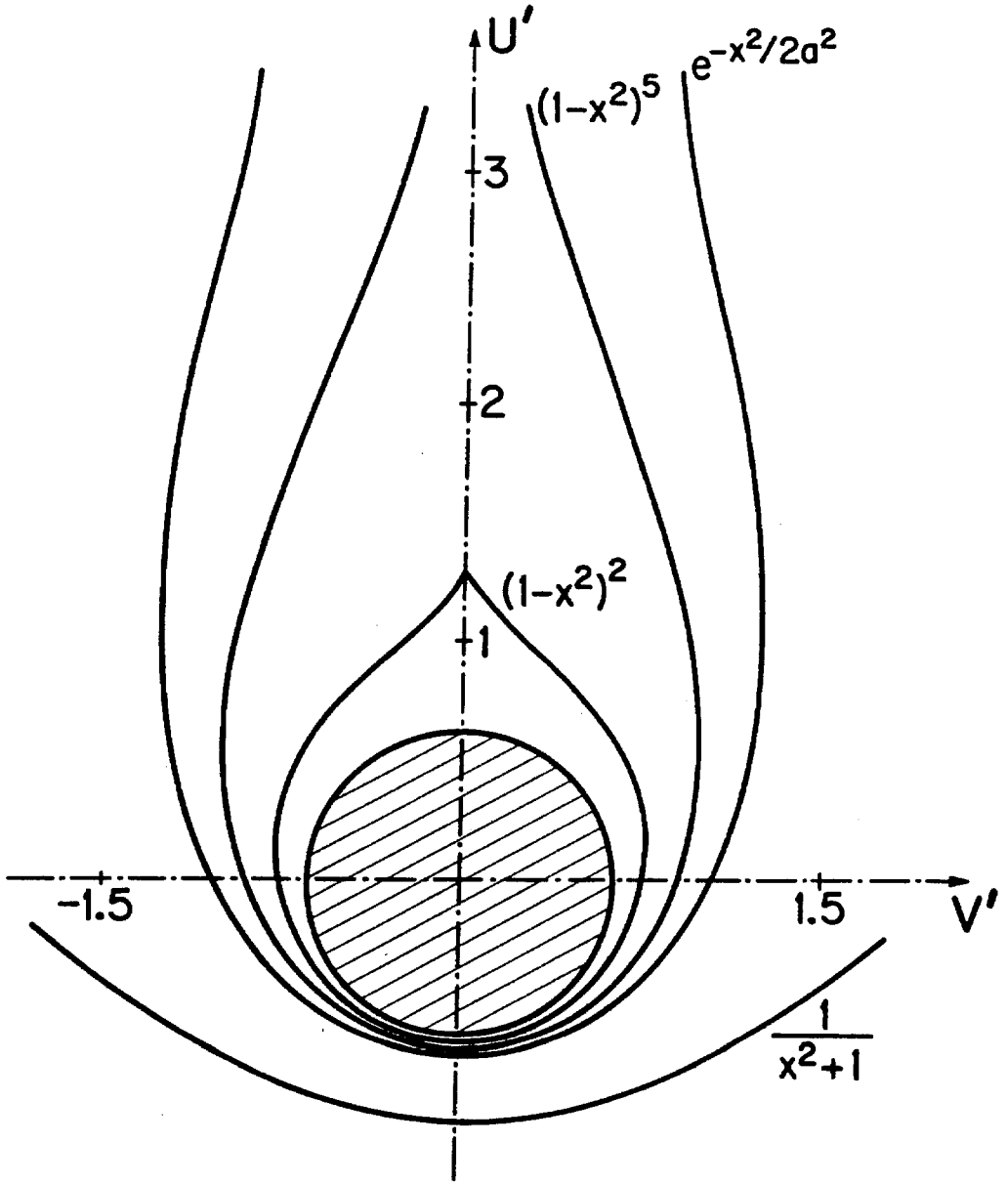

Figure 5.3 -- Regions of beam stability as a function of the complex impedance of a storage ring.

impedance of the accumulator must be on the order of one ohm to be

stable longitudinally. (The actual impedance may be a bit higher, since the electron cooling force will help stabilize operation for the low frequency instabilities.)

Transverse Stability -- At the completion of the stochastic cooling process the lowest existing sideband is unstable against transverse oscillations. After electron cooling is completed it is likely that the first 40 sidebands will prove unstable. The correction for this instability is a damper which has been placed in the ring. This damper may need improvement if the higher beam density made possible by electron cooling is to be realized.

Impedance Estimates -- Estimates of the impedance of the the various structures within the accumulator ring are presented in a p-bar note[5.7]. The results of that note follow.

There are three RF cavities in the ring. Two are narrow band cavities with resistances on band of 500 to 1000 Ω. The third cavity is a broad band cavity of 50 Ω resistance.

The stochastic system has an upper bound to its impedance of around 50 Ω. The impedance is inductive at low frequencies, resistive in band, and capacitive at high frequencies.

A beam profile monitor pickup has a resistance of about 12.5 Ω.

Other broadband impedances result from irregularities in the bellows, and the DC resistance of the stainless steel in the ring. This amounts to about 2 to 3 Ω.

Maximizing the Machine Performance -- The resistance of the RF cavities and the beam profile pickup are much higher than the amount allowed by the Keil-Schnell criterion. These resistances can be lowered by using negative feedback. A monitor must pick up a signal as the beam begins to bunch, and be amplified and sent to the cavities in such a way as to counteract this bunching. This technique was applied in the operation of the Intersecting Storage Rings (ISR) at CERN. The inductive impedance of the stochastic system should

represent no problem, as the inductance can be fairly large without provoking instability. (See Figure 5.3.)

Even with the reduction in impedance made possible by feedback systems the total impedance may still be too large to accommodate beams of $\Delta p/p = 10^{-5}$. What was experienced in the FNAL electron cooling experiment[5.8] was that the beam would cool down to the point where an instability would make it suddenly grow until it got to a point where cooling was once again dominant. In intermediate energy electron cooling it is possible to increase the equilibrium value of the final cool down. If the electron current is reduced a new equilibrium with intrabeam scattering will result. This new equilibrium point can be chosen to make the antiproton beam the coolest possible without provoking instability.

Residual Gas Scattering Effect -- As the antiproton beam traverses the accumulator ring it will diffuse do to Coulomb collisions with residual gas. The emittance growth is proportional to the square of the increase of the rms angular divergence of the beam. (The linear term averages to zero.)

$$\frac{d\varepsilon}{dt} = \beta_{Twiss} \left(\frac{d\Theta^2}{dt}\right) \tag{5.21}$$

The formulas for multiple scattering and radiation length are found in the Particle Properties Data Booklet[5.9]. Growth of the square of the beam rms angular divergence is given by:

$$\Delta(\Theta^2) = \left(\frac{15\ \text{MeV}}{p\beta c}\right)^2 \frac{L}{L_r} \tag{5.22}$$

where $p\beta c = 8$ GeV, and

$$L_r = 3.02\times10^2\text{m at 1 atm} \Rightarrow L_r = 10^{15}\text{m at } 3\times10^{-10}\ \text{Torr}\ . \tag{5.23}$$

Thus,

$$\frac{d\varepsilon}{dt} = \frac{\beta_{Twiss}\beta c}{L_r}\left(\frac{15\ \text{MeV}}{8\ \text{GeV}}\right)^2 = 1\times10^{-11}\text{m/s}. \tag{5.24}$$

Since the transverse equilibrium is expected to be of the order of 5×10^{-7}m the diffusion growth time due to residual gas scattering is on the order of 10,000 s, much larger than the diffusion growth time due to IBS, and therefore is unimportant in the determination of where equilibrium will take place.

Appendix 1 -- Electron Beam Optics in a Transport Line

```
C       PROGRAM TRAN3
C       THIS PROGRAM CALCULATES BEAM RADII BY NUMERICALLY
C       INTEGRATING THE TWISS PARAMETERS
C       IT THEN FINDS THE AVERAGE BEAM DIVERGENCE ANGLE
C       OF THE BEAM OVER THE DISTANCE OF EXPANSION

C       THE VARIABLES

      REAL Z,SOLNO,SOL5,FL5,SOL6,FL6
      REAL SOLE4HI,SOLE4LO,DRDZHI,DRDZLO
      REAL I0,K1,K2,K3,K4,K5,MAG,DRDZ0,RADI0

C                   WE NOW READ IN THE INITIAL VALUES

      OPEN(UNIT=11,TYPE='OLD',FILE='TRAN3IN.DAT')
        READ(11,*)  (K1,K2,K3,K4,K5)
        READ(11,*)  (POS1,POS2,POS3,POS4,POS5)
        READ(11,*)  (EMMIT,COUNTB,RMIN,ERROR,POSEND)
        READ(11,*)  (SOL5,FL5,SOL6,FL6,GAMMAR)
      CLOSE (11)
C       MORE READING OF INITIAL VALUES

      OPEN (UNIT=10,TYPE='OLD',FILE='PELL3IN.DAT')
      READ(10,*)  (RADI0,DRDZ0,I0,E0,PHI0)
      READ(10,*)  (STEP,PELL,COUNTA,EMMIT0)
      READ(10,*)  (SOL1,SOL2,FL1,FL2)
      READ(10,*)  (SOL3,SOL4,FL3,FL4)
      CLOSE (UNIT=10)

C             INITIALIZE TOP DRAWER FILE

      WRITE (12,*)  'SET DEVICE IMGN300'
      WRITE (12,*)  'SET FONT DUPLEX'
      WRITE (12,*)  'TITLE LEFT ''RADIUS (CM.)'' '
      WRITE (12,*)  'TITLE SIZE 2.0'
      WRITE (12,*)  'TITLE BOTTOM ''BEAMLINE DISTANCE (M.)'' '
      WRITE (12,*)  'SET ORDER Y X'
      WRITE (12,*)  '0.0 0.0'
C                   WE NOW SET INITIAL PARAMETERS

      K=0
      J=0
      N=0
222     CONTINUE
      RADI=RADI0
      DRDZ=DRDZ0
      POS=0.0
      SOLNO=0.0
      BETA=((RADI)**2)/EMMIT
      ALPHA=-(RADI*DRDZ)/EMMIT
      GAMMA=(1+(ALPHA)**2)/BETA
      BETAR=(1-(1/((GAMMAR)**2)))**0.5
      XI=(2*I0)/((1.7E4)*((BETAR*GAMMAR)**3)*EMMIT)
      MAG=K1
C                 NOW COMES THE CALCULATING SECTION

111     CONTINUE
      DA=((MAG*BETA)-GAMMA-XI)*STEP
      ALPHA=ALPHA+DA
      DB=-2*ALPHA*STEP
      BETA=BETA+DB
      GAMMA=(1+(ALPHA*ALPHA))/BETA
      POS=POS+STEP
      COUNT1=COUNT1+STEP
      COUNT2=COUNT2+STEP
      RADI=(BETA*EMMIT)**0.5
      DRDZ=-(ALPHA*EMMIT)/RADI
      DRDZSUM=DRDZSUM+DRDZ*STEP

C             HERE WE HAVE CONDITIONAL PRINTING OUT OF VALUES

      IF (COUNT1.GT.COUNTA) THEN
      COUNT1=0
      POSNOW=POS+PELL
      RADICENT=RADI*100
      WRITE(12,1004)  (RADICENT,POSNOW)
1004     FORMAT (6E20.8)
      ENDIF
C                 CONDITIONAL SOLENOID PROCEDURE

      IF (POS.GT.SOL5.AND.SOLNO.LT.0.5) THEN
            IF (FL5.GT.0.0)       THEN
            DRDZ=DRDZ-(RADI/FL5)
            ALPHA=-(RADI*DRDZ)/EMMIT
            GAMMA=(1+(ALPHA)**2)/BETA
            ENDIF
      SOLNO=1.0
      ENDIF

      IF (POS.GT.SOL6.AND.SOLNO.LT.1.5) THEN
            IF (FL6.GT.0.0)       THEN
            DRDZ=DRDZ-(RADI/FL6)
            ALPHA=-(RADI*DRDZ)/EMMIT
            GAMMA=(1+(ALPHA)**2)/BETA
            ENDIF
      SOLNO=2.0
      ENDIF
C                 RESET MAGNET PARAMETERS

      IF (POS.GT.POS2) MAG=K2
      IF (POS.GT.POS3) MAG=K3
      IF (POS.GT.POS4) MAG=K4
      IF (POS.GT.POS5) MAG=K5

C             CONDITIONAL PROGRAM TERMINATION

      IF (POS.GT.POSEND) THEN
      DRDZAVE=DRDZSUM/(((2.0)**0.5)*POSEND)
      WRITE(12,*) DRDZAVE
      GOTO 999
      ENDIF
      GOTO 111
999     END
```

Appendix 2 -- Complete Pelletron Optics Code Package

```
C           PELLET3.FOR
C           THIS PROGRAM CALCULATES BEAM RADII BY NUMERICALLY
C           INTEGRATING THE TWISS PARAMETERS

C     THE VARIABLES

      REAL Z,SOLNO,SOL1,FL1,SOL2,FL2,SOL3,FL3,SOL4,FL4
      REAL SOLE4HI,SOLE4LO,DRDZHI,DRDZLO,TERM2,DXDZ
      REAL I0,K1,K2,K3,K4,K5,MAG,DRDZ0,RADI0,FL6

C      THIS SECTION READS IN INITIAL VALUES

      OPEN (UNIT=10,TYPE='OLD',FILE='PELL3IN.DAT')
      READ(10,*) (RADI0,DRDZ0,I0,E0,PHI0)
      READ(10,*) (STEP,POSEND,COUNTA,EMMIT0)
      READ(10,*) (SOL1,SOL2,FL1,FL2)
      READ(10,*) (SOL3,SOL4,FL3,FL4)
      CLOSE (UNIT=10)

C           INITIALIZE TOP DRAWER FILE

      WRITE (12,*) 'SET DEVICE IMGN300'
      WRITE (12,*) 'SET FONT DUPLEX'
      WRITE (12,*) 'TITLE LEFT ''RADIUS (CM.)'' '
      WRITE (12,*) 'TITLE SIZE 2.0'
      WRITE (12,*) 'TITLE BOTTOM ''BEAMLINE DISTANCE (M.)'' '
      WRITE (12,*) 'SET ORDER Y X'
C            WE NOW SET INITIAL PARAMETERS

222      CONTINUE

      POS=0.0
      SOLNO=0.0
      RADI=RADI0
      DRDZ=DRDZ0
      PHI=PHI0
      ALP0=E0/5.11E5
      GAMMAR=1+(PHI0/5.11E5)
      BETAR=(1-(1/((GAMMAR)**2)))**0.5
      EMMIT=EMMIT0/(BETAR*GAMMAR)
      XRADI=RADI0*((BETAR*GAMMAR)**0.5)
      BETA=((XRADI)**2)/EMMIT0
      TERM2=(RADI*ALP0*GAMMAR)/(2*((BETAR*GAMMAR)**1.5))
      DXDZ=DRDZ*((BETAR*GAMMAR)**0.5)+TERM2
      ALPHA=-(XRADI*DXDZ)/EMMIT0
      GAMMA=(1+(ALPHA)**2)/BETA
C           NOW COMES THE CALCULATING SECTION

111      CONTINUE
      XI=(2*I0)/((1.7E4)*((BETAR*GAMMAR)**3.))
      XI2=((ALP0**2)*((GAMMAR**2)+2))/(4*(BETAR*GAMMAR)**4)
      DA=(-GAMMA-(((XI/(RADI**2))-XI2)*BETA))*STEP
      ALPHA=ALPHA+DA
      DB=-2*ALPHA*STEP
      BETA=BETA+DB
      GAMMA=(1+(ALPHA*ALPHA))/BETA
      POS=POS+STEP
      COUNT1=COUNT1+STEP
      COUNT2=COUNT2+STEP
      XRADI=(BETA*EMMIT0)**0.5
      RADI=(XRADI)/((BETAR*GAMMAR)**0.5)
      RADI12=RADI11
      RADI11=RADI
      DRDZ=(RADI11-RADI12)/STEP
      PHI=(PHI+(E0*STEP))
      GAMMAR=1+(PHI/5.11E5)
      BETAR=(1-(1/((GAMMAR)**2)))**0.5
C            HERE WE HAVE CONDITIONAL PRINTING OUT OF VALUES

      IF (COUNT1.GT.COUNTA) THEN
      COUNT1=0
      RADICENT=RADI*100
      WRITE(12,1004) (RADICENT,POS)
1004     FORMAT (6E20.8)
      ENDIF

C            CONDITIONAL SOLENOID PROCEDURE

      IF (POS.GT.SOL1.AND.SOLNO.LT.0.5) THEN
            IF (FL1.GT.0.0) THEN
            DRDZ=DRDZ-(RADI/FL1)
            TERM2=(RADI*ALP0*GAMMAR)/(2*((BETAR*GAMMAR)**1.5))
            DXDZ=DRDZ*((BETAR*GAMMAR)**0.5)+TERM2
            ALPHA=-(XRADI*DXDZ)/EMMIT0
            GAMMA=(1+(ALPHA*ALPHA))/BETA
            ENDIF
      SOLNO=1.0
      ENDIF
C      THE SOLENOIDAL PROCEDURE -- CONTINUED
      IF (POS.GT.SOL2.AND.SOLNO.LT.1.5) THEN
            IF (FL2.GT.0.0) THEN
            DRDZ=DRDZ-(RADI/FL2)
            TERM2=(RADI*ALP0*GAMMAR)/(2*((BETAR*GAMMAR)**1.5))
            DXDZ=DRDZ*((BETAR*GAMMAR)**0.5)+TERM2
            ALPHA=-(XRADI*DXDZ)/EMMIT0
            GAMMA=(1+(ALPHA*ALPHA))/BETA
            ENDIF
      SOLNO=2.0
      ENDIF

C            CONDITIONAL PROGRAM TERMINATION

      IF (POS.LT.POSEND) GOTO 111
      CALL SLO3(RADI,DRDZ,E0,GAMMAR,DRDZ1)
      CALL TRAN3(RADI,DRDZ1,GAMMAR,PHI,ZFINAL,RADI2,DRDZ2)
      CALL SLO3(RADI2,DRDZ2,E0,GAMMAR,DRDZ3)
      CALL UPPELL(RADI2,DRDZ3,PHI,ZFINAL)
      CLOSE (12)
      STOP
      END


      SUBROUTINE SLO3(R,DRDZ,E0,GAMMA,DRDZ1)

C      THE VARIABLES

      REAL GAMMA,DRDZ1,DRDZ,R,E0
```

```
C      THE REST OF THIS GLORIOUS SUBROUTINE

      OPEN (1,TYPE='NEW',FILE='SLOUT.DAT')
      WRITE (1,1111) (DRDZ)
      DRDZ1=DRDZ+R*((E0)/(4*GAMMA*511000.0))
      WRITE (1,1111) (DRDZ1)
1111     FORMAT (6E20.8)
      CLOSE (1)
      END


      SUBROUTINE TRAN3(RADI,DRDZ,GAMMAR,PHI,ZFINAL,RADI1,DRDZ1)

C      THIS PROGRAM CALCULATES BEAM RADII BY NUMERICALLY          C
C      INTEGRATING THE TWISS PARAMETERS                      C

C      THE VARIABLES

      REAL Z,SOLNO,SOL5,FL5,SOL6,FL6
      REAL SOLE4HI,SOLE4LO,DRDZHI,DRDZLO
      REAL I0,K1,K2,K3,K4,K5,MAG,DRDZ0,RADI0

C                  WE NOW READ IN THE INITIAL VALUES

      OPEN(UNIT=11,TYPE='OLD',FILE='TRAN3IN.DAT')
        READ(11,*) (K1,K2,K3,K4,K5)
        READ(11,*) (POS1,POS2,POS3,POS4,POS5)
        READ(11,*) (EMMIT,COUNTB,RMIN,ERROR,POSEND)
        READ(11,*) (SOL5,FL5,SOL6,FL6)
      CLOSE (11)
C      MORE READING IN OF INITIAL VALUES

      OPEN (UNIT=10,TYPE='OLD',FILE='PELL3IN.DAT')
      READ(10,*) (RADI0,DRDZ0,I0,E0,PHI0)
      READ(10,*) (STEP,PELL,COUNTA,EMMIT0)
      READ(10,*) (SOL1,SOL2,FL1,FL2)
      READ(10,*) (SOL3,SOL4,FL3,FL4)
      CLOSE (UNIT=10)

C                  WE NOW SET INITIAL PARAMETERS

      K=0
      J=0
      N=0
222      CONTINUE
      POS=0.0
      SOLNO=0.0
      BETA=((RADI)**2)/EMMIT
      ALPHA=-(RADI*DRDZ)/EMMIT
      GAMMA=(1+(ALPHA)**2)/BETA
      BETAR=(1-(1/((GAMMAR)**2)))**0.5
      XI=(2*I0)/((1.7E4)*((BETAR*GAMMAR)**3)*EMMIT)
      MAG=K1

C                  NOW COMES THE CALCULATING SECTION

111      CONTINUE
      DA=((MAG*BETA)-GAMMA-XI)*STEP
      ALPHA=ALPHA+DA
      DB=-2*ALPHA*STEP
      BETA=BETA+DB
      GAMMA=(1+(ALPHA*ALPHA))/BETA
      POS=POS+STEP
      COUNT1=COUNT1+STEP
      COUNT2=COUNT2+STEP
      RADI=(BETA*EMMIT)**0.5
      DRDZ=-(ALPHA*EMMIT)/RADI

C          HERE WE HAVE CONDITIONAL PRINTING OUT OF VALUES

      IF (COUNT1.GT.COUNTA) THEN
      COUNT1=0
      POSNOW=POS+PELL
      RADICENT=RADI*100
      WRITE(12,1004) (RADICENT,POSNOW)
1004     FORMAT (6E20.8)
      ENDIF

C                  RESET MAGNET PARAMETERS

      IF (POS.GT.POS2) MAG=K2
      IF (POS.GT.POS3) MAG=K3
      IF (POS.GT.POS4) MAG=K4
      IF (POS.GT.POS5) MAG=K5

C                  CONDITIONAL SOLENOID PROCEDURE

      IF (POS.GT.SOL5.AND.SOLNO.LT.0.5) THEN
            IF (FL5.GT.0.0)       THEN
            DRDZ=DRDZ-(RADI/FL5)
            ALPHA=-(RADI*DRDZ)/EMMIT
            GAMMA=(1+(ALPHA)**2)/BETA
            ENDIF
      SOLNO=1.0
      ENDIF
C       CONDITIONAL SOLENOID PROCEDURE -- CONTINUED

      IF (POS.GT.SOL6.AND.SOLNO.LT.1.5) THEN
            IF (FL6.GT.0.0)       THEN
            DRDZ=DRDZ-(RADI/FL6)
            ALPHA=-(RADI*DRDZ)/EMMIT
            GAMMA=(1+(ALPHA)**2)/BETA
            ENDIF
      SOLNO=2.0
      ENDIF

C          CONDITIONAL PROGRAM TERMINATION

      IF (POS.GT.POSEND) GOTO 888
      GOTO 111
888      CONTINUE
      RADI1=RADI
      DRDZ1=DRDZ
      ZFINAL=POSEND+PELL
      RETURN
999      END
```

```
      SUBROUTINE UPPELL(RADI,DRDZ,PHI,ZFINAL)
C      THIS SUBROUTINE CALCULATES BEAM RADII BY NUMERICALLY
C      INTEGRATING THE TWISS PARAMETERS

C      THE VARIABLES

      REAL Z,SOLNO,SOL3,SOLEFF3,SOL4,SOLEFF4,FL6
      REAL SOLE4HI,SOLE4LO,DRDZHI,DRDZLO,TERM2,DXDZ
      REAL I0,K1,K2,K3,K4,K5,MAG,DRDZ0,RADI0

C            THIS SECTION READS IN INITIAL VALUES

      OPEN (UNIT=10,TYPE='OLD',FILE='PELL3IN.DAT')
      READ(10,*)  (RADI0,DRDZ0,I0,E0,PHI0)
      READ(10,*)  (STEP,POSEND,COUNTA,EMMIT0)
      READ(10,*)  (SOL1,SOL2,FL1,FL2)
      READ(10,*)  (SOL3,SOL4,FL3,FL4)
      CLOSE (10)
C      MORE READING IN OF INITIAL VALUES

      OPEN(UNIT=11,TYPE='OLD',FILE='TRAN3IN.DAT')
        READ(11,*)  (K1,K2,K3,K4,K5)
        READ(11,*)  (POS1,POS2,POS3,POS4,POS5)
        READ(11,*)  (EMMIT,COUNTB,RMIN,ERROR,POSEND2)
        READ(11,*)  (SOL5,FL5,SOL6,FL6)
      CLOSE (11)

C            WE NOW SET INITIAL PARAMETERS

222     CONTINUE
      POS=ZFINAL
      ALP0=(-1*E0)/5.11E5
      GAMMAR=1+(PHI/5.11E5)
      BETAR=(1-(1/((GAMMAR)**2)))**0.5
      EMMIT=EMMIT0/(BETAR*GAMMAR)
      XRADI=RADI*((BETAR*GAMMAR)**0.5)
      BETA=((XRADI)**2)/EMMIT0
      TERM2=(RADI*ALP0*GAMMAR)/(2*((BETAR*GAMMAR)**1.5))
      DXDZ=DRDZ*((BETAR*GAMMAR)**0.5)+TERM2
      ALPHA=-(XRADI*DXDZ)/EMMIT0
      GAMMA=(1+(ALPHA)**2)/BETA

C            NOW COMES THE CALCULATING SECTION

111     CONTINUE
      XI=(2*I0)/((1.7E4)*((BETAR*GAMMAR)**3.))
      XI2=((ALP0**2)*((GAMMAR**2)+2))/(4*(BETAR*GAMMAR)**4)
      DA=(-GAMMA-(((XI/(RADI**2))-XI2)*BETA))*STEP
      ALPHA=ALPHA+DA
      DB=-2*ALPHA*STEP
      BETA=BETA+DB
      GAMMA=(1+(ALPHA*ALPHA))/BETA
      POS=POS+STEP
      COUNT1=COUNT1+STEP
      XRADI=(BETA*EMMIT0)**0.5
      RADI=(XRADI)/((BETAR*GAMMAR)**0.5)
      RADI12=RADI11
      RADI11=RADI
      DRDZ=(RADI11-RADI12)/STEP
      PHI=(PHI-(E0*STEP))
      GAMMAR=1+(PHI/5.11E5)
      BETAR=(1-(1/((GAMMAR)**2)))**0.5
C            HERE WE HAVE CONDITIONAL PRINTING OUT OF VALUES

      IF (COUNT1.GT.COUNTA) THEN
      COUNT1=0
      RADICENT=RADI*100
      WRITE(12,1004)  (RADICENT,POS)
1004     FORMAT (6E20.8)
      ENDIF

C            CONDITIONAL SOLENOID PROCEDURE

      IF (POS.GT.SOL3.AND.SOLNO.LT.2.5) THEN
            IF (FL3.GT.0.0)       THEN
            DRDZ=DRDZ-(RADI/FL3)
            TERM2=(RADI*ALP0*GAMMAR)/(2*((BETAR*GAMMAR)**1.5))
            DXDZ=DRDZ*((BETAR*GAMMAR)**0.5)+TERM2
            ALPHA=-(XRADI*DXDZ)/EMMIT0
            GAMMA=(1+(ALPHA*ALPHA))/BETA
            ENDIF
      SOLNO=3.0
      ENDIF
C      CONDITIONAL SOLENOID PROCEDURE -- CONTINUED

      IF (POS.GT.SOL4.AND.SOLNO.LT.3.5) THEN
            IF (FL4.GT.0.0)       THEN
            DRDZ=DRDZ-(RADI/FL4)
            TERM2=(RADI*ALP0*GAMMAR)/(2*((BETAR*GAMMAR)**1.5))
            DXDZ=DRDZ*((BETAR*GAMMAR)**0.5)+TERM2
            ALPHA=-(XRADI*DXDZ)/EMMIT0
            GAMMA=(1+(ALPHA*ALPHA))/BETA
            ENDIF
      SOLNO=4.0
      ENDIF

C            CONDITIONAL PROGRAM TERMINATION

      Z2=POSEND+ZFINAL
      IF (POS.LT.Z2) GOTO 111
      WRITE(12,*)  'JOIN'
      WRITE(12,*)  'TITLE SIZE 1.0'
      WRITE(12,*)  'TITLE 1.0 9.5',' '' ',DRDZ,FL5,FL6,FL4,' '' '
      RETURN
      END
```

Appendix 3 -- Ideal Cooling Time Calculation

```
C            PROGRAM EMIT1
C      THIS PROGRAM CALCULATES ELECTRON COOLING
C      FOR AN IDEALLY COLD ELECTRON BEAM
C      NO IBS, NO BETATRON OSCILLATIONS


C            DECLARATION OF THE VARIABLES

      REAL THETAX(10),THETAZ(10),DP(10),EPX(10),EPZ(10)
      REAL DEPX(10),DEPZ(10),DDP(10),K,K2,DT,T,TDIS,TDISA,PI
      REAL BX(10),BZ(10),BS(10),BETA,GAMMA,P0,BTWISS
      REAL BT(10),NE,RE,RP,LAM,ETA,C,RAD,E,IE,PER
      REAL AP,BP,CP,AE,BE,CE,THETA(10),DPG(10)
      INTEGER I,J,NL
C      READ IN VARIABLES AND SET CONSTANTS

      OPEN (UNIT=1,TYPE='OLD',FILE='EMIT1IN.DAT')
      READ (1,*) AP,BP,CP,TDISA,DT
      READ (1,*) IE,RAD,LAM,ETA,BTWISS
      READ (1,*) GAMMA,AE,BE,CE
      CLOSE (1)

      AE=AE+1E-20
      BE=BE+1E-20
      CE=CE+1E-20

      PI=3.14
      C=3.0E8
      E=1.6E-19
      RE=2.82E-15
         RP=1.53E-18
C            INITIALIZATION OF PARAMETERS

      TDIS=TDISA
      BETA=(1-(1/GAMMA**2))**0.5
      THETAX(1)=AP/(BETA*GAMMA)
      THETAZ(1)=BP/(BETA*GAMMA)
      DP(10)=CP/BETA

      DO 0010 I=1,10
      PER=(1.-((FLOAT(I)-1.)/9.))
      THETAX(I)=PER*THETAX(1)
      THETAZ(I)=PER*THETAZ(1)
      THETA(I)=(THETAX(I)**2+THETAZ(I)**2)**0.5
      DP(I)=((1-(THETA(I)**2/THETA(1)**2))**0.5)*DP(10)
      EPX(I)=PI*BTWISS*THETAX(I)**2
      EPZ(I)=PI*BTWISS*THETAZ(I)**2
0010      CONTINUE

      NE=IE/(PI*RAD**2*BETA*C*GAMMA*E)
      K2=(4*PI*NE*RE*RP*LAM*ETA*C)/((BETA*GAMMA)**3)
      K=K2*BTWISS*2*PI
      K2=K2*BETA
      NL=10
C                  CALCULATION

0100      CONTINUE
      DO 0700 I=1,NL
      DPG(I)=DP(I)/GAMMA
      IF (EPX(I).LT.1E-19) GOTO 0200
DEPX(I)=(K*THETAX(I)**2)/((THETAX(I)**2+THETAZ(I)**2+DPG(I)**2)**1.5)
      EPX(I)=EPX(I)-DEPX(I)*DT
      IF (EPX(I).LT.1E-19) GOTO 0200
      THETAX(I)=((EPX(I))/(PI*BTWISS))**0.5
      BX(I)=BETA*GAMMA*THETAX(I)
0200      CONTINUE
      IF (EPZ(I).LT.1E-19) GOTO 0300
DEPZ(I)=(K*THETAZ(I)**2)/((THETAX(I)**2+THETAZ(I)**2+DPG(I)**2)**1.5)
      EPZ(I)=EPZ(I)-DEPZ(I)*DT
      IF (EPZ(I).LT.1E-19) GOTO 0300
      THETAX(I)=((EPX(I))/(PI*BTWISS))**0.5
      BZ(I)=BETA*GAMMA*THETAZ(I)
0300      CONTINUE
      DDP(I)=(K2*DP(I))/((THETAX(I)**2+THETAZ(I)**2+DPG(I)**2)**1.5)
      DP(I)=DP(I)-DDP(I)*DT
      BS(I)=BETA*DP(I)
0700      CONTINUE
      T=T+DT*GAMMA
      TDIS=TDIS+DT*GAMMA


C      CONDITIONAL PRINTOUT OF VALUES

      IF (TDIS.GT.TDISA) THEN
      TDIS=0.0
      OPEN (UNIT=3,TYPE='NEW',FILE='OUT1.DAT')
      WRITE (3,0800) (BX(I),I=1,10)
      WRITE (3,0800) (BZ(I),I=1,10)
      WRITE (3,0800) (BS(I),I=1,10)
      WRITE (3,*) 'TIME = ',T
      CLOSE (3)
      CALL TOTD
      ENDIF
0800      FORMAT (E12.6)
C      CONDITIONAL PROGRAM TERMINATION

      DO 0900 I=1,NL
      BT(I)=((BX(I)**2/AE**2)+(BZ(I)**2/BE**2)+(BS(I)**2/CE**2))**0.5
      IF (BT(I).LE.1.0) THEN
      DO 0910 J=1,NL
0910      CONTINUE
      NL=NL-1
            IF (NL.LE.0.5) THEN
            OPEN (UNIT=3,TYPE='NEW',FILE='OUT1.DAT')
            WRITE (3,0800) (BX(J),J=1,10)
            WRITE (3,0800) (BZ(J),J=1,10)
            WRITE (3,0800) (BS(J),J=1,10)
            WRITE (3,*) 'TIME = ',T
            CLOSE (3)
            CALL TOTD
            GOTO 1000
            ENDIF
      ENDIF
0900      CONTINUE
      GOTO 0100
1000      STOP
      END
```

Appendix 4 -- Calculation of the Effect of Electron Temperature
.c
<on the Electron Cooling Force>

```
C      PROGRAM ECOOL3 -- INCLUDES ELECTRON VELOCITIES

C                    THE VARIABLES

      REAL*8 PI,C,E,RE,RP,BETA,GAMMA,AP,AE,BE,CE
      REAL*8 THETXO
      REAL*8 PER,NE,IE,RAD,K2,LAM,ETA,K,BTWISS,T,EPE,EPX
      REAL*8 THETAX,DX,DZ,DDP,X(10000),Z(10000),DP(10000),DIST,KTOT
      REAL*8 DEPX,DENOM1,DDEPX1,DT,BX,DENOM2,DDEPX2
      INTEGER I,J,L,NX,NY,NZ,NIN,NIN2

C      READ IN VARIABLES

      OPEN (UNIT=1,TYPE='OLD',FILE='EMIT3IN.DAT')
      READ (1,*) AP,BP,CP,TDISA,DT
      READ (1,*) IE,RAD,LAM,ETA,BTWISS
      READ (1,*) GAMMA,AE,BE,CE
      READ (1,*) NX,NY,NZ
      CLOSE (1)
C        SET CONSTANTS

      PI=3.14
      C=3.0E8
      E=1.6E-19
      RE=2.82E-15
      RP=1.53E-18

C              INITIALIZATION OF PARAMETERS

      BETA=(1-(1/GAMMA**2))**0.5
      TAE=AE/(BETA*GAMMA)
      TBE=BE/(BETA*GAMMA)
      TCE=CE/(BETA*GAMMA)
C      THE GAMMA COMES IN THE FORMULA FOR COOLING FOR THE LONGITUDINAL
C      TCE. NOT IN THE TRANSFORMATION TO THETA AS IN TAE AND TBE
      THETXO=AP/(BETA*GAMMA)
      NE=IE/(PI*RAD**2*BETA*C*GAMMA*E)
      K2=(4*PI*NE*RE*RP*LAM*ETA*C)
      KTOT=(K2*BTWISS*2*PI)/((BETA*GAMMA)**3)

      DX=AE/(NX*BETA*GAMMA)
      DZ=BE/(NY*BETA*GAMMA)
      DDP=CE/(NZ*BETA*GAMMA)
C      MORE INITIALIZATION OF PARAMETERS

      DO 0150 I=1,NX
       X(I)=I*DX
0150     CONTINUE
      DO 0160 I=1,NY
       Z(I)=I*DZ
0160     CONTINUE
      DO 0165 I=1,NZ
       DP(I)=I*DDP
0165     CONTINUE

      THETAX=THETXO
      NIN=0
C                    RENORMALIZE K

      DO 0173 I=1,NX
       DO 0172 J=1,NY
        DO 0171 L=1,NZ
         DIST=(X(I)**2)/TAE**2+(Z(J)**2)/TBE**2+(DP(L)**2)/TCE**2
         IF (DIST.LT.1) THEN
          NIN=NIN+1
         END IF
0171        CONTINUE
0172       CONTINUE
0173      CONTINUE
      K=KTOT/(2*NIN)
C                    CALCULATION

0179      CONTINUE
      DEPX=0.0
      DO 0200 I=1,NX
       DO 0190 J=1,NY
        DO 0180 L=1,NZ
         DIST=(X(I)**2)/TAE**2+(Z(J)**2)/TBE**2+(DP(L)**2)/TCE**2
         IF (DIST.LT.1.0) THEN
         DENOM1=((THETAX-X(I))**2+Z(J)**2+DP(L)**2)**1.5
         DENOM2=((THETAX+X(I))**2+Z(J)**2+DP(L)**2)**1.5
         DDEPX1=(K*(THETAX-X(I))*THETAX)/DENOM1
         DDEPX2=(K*(THETAX+X(I))*THETAX)/DENOM2
         DEPX=DEPX+DDEPX1+DDEPX2
         END IF
0180        CONTINUE
0190       CONTINUE
0200      CONTINUE
C            CONDITIONAL PROGRAM TERMINATION

      OPEN (UNIT=4,TYPE='NEW',FILE='OUT3.DAT')
      NIN2=NIN*8
      WRITE (4,*) THETAX,DEPX,NIN2
      CLOSE (4)
0500      CONTINUE
      STOP
      END
```

Appendix 5 -- The Effect of Betatron Oscillations on the Cooling Time

```
C                        PROGRAM EMIT4
C      THIS PROGRAM CALCULATES THE EFFECT OF BETATRON OSCILATIONS
C                   ON THE COOLING TIME

C                   THE VARIABLES

      REAL DEP0,THETAX,THETAZ,PI,DPSIX,DPSIZ,PSIX,PSIZ,GOOF,FUNC
      REAL THETAE,RATIO,DDEP,DEP,DPG

C      READ IN VARIABLES AND SET CONSTANTS AND INITIAL CONDITIONS

      OPEN (UNIT=1,TYPE='OLD',FILE='EMIT4IN.DAT')
      READ (1,*) THETAX,THETAZ,THETAE,DPG
      READ (1,*) DPSIX,DPSIZ
      CLOSE (1)

      DEP0=(THETAX**2)/(((THETAX**2)+(THETAZ**2)+(DPG**2))**1.5)
      PI=3.141592654
      NI=PI/(2*DPSIX)
      NJ=PI/(2*DPSIZ)

C                   THE CALCULATION

      DO 0100 I=1,NI
       PSIX=(FLOAT(I)-0.5)*DPSIX
       A=SIN(PSIX)
       GOOF1=THETAX*(SIN(PSIX))
       IF (GOOF1.LT.THETAE) GOOF1=THETAE
        DO 0200 J=1,NJ
        PSIZ=(FLOAT(J)-0.5)*DPSIZ
        GOOF2=THETAZ*(SIN(PSIZ))
        IF (GOOF2.LT.THETAE) GOOF2=THETAE
        DENOM=((GOOF1**2)+(GOOF2**2)+(DPG**2))**1.5
        FUNC=(SIN(PSIX))**2/DENOM
        DDEP=FUNC*DPSIX*DPSIZ
        NTOT=NTOT+1
        DEP=DEP+DDEP
0200       CONTINUE
0100      CONTINUE
C      FINAL MOP-UP, PRINTOUT, AND TERMINATION

      DEP=(DEP*(THETAX**2)*4)/(PI**2)
      RATIO=DEP/DEP0
      PRINT *,RATIO,NI,NJ,DEP0,DEP
      PRINT *,THETAX,THETAZ,THETAE,NTOT
      PRINT *,DPSIX,DPSIZ,PSIX,PSIZ
      STOP
      END
```

Appendix 6 -- The Effect of Intrabeam Scattering on the Cooling Time

Note -- This appendix contains two versions of the code EMIT2. I have used two different assumptions to find the effect of Intrabeam Scattering. Both codes use subroutine IBS.

```
C            PROGRAM EMIT2

C      THIS PROGRAM CALCULATES ELECTRON COOLING
C                INCLUDING IBS
C         (FOR AN IDEALLY COLD ELECTRON BEAM)
C            (NO BETATRON OSCILLATIONS)

C            DECLARATION OF THE VARIABLES

      REAL THETAX,DP,EPX
      REAL DEPX,DDP,K,K2,DT,T,TDIS,TDISA,PI,AX(10),AS(10)
      REAL BX(10),BS(10),BETA,GAMMA,P0,BTWISS,BXX,BSS
      REAL BT,NE,RE,RP,LAM,ETA,C,RAD,E,IE,PER
      REAL AP,BP,CP,AE,BE,CE,THETA,DPG,TANGENT
      INTEGER I,J,NL
C      READ IN VARIABLES AND SET CONSTANTS

      OPEN (UNIT=3,TYPE='NEW',FILE='OUT1.DAT')
      OPEN (UNIT=1,TYPE='OLD',FILE='EMIT2IN.DAT')
      READ (1,*) AP,BP,CP,TDISA,DT
      READ (1,*) IE,RAD,LAM,ETA,BTWISS
      READ (1,*) GAMMA,AE,BE,CE,TOGGLE
      CLOSE (1)

      AE=AE+1E-20
      BE=BE+1E-20
      CE=CE+1E-20

      PI=3.14
      C=3.0E8
      E=1.6E-19
      RE=2.82E-15
      RP=1.53E-18
C            INITIALIZATION OF PARAMETERS

      TDIS=TDISA
      BETA=(1-(1/GAMMA**2))**0.5
      THETAX=AP/(BETA*GAMMA)
      DP=CP/BETA
      TANGENT=DP/THETAX
         EPX=PI*BTWISS*THETAX**2
      BSS=BETA*DP

      NE=IE/(PI*RAD**2*BETA*C*GAMMA*E)
      K2=(4*PI*NE*RE*RP*LAM*ETA*C)/((BETA*GAMMA)**3)
         K=K2*BTWISS*2*PI
      K2=K2*BETA
C                    CALCULATION

0100     CONTINUE
      DPG=DP/GAMMA
      IF (TOGGLE.GT.0) THEN
      CALL IBS(DP,EPX,XRATE,YRATE)
      ELSE
      XRATE=0.
      YRATE=0.
      ENDIF
      DDEPX=EPX*XRATE
      DEPX=(K*THETAX**2)/((THETAX**2+DPG**2)**1.5)
      EPX=EPX-((DEPX-DDEPX)*DT)
      THETAX=((EPX)/(PI*BTWISS))**0.5
      BXX=BETA*GAMMA*THETAX

      IF (BSS.GT.CE) THEN
      DP=TANGENT*THETAX
      BSS=BETA*DP
      ENDIF

      T=T+DT*GAMMA
      TDIS=TDIS+DT*GAMMA
C      CONDITIONAL PROGRAM TERMINATION

      IF (BXX.GT.AE) GOTO 0100
0900     WRITE (3,0800) BXX,BSS,T
      CLOSE (3)
1000     STOP
      END


         SUBROUTINE IBS(DP,EPX,XRATE,YRATE)

CC       THIS SUBROUTINE CALCULATES THE EMITTANCE GROWTH
CC           CAUSED BY INTRABEAM SCATTERING

CC                THE VARIABLES

      REAL DP,EPX,XRATE,YRATE,DP1,EPX1

CC        BEST FIT EQUATION FOR DATA FROM BJORKEN & MTINGWA

      DP1=(DP*1E4)
      EPX1=(EPX*1E6)/(6*3.14)
      DSTUFF=(((DP1)**(-0.24))-.4*((DP1)**(.3)))/3600.
      XRATE=10.*(1.28E-2)*(EPX1**-2.48)*(1+2.5*EPX1*DP1)*DSTUFF
      YRATE=10.*(.42*(DP1**-2.24)*(EPX1**-1.47))/3600.
      RETURN
      END


C            PROGRAM EMIT2

C      THIS PROGRAM CALCULATES ELECTRON COOLING INCLUDING IBS
C         (FOR AN IDEALLY COLD ELECTRON BEAM)
C            (NO BETATRON OSCILLATIONS)

C            DECLARATION OF THE VARIABLES

      REAL THETAX,DP,EPX
      REAL DEPX,DDP,K,K2,DT,T,TDIS,TDISA,PI,AX(10),AS(10)
      REAL BX(10),BS(10),BETA,GAMMA,P0,BTWISS,BXX,BSS
      REAL BT,NE,RE,RP,LAM,ETA,C,RAD,E,IE,PER
      REAL AP,BP,CP,AE,BE,CE,THETA,DPG
         INTEGER I,J,NL
```

```
C      READ IN VARIABLES

       OPEN (UNIT=3,TYPE='NEW',FILE='OUT1.DAT')
       OPEN (UNIT=1,TYPE='OLD',FILE='EMIT2IN.DAT')
       READ (1,*) AP,BP,CP,TDISA,DT
       READ (1,*) IE,RAD,LAM,ETA,BTWISS
       READ (1,*) GAMMA,AE,BE,CE
       CLOSE (1)
C      SET CONSTANTS

       AE=AE+1E-20
       BE=BE+1E-20
       CE=CE+1E-20

       PI=3.14
       C=3.0E8
       E=1.6E-19
          RE=2.82E-15
       RP=1.53E-18
C            INITIALIZATION OF PARAMETERS

       TDIS=TDISA
       BETA=(1-(1/GAMMA**2))**0.5
       THETAX=AP/(BETA*GAMMA)
       DP=CP/BETA
       EPX=PI*BTWISS*THETAX**2
       BSS=BETA*DP
       BXX=BETA*GAMMA*THETAX
       B=(BSS**2+BXX**2)**0.5

          NE=IE/(PI*RAD**2*BETA*C*GAMMA*E)
       K2=(4*PI*NE*RE*RP*LAM*ETA*C)/((BETA*GAMMA)**3)
       K=K2*BTWISS*2*PI
          K2=K2*BETA
C                   CALCULATION

0100      CONTINUE
       DPG=DP/GAMMA

       CALL IBS(DP,EPX,XRATE,YRATE)
       DDEPX=EPX*XRATE
       DEPX=1.5*(K*THETAX**2)/((THETAX**2+DPG**2)**1.5)
       EPX=EPX-((DEPX-DDEPX)*DT)
       THETAX=((EPX)/(PI*BTWISS))**0.5
       BXX=BETA*GAMMA*THETAX

       IF (BSS.GT.CE) THEN
       DDDP=0.5*DP*YRATE
       DDP=10*(K2*DP)/((THETAX**2+DPG**2)**1.5)
       DP=DP-(DDP-DDDP)*DT
       BSS=BETA*DP
       ENDIF

       B1=B
       B=(BSS**2+BXX**2)**0.5
       T=T+DT*GAMMA
       TDIS=TDIS+DT*GAMMA
C      CONDITIONAL PRINTOUT OF VALUES

       IF (TDIS.GT.TDISA) THEN
             TDIS=0.0
             WRITE (3,0800) BXX,BSS,T
0800             FORMAT (E12.6,3X,E12.6,3X,E12.6)
       ENDIF

C      CONDITIONAL PROGRAM TERMINATION

       IF (B.LT.B1) GOTO 0100
0900      WRITE (3,0800) BXX,BSS,T
       CLOSE (3)
1000      STOP
       END
```

Appendix 7 -- Calculation of the Ideal Electron Cooling Rates

```
C      PROGRAM ECOOLRATE -- CALCULATES ELECTRON COOLING RATES

C            DECLARATION OF VARIABLES

      REAL PI,C,E,RE,RP,IE,RAD,GAMMA,LAM,ETA,BTWISS,DPG(6),EPX(7)
      REAL BETA,NE,K2,K,THETAX,DEPX,XRATE(7,6),DP(6)

C      SET CONSTANTS

      PI=3.14
      C=3.0E8
      E=1.6E-19
      RE=2.82E-15
      RP=1.53E-18
C      READ IN AND DETERMINE INITIAL VALUES

      OPEN (UNIT=1,TYPE='OLD',FILE='IN.DAT')
      READ (1,*) IE,RAD,GAMMA,LAM,ETA
      READ (1,*) BTWISS

      BETA=(1-(1/GAMMA**2))**0.5
      NE=IE/(PI*RAD**2*BETA*C*GAMMA*E)
      K2=(4*PI*NE*RE*RP*LAM*ETA*C)/((BETA*GAMMA)**3)
      K=K2*BTWISS*2*PI

C            INITIALIZE EPX

      EPX(1)=2.27E-25
      EPX(2)=1.0E-10
      EPX(3)=1.0E-9
      EPX(4)=1.0E-8
      EPX(5)=3.63E-8
      EPX(6)=1.0E-7
      EPX(7)=1.0E-6
            INITIALIZE DP

      DP(1)=7.5E-17
      DP(2)=1.0E-6
      DP(3)=1.0E-5
      DP(4)=3.0E-5
      DP(5)=5.0E-5
      DP(6)=1.0E-4

C                  CALCULATION

      DO 0100 I=1,7
      DO 0200 J=1,6
      DPG(J)=DP(J)/GAMMA
      THETAX=((EPX(I))/(BTWISS))**0.5
      DEPX=(K*THETAX**2)/((THETAX**2+DPG(J)**2)**1.5)
      XRATE(I,J)=(DEPX/EPX(I))*(3600./GAMMA)
0200      CONTINUE
0100      CONTINUE

C      THE REASON THERE IS NO PI IN THE EQUATION FOR THETAX
C      COMES FROM THE FACT THAT BJORKEN AND MTINGWA DEFINED          C
C      THE EMITTANCE TO NOT INCLUDE THE PI                           C

C            WRITE THE RESULTS TO A FILE AND TERMINATE PROGRAM

      OPEN (UNIT=2,TYPE='NEW',FILE='OUT.DAT')
      WRITE (2,12) ((XRATE(I,K),I=1,7),K=1,6)
12      FORMAT (E9.3,1X,E9.3,1X,E9.3,1X,E9.3,1X,E9.3,1X,E9.3,1X,E9.3)
      CLOSE (2)
      END
```

Acknowledgments

I wish to thank the many people who have made this draft possible.

Professors David Cline and Frederick Mills were the research directors of this project over the past four years. Their expertise covered the whole range of topics considered within these pages. I am deeply indebted to both of them for their help and guidance.

Experimental work on this project was largely carried out at National Electrostatics Corporation. Mark Sundquist, Jim Adney, Jim Ferry, and Ray Herb were all instrumental members of the research team.

Experts at Fermi National Laboratory contributed greatly in specific areas. Sekazi Mtingwa provided crucial information on the influence intrabeam scattering has on an antiproton beam. The study of beam instabilities in the accumulator was performed by John Marriner.

Sandro Ruggiero and Jim Simpson of Argonne National Lab contributed to my early understanding of the cooling process.

Others who contributed: Dan Anderson painstakingly proofed all calculations and computer codes used in this analysis. Bill Cummings, Dan Anderson, Scott Winkowsi, and Steve Dehais were all helpful in the experimental effort. Mike Procario and Dan Gee were extremely helpful on computer related matters. Jamie Rosenzweig provided lively and thoughtful counsel periodically throughout this effort.

Thanks to all.

References

1.1 G.I. Budker, The 1966 Proc. Int. Symp. Electron and Positron Storage Rings, Saclay. Atomnaya Energiya 22: 346.

1.2 L. Spitzer, "Physics of Fully Ionized Gases", pp. 80-81, New York: Interscience, 1956.

1.3 S. Van der Meer, "Stochastic Stacking in the Antiproton Accumulator", CERN/PS/AA/78-22, 16 October 1978.

1.4 F. Sacherer, "Stochastic Cooling Theory", CERN-ISR-TH/78-11.

1.5 G.I. Budker, et al., "Experimental Studies of Electron Cooling", Particle Accelerators, 1976, Vol. 7, pp. 197-211.

1.6 M. Bell, et al., "Electron Cooling Experiment at CERN", Physics Letters, Vol. 87B, number 3, 5 November 1979.

1.7 T. Ellison, et al., "Electron Cooling and Accumulation of 200 MeV Protons at Fermilab", IEEE Trans. Nuc. Sci., Vol. NS-30, No. 4, August 1983, 2636-2638.

1.8 J.D. Jackson, "Classical Electrodynamics", equation 13.13.

2.1 D.B. Cline, et al., "Intermediate Energy Electron Cooling for Antiproton Sources using a Pelletron Accelerator", IEEE Trans. Nuc. Sci., Vol. NS-30, No. 4, August 1983, 2370-2372.

2.2 W. Kells, AIP Conference Proceedings No. 87, pp. 656, American Institute of Physics, New York 1982.

2.3 E.D. Courant and H.S. Snyder, Annals of Physics: 3, 1, 1958.

2.4 T. Ellison, et al., "Electron Cooling and Accumulation of 200 MeV Protons at Fermilab", IEEE Trans. Nuc. Sci., Vol. NS-30, No. 4, August 1983, 2636-2638.

2.5 W.B. Herrmannsfeldt, et al., "The Electron Beam for the Fermilab Electron Cooling Experiment", IEEE Trans. Nuc. Sci., Vol. NS-26, No. 3, June 1979, 3237-3240.

2.6 W. Kells, et al., "Electron Cooling for the Fermilab P-bar Source", IEEE Trans. Nuc. Sci, Vol. NS-28, No. 3, June 1981, 2583-2584.

2.7 R. Forster, et al., "Electron Cooling Experiments at Fermilab", IEEE Trans. Nuc. Sci, Vol. NS-28, No. 3, June 1981, 2386-2388.

2.8 D.J. Larson, et al., "Beam Envelope Solution of a Finite Emittance Beam Including Space Charge and Acceleration", to be published. (Reported to the 1985 Particle Accelerator Conference held in Vancouver. IEEE report.)

2.9 Septier, "Focusing of Charged Particles", pp. 321-345.

3.1 "Design Report - Tevatron I Project" Fermi National Accelerator Laboratory, September 1983.

3.2 S. Van der Meer, "Stochastic Damping of Betatron Oscillations in the ISR", CERN/ISR-PO/72-31 (1972), unpublished.

3.3 B.F. Bayanov et al., "A Lithium Lens for Axially Symmetric Focusing of High Energy Particle Beams" Nucl. Inst. Methods 190, pp. 9-14, 1981.

3.4 J.D. Simpson, Argonne National Lab, unpublished.

3.5 D.B. Cline, et al., "Intermediate Energy Electron Cooling for Antiproton Sources using a Pelletron Accelerator", IEEE Trans. Nuc. Sci., Vol. NS-30, No. 4, August 1983, 2370-2372.

3.6 J.D. Jackson, "Classical Electrodynamics", equation 13.13.

4.1 J.D. Jackson, "Classical Electrodynamics", equation 13.13.

4.2 E.D. Courant and H.S. Snyder, Annals of Physics: 3, 1, 1958.

4.3 J.D. Bjorken and S.K. Mtingwa, "Intrabeam Scattering", Particle Accelerators Vol. 13 pp. 115-143, 1983.

4.4 A. Piwinski, Proc. 9th Int. Conf. on High Energy Accelerators, 1974, p. 405.

4.5 S.K. Mtingwa, private communication.

5.1 J.D. Bjorken and S.K. Mtingwa, "Intrabeam Scattering", Particle Accelerators Vol. 13 pp. 115-143, 1983.

5.2 E.D. Courant and H.S. Snyder, Annals of Physics: 3, 1, 1958.

5.3 S.K. Mtingwa, private communication.

5.4 W. Schnell, "Coherent Instabilities of Proton Beams in Accelerators and Storage Rings -- Experimental Results, Diagnosis and Cures", Theoretical aspects of the behavior of beams via accelerators and storage rings, Erice, Sicily, Nov. 10-22, 1976 (CERN 1977), pp. 231-64.

5.5 A. Hofmann, "Single-beam Collective Phenomena -- Longitudinal", Theoretical aspects of the behavior of beams via accelerators and storage rings, Erice, Sicily, Nov. 10-22, 1976 (CERN 1977), pp. 139-74.

5.6 E. Keil and W. Schnell, CERN Report ISR-TH-RF/69-48 (1969).

5.7 J. Marriner, et al., "Stability Criterion and Wall Impedance for the Antiproton Accumulator", to be published as a p-bar note.

5.8 F.E. Mills, private communication.

5.9 Particle Properties Data Booklet, April 1985.